arXiv:2608.02865v1 [physics.chem-ph] 3 Aug 2026

A concentration-independent paradigm rendering weak interactions inherently quantifiable

Masahiko Yoshimura[1†], Fuyuki Matsuda[1†], Yoshiki Ikeda[1†], Chihiro Mori[1], Tomoko Yoneda[1], Minako Kikukawa[1], Rie Murakami[1], Chiharu Nogami[2], Yukihiko Sugita[3,4,5], Yoshiko Nakada-Nakura[1], Masahiko Tsujimoto[1], Daishi Fujita[1,6*]

[1]Institute for Integrated Cell-Material Sciences (iCeMS), Institute for Advanced Study, Kyoto University, Yoshida, Sakyo-ku, Kyoto, 606-8501, Japan.
[2]Faculty of Science, Kyoto University, Sakyo-ku, Kyoto, 606-8502, Japan.
[3]Institute for Life and Medical Sciences, Kyoto University, 53 Shogoin Kawahara-cho, Sakyo-ku, Kyoto, 606-8507, Japan.
[4]Graduate School of Biostudies, Kyoto University, Yoshida-Konoecho, Sakyo-ku, Kyoto, 606-8501, Japan.
[5]Hakubi Center for Advanced Research, Kyoto University, Kyoto, Japan.
[6]Inamori Research Institute for Science, Kyoto, Japan.

*Corresponding author(s). E-mail(s): dfujita@icems.kyoto-u.ac.jp;
†These authors contributed equally to this work.

Present Address:
Chiharu Nogami: Institute for Life and Medical Sciences, Kyoto University, 53 Shogoin Kawahara-cho, Sakyo-ku, Kyoto 606-8507, Japan; Graduate School of Biostudies, Kyoto University, Yoshida-Konoecho, Sakyo-ku, Kyoto 606-8501, Japan.

Abstract

A vast class of weak, millimolar-affinity molecular interactions governs cellular function, yet their quantitative characterization has remained largely beyond the reach of conventional methods. For over a century, biochemistry has worked within a concentration-based framework in which molarity scales with molecular

number per volume ($\boldsymbol{N/V}$), and experiments have usually, and often implicitly, changed concentration by moving $\boldsymbol{N}$ while holding $\boldsymbol{V}$ fixed. The weak-interaction measurement bottleneck arises from this paradigm itself: reading weak binding through bulk concentration requires concentrations that often exceed practical limits, a constraint rooted in the framework rather than in instrumental sensitivity. Here we show that shifting experimental control from molecular number $\boldsymbol{N}$ to accessible volume $\boldsymbol{V}$ directly overcomes this bottleneck and provides access to previously intractable affinity ranges through nanoscale spatial confinement. In practical terms, controlling accessible volume $\boldsymbol{V}$ means controlling what biochemists have long called "local concentration" and "proximity effects"; this shift can be viewed as recasting these previously ambiguous notions as quantitative variables grounded in first principles. Implemented in DNA nanocavities that impose controlled confinement, the approach showed that geometric arrangement alone can override solution-phase binding hierarchies. The same spatial control quantified a protein–peptide interaction of order **10 mM** from femtomoles per well, totalling under a picomole per titration. Even so, a standard plate reader gave a signal-to-noise ratio near $\mathbf{10^3}$, leaving headroom for still weaker interactions. The same affinity-and-geometry readout also enabled rational screening for protein–protein-interaction modulators, identifying compounds that enhance weak associations by reweighting local encounters rather than by binding tightly on their own or forming a stable ternary complex. Together, this volume-based paradigm and its experimental implementation provide a general strategy for probing and modulating previously inaccessible biochemical phenomena.

Cellular function hinges on a hidden majority of molecular interactions that current biochemical methods fail to capture[1–3]. The structural and thermodynamic bases of high-affinity binding, characterized by equilibrium dissociation constants (K_d) in the nanomolar to micromolar range, are well understood. By contrast, many functionally critical interactions exhibit weak affinity (K_d in the millimolar range), such that most binding partners remain unbound at typical intracellular concentrations[4]. These low-occupancy interactions are essential for cellular homeostasis, mediating dynamic protein assemblies[5–8], metabolic channelling[9–13] and plasticity within signalling networks[14, 15]. Yet their low occupancy renders them largely invisible to conventional ensemble assays, and a comprehensive database analysis reveals that millimolar-affinity interactions remain almost entirely unquantified in the literature (Fig. 1), creating a persistent methodological gap. Chien and Gierasch accordingly described their quantitative detection and characterization as "dream experiments"[16], reflecting both their biological importance and persistent experimental inaccessibility. What has kept them beyond reach?

The answer lies not in instrumentation alone, but in the molar-concentration metric through which binding is conventionally measured. For over a century, the dissociation constant (K_d) has dominated because its molar units are simple and intuitive; for a 1:1 interaction, it is the free-ligand concentration at half occupancy. Molar concentration scales with molecular number per volume (N/V), and routine titrations change it almost entirely by increasing N at fixed V. This practice works well for

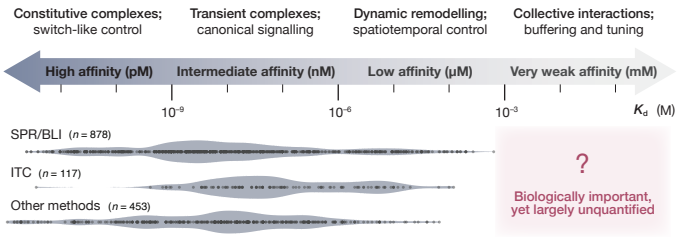


Fig. 1 Millimolar-affinity protein interactions are largely unquantified by standard binding assays. Reported dissociation constants (K_d) for wild-type protein–protein interactions in the PPB-Affinity dataset[20] (n = 1,460, 1990–2018). The K_d axis is logarithmic; larger values indicate weaker binding. Points denote individual reported interactions, grouped by method: SPR/BLI (surface plasmon resonance or biolayer interferometry, n = 878), ITC (isothermal titration calorimetry, n = 117) and other methods (n = 453). The axis starts at 10^{-12} M, so 12 sub-picomolar records fall outside it and 1,448 of the 1,460 are drawn. Grey violin density envelopes summarize the displayed method-specific distributions. Upper annotations show illustrative biological contexts rather than definitive categories. Coverage is dense from picomolar to micromolar and thins sharply at high micromolar K_d. Across all 1,460 records, none exceeds 1 mM and the weakest reported interaction is 0.635 mM. The millimolar range highlighted in pale pink is therefore the weak-interaction frontier targeted here.

strong interactions, whose affinity range is reached at modest concentrations, but weak interactions expose its ceiling: measuring millimolar K_d values demands comparable or higher free-ligand concentrations, conditions that routinely exceed solubility limits or exhaust sample availability. For example, even well-behaved proteins suitable for crystallization rarely reach concentrations above 10 mg/mL ($\sim$ 200 μM for a 50 kDa protein)[17–19], which puts millimolar measurements out of reach across all major techniques (Fig. 1). Critically, this ceiling is an artefact of the concentration paradigm itself. This single concentration coordinate dictates measurement protocols; instrumentation follows accordingly, and the resulting self-imposed constraints come to be mistaken for natural limits. We term this framework the concentration-based (N-controlled) paradigm and challenge it at its foundations.

A complementary experimental route is to control the denominator of N/V: instead of adding molecules, to control the space available to them. At the molecular scale, this route can be implemented by controlling the accessible volume of each interaction partner, opening a parallel experimental axis. We call this the volume-based (V-controlled) paradigm. Flexible tethers define each partner's range of motion, and the overlap of these ranges sets how readily the pair can meet (Fig. 2a,b). In this light, what biochemists call "local concentration" and "proximity effects" can be viewed as consequences of the volume available to each partner[21–23]. DNA nanocavities realize this scheme by creating nanoscale zones for tethered motion while remaining connected to the surrounding solution through openings. These engineered zones form a minimal single-pair platform whose cavities function as "molecular interrogation rooms" in which pairwise behaviour can be perturbed and examined (Fig. 3a).

This study demonstrates the experimental impact of the rigorous theoretical framework developed in our companion paper[24] by translating it into an intuitive, bench-compatible strategy for weak intermolecular interactions. The full mathematical treatment is provided there; this article focuses on the core distinction needed at the

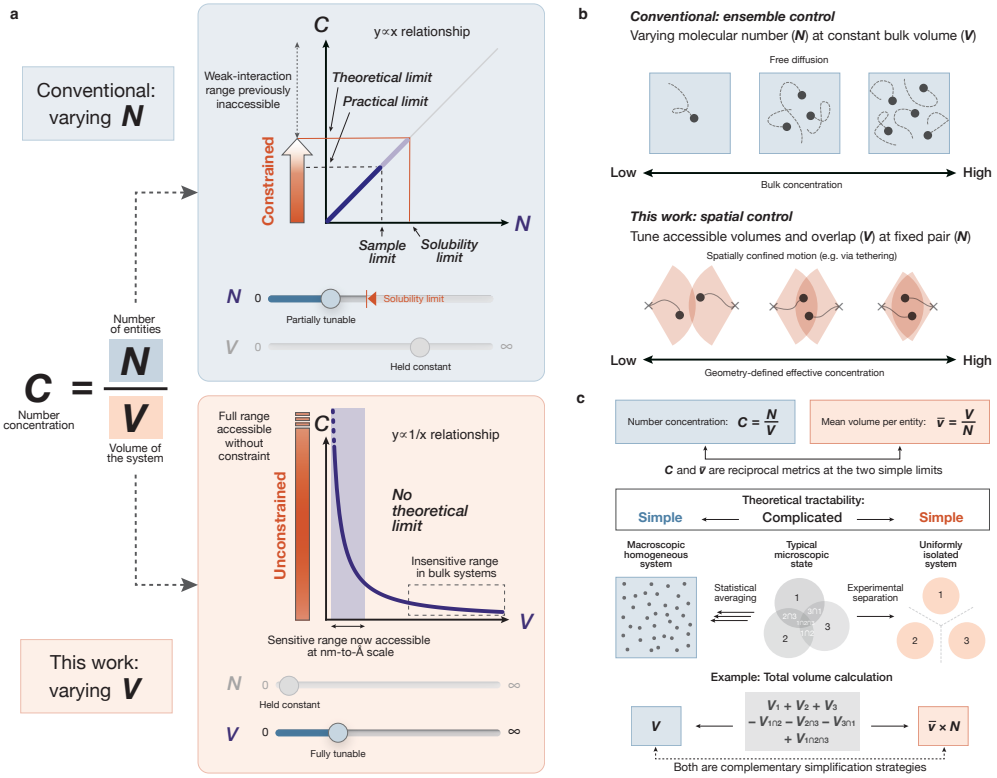


Fig. 2 The denominator side of concentration control has no theoretical ceiling. a, Conventional titration changes concentration (C) by varying the number of entities (N) at constant bulk volume (V). This titration gives the familiar $C \propto N$ relationship, but the accessible range is capped by sample availability and solubility, leaving weak-interaction regimes experimentally inaccessible. The volume-based route instead varies the denominator. Because $C \propto 1/V$, the ideal curve has no ceiling when interacting partners are confined together, and it approaches zero as they are fully separated. At macroscopic length scales this reciprocal curve is nearly insensitive to practical changes in V; nanoscale architectures make the sensitive nm-to-Å range experimentally accessible. **b**, Physical interpretation of the two perturbations. Conventional ensemble assays perturb a shared bulk system by adding molecules. In the present approach, a fixed molecular pair is perturbed by changing the overlap of the regions its partners can explore, for example by tethering each partner to a fixed anchor. Moving the same pair closer together or farther apart tunes a geometry-defined effective concentration, emulating a concentration titration and extending its range without increasing bulk abundance. **c**, Complementary simplification limits. Number concentration ($C = N/V$) is natural for macroscopic homogeneous systems, where statistical averaging simplifies many-particle behaviour. Mean volume per entity ($\bar{v} = V/N$) becomes natural at the opposite limit, where entities are experimentally isolated in addressable regions. Typical microscopic states lie between these limits, so overlapping volumes generate cross terms: three components already require seven terms. Thus, macroscopic pooling and spatial isolation are complementary simplification strategies; the full formal treatment is given in the companion paper[24].

bench: concentration-based control changes molecular number, whereas volume-based control changes the space available for interaction. We first clarify this distinction,

then implement it in DNA nanocavities and finally test it through three demonstrations. Controlled geometry shows that spatial arrangement can overturn solution-phase binding hierarchies; calibrated competition yields absolute K_d values deep in the millimolar regime; and a final screen identifies protein–protein-interaction modulators that enhance weak associations by reweighting local encounters rather than by high isolated affinity. These demonstrations move the volume-based paradigm from a theoretical coordinate change to a practical route for measuring and manipulating weak interactions beyond the reach of conventional methods.

A volume-centric theoretical framework

To deliver the intuitive account promised above, we begin with the elementary equilibrium $\mathrm{A} + \mathrm{B} \rightleftharpoons \mathrm{AB}$, leaving the full macro-to-micro derivation to the companion paper[24]. We write concentrations as number concentrations, $[X] = N_X/V_X$, so that Avogadro factors do not obscure the argument; lowercase symbols denote molar concentrations throughout. The usual molar K_d differs only by the constant unit conversion.

The key step is to view the concentration axis from its denominator side. Number concentration scales as N/V; read in reverse, this ratio points to V/N, a mean volume per molecule. In ordinary bulk solution, this quantity is only a notional partition, not the physical range explored by a freely diffusing molecule. Suppose, however, that the volume available to species X is divided into N_X compartments, one for each X molecule, each specified by a mean accessible volume $\overline{v}_X$, so that the partition satisfies $V_X = N_X \overline{v}_X$. Substituting this relation into the equilibrium expression gives the key cancellation, where molecule numbers drop out and only accessible volumes remain:

$$K_\mathrm{d} = \frac{[\mathrm{A}][\mathrm{B}]}{[\mathrm{AB}]} = \frac{\dfrac{N_A}{V_A}\cdot\dfrac{N_B}{V_B}}{\dfrac{N_{AB}}{V_{AB}}} \xrightarrow[V_X = N_X \cdot \overline{v}_X]{\text{mutual isolation}} \frac{\dfrac{\cancel{N_A}}{\cancel{N_A}\cdot \overline{v}_A}\cdot\dfrac{\cancel{N_B}}{\cancel{N_B}\cdot \overline{v}_B}}{\dfrac{\cancel{N_{AB}}}{\cancel{N_{AB}}\cdot \overline{v}_{AB}}} = \frac{\overline{v}_{AB}}{\overline{v}_A \cdot \overline{v}_B} \tag{1}$$

This visual cancellation is the essence of the V-paradigm. Under this construction, equilibrium is no longer governed by pooled molecule numbers; it closes instead on accessible volumes. Because ordinary bulk solution contains no such compartments, the construction remains hypothetical until nanoscale architecture imposes mutual isolation. At that point, V/N ceases to be a formal reciprocal and becomes an experimental variable.

Viewed from the denominator side, the formal concentration axis has no ceiling. Shrinking co-localized accessible regions towards a shared point drives the effective concentration upward without a formal bound; separating those regions completely drives it to zero. Thus, in the limiting case, $0 \leq c < \infty$ becomes accessible. Conventional macroscopic volume changes lie on the insensitive part of this reciprocal curve; nanoscale architectures move the experiment into its sensitive range, where linker length, cavity geometry and steric exclusion can tune accessible volume directly (Fig. 2a,b).

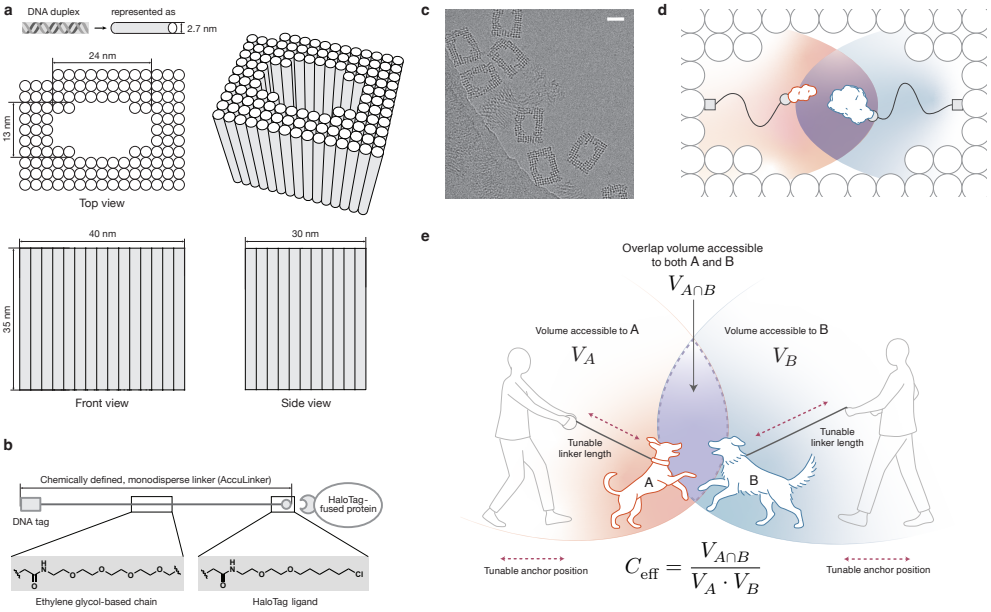


Fig. 3 DNA nanocavities define accessible volumes that convert pairwise geometry into molar effective concentration. a, DNA-nanocavity scaffold. DNA duplexes are represented as 2.7-nm cylinders, with orthogonal and perspective views showing the designed dimensions. **b**, Stepwise-synthesized, length-defined AccuLinker for tethering proteins to DNA tags. The ethylene glycol-based chain can be functionalized with different terminal ligands; the implementation shown uses a HaloTag ligand[25] to attach a HaloTag-fused protein. **c**, Representative cryo-EM image of assembled DNA nanocavities embedded in thin vitreous ice. Scale bar, 25 nm. **d**, Physical implementation. Two tethered partners explore partially overlapping regions inside a nanocavity connected to the surrounding solution. The red-shaded and blue-shaded regions denote the volumes accessible to each partner; the purple region denotes the shared region in which encounters can occur. **e**, Conceptual abstraction of panel d, drawn as two tethered animals exploring overlapping ranges. Linker length and anchor position set the volumes accessible to A and B, V_A and V_B, and their overlap, $V_{A\cap B}$. These volumes determine c_{eff}, a first-principles molar effective concentration that places local pair geometry on the same scale as flask molarity. In the idealized case shown, the number-based effective concentration is $C_{\text{eff}} = V_{A\cap B}/(V_A V_B)$, which holds when A and B are independent and uniformly distributed, and dividing by the Avogadro constant gives the molar value c_{eff}. The full framework extends this relation to non-uniform spatial distributions[24]. The analogy shows how encounter likelihood can be tuned by changing overlap rather than molecular number.

Experimental platform: linker-mediated volume control

To realize denominator-side control experimentally, we needed confinement that isolates one specified molecular pair from all other pairs without sealing that pair from solution. We therefore built through-hole DNA nanocavities in which steric walls separate one linker-tethered pair from neighbouring pairs, removing cross-pair terms from the population readout while maintaining continuity with the surrounding solution (Fig. 3a,d). We term this platform the Zonal Engineered Nano (ZEN) architecture. In

each ZEN box, anchor position and linker length specify the accessible range of each partner and the overlap between these ranges (Fig. 3d,e).

To obtain the design freedom needed to place anchors at defined internal coordinates, we constructed the nanocavities using DNA bricks[26, 27], a modular variant of DNA origami that provides sub-nanometre positioning precision and breadboard-like repositionability. The self-assembled cuboid contains an elliptical cylindrical through-hole, with single-stranded DNA overhangs at defined coordinates positioning tether anchors across a range of diagonal distances (Fig. 3a; Supplementary Figs. S1, S2 and S5). Cryo-EM and negative-stain TEM (nsTEM) confirmed the structural integrity of the assemblies (Fig. 3c; Supplementary Fig. S4). Gel electrophoresis indicated efficient assembly, with a maximum isolated-product yield of 48% (Supplementary Fig. S3).

In the ZEN architecture, accessible-volume control rests on length-defined linkers with modular end chemistry. We therefore synthesized AccuLinkers, ethylene glycol-based monodisperse linkers made by stepwise synthesis rather than polymerization, so that each design has a predetermined exploration radius (Fig. 3b; Supplementary Figs. S5, S6, S11, S12 and S13). The spacer can be functionalized with different terminal ligands; in the implementation used in this study, a HaloTag ligand[25] was installed to covalently attach HaloTag-fused proteins, while the opposite terminus carried ssDNA complementary to a specific sequence inside the cavity. Together with anchor position and cavity geometry, linker length sets each partner's accessible range, and the cavity walls restrict unintended encounters. Fluorescence monitoring showed that a 10-fold excess of protein–ssDNA conjugate drove cavity loading to a plateau within 2 h; after excess-conjugate removal, the material corresponded to the saturated attachment condition and exhibited the expected site-specific localization (Supplementary Figs. S7, S8, S9 and S10). Varying linker length and anchor position across ZEN populations therefore yields fraction-bound measurements that report overlap-dependent binding.

Spatial control reshapes binding preferences

Fig. 3d,e illustrates the central premise that only the shared accessible region contributes directly to molecular encounters. We therefore asked whether this overlap principle can predict partner choice in a three-component ZEN box. LgBiT is the large fragment of the NanoBiT split-luciferase system, SmBiT is the luminescent peptide partner that restores signal upon binding LgBiT, and DarkBiT is a non-luminescent SmBiT analogue that competes for the same LgBiT site[28, 29]; the HaloTag-fused variants used here are SmBiT114 and DarkBiT **1**. We implemented this system in seven ZEN designs, each containing one copy of each component in the same cavity volume; only linker length and anchor position were varied (Fig. 4a). A copy-number-per-cavity-volume view of local concentration would therefore assign all designs the same value. We estimated the regions accessible to each component by simple Monte Carlo sampling of tethered motion (Supplementary Fig. S14), then redrew the same overlap patterns as simplified schematics to show whether LgBiT overlaps more with

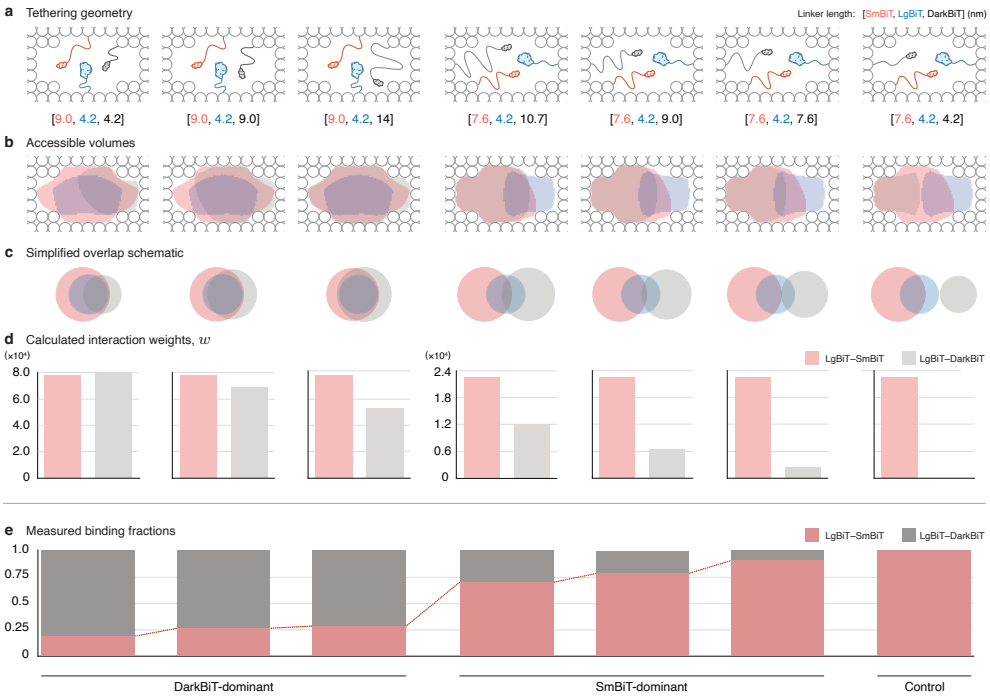


Fig. 4 Designed spatial overlap inverts the binding hierarchy in a single nanocavity. In Zonal Engineered Nano (ZEN) cavities, defined tethering geometries position LgBiT, the large luciferase fragment, and two peptide partners (all tethered through HaloTag fusions). SmBiT114 (labelled SmBiT) restores luciferase activity when bound to LgBiT; DarkBiT **1** (labelled DarkBiT) has higher solution-phase affinity for LgBiT but does not restore activity. Bold numerals denote compound names. Unbound LgBiT and LgBiT–DarkBiT **1** are dark, so luminescence reports the LgBiT–SmBiT binding fraction. **a**, Tethering geometries, specifying DNA-helix attachment positions and linker lengths in nm ([SmBiT, LgBiT, DarkBiT]). **b**, Accessible volumes calculated for each of the seven designs with a simple tethered-sphere Monte Carlo model. Red, blue and grey denote the regions explored by SmBiT, LgBiT and DarkBiT **1**, respectively. **c**, Simplified overlap schematics preserving the relative fractions from panel b while regularizing the shapes for visual comparison. Because SmBiT and DarkBiT **1** both compete for LgBiT, comparing the red–blue and grey–blue overlaps indicates which interaction is geometrically favoured. **d**, Calculated interaction weights, w, for LgBiT–SmBiT and LgBiT–DarkBiT **1**. These geometry-derived weights are the overlap terms underlying the c_{eff} construction in Fig. 3, with common constants omitted when comparing the two competitors. Geometry progressively favours SmBiT despite the stronger solution-phase affinity of DarkBiT **1**. **e**, Measured binding fractions for the same nanocavity designs. This experimental readout validates the calculation in panels b–d: the dominant partner switches from DarkBiT **1** to SmBiT in the order predicted by the calculated weights. In the control design, DarkBiT **1** is tethered but cannot reach LgBiT. Predictive agreement of the w-based model across tethering geometries is reported in the companion analysis (Pearson $r = 0.994$, RMSE = 1.09-fold)[24].

SmBiT or DarkBiT **1** (Fig. 4b,c). For the two possible LgBiT complexes, LgBiT–SmBiT and LgBiT–DarkBiT **1**, we calculated an interaction weight, w, a pair-specific overlap measure that provides the geometric basis for c_{eff}. In the uniform-independent

limit, $w_{XY} \propto V_{X\cap Y}/(V_X V_Y)$, with the general probability-distribution form given in the companion framework[24] (Fig. 4d).

The same geometries were then read out with a three-component NanoBiT competition assay to test whether designed overlap can override the solution-phase binding hierarchy. DarkBiT **1** binds LgBiT more strongly in solution ($K_d \approx 10$ μM; Supplementary Fig. S15) than SmBiT114 ($K_d \approx 0.3$ mM; Fig. 5b)[28, 29]. Because linker length and anchor position are programmable variables, the balance of w can in principle be tuned continuously; the seven designs sampled this range, from configurations favouring LgBiT–DarkBiT **1** to those favouring LgBiT–SmBiT (Fig. 4a–d). Despite this tens-of-fold affinity advantage in solution, the measured binding fractions followed the geometry-derived order, with the favoured partner switching from DarkBiT **1** to SmBiT across the same designs (Fig. 4e). The w-based predictions matched the measured fractions with Pearson $r > 0.99$ in the companion analysis, supporting w as a quantitative readout of designed overlap[24].

These results show that nanostructured space can make geometry the primary control axis for binding preference. That axis is invisible in a copy-number-per-volume view of concentration. The same set of components can form different local complexes when linker-defined accessible regions are rearranged; in some geometries, this spatial arrangement is sufficient to invert the solution-phase K_d hierarchy. Pairwise K_d values still define intrinsic affinities, but local preference follows the geometry-defined encounter landscape. Quantitatively, the hierarchy switch is captured by w, or by c_{eff} in molar units, consistent with the high prediction–measurement correlation across geometries. Programmable geometry thereby becomes the operational control axis of the V-paradigm: an experimentally set variable, analogous to concentration in conventional assays, whose effect is quantified by w.

Detection of millimolar-affinity interactions

Geometry-controlled hierarchy inversion reveals a practical strength of the V-paradigm: competition balance is no longer set by solution K_d alone, because accessible-volume geometry provides a second, programmable axis. We used this axis in an open titration format. For each design, one SmBiT variant and LgBiT were tethered in the same ZEN geometry, setting the local encounter balance for the luminescent pair, while DarkBiT **2**, the free DarkBiT peptide, was added from bulk as a competitor for the same LgBiT site (Fig. 5a–c). An otherwise ultra-weak tethered interaction thereby becomes a standard-format inhibition assay: ZEN samples are aliquoted into a microtitre plate, mixed with a DarkBiT **2** concentration series and read by luminescence on a standard plate reader. We applied this strategy to a community-validated NanoBiT toolkit of six SmBiT variants, chosen because it spans orders of magnitude in reported affinity and includes SmBiT230, the weakest member, for which no conventional K_d has been assigned[28, 29].

The resulting inhibition curves retained quantitative affinity information across the SmBiT series. Bayesian fitting of the companion response model without literature anchors recovered a strong log-linear relation to the reported affinities, showing that the competition responses alone support K_d inference (Fig. 5a)[24]. The estimates

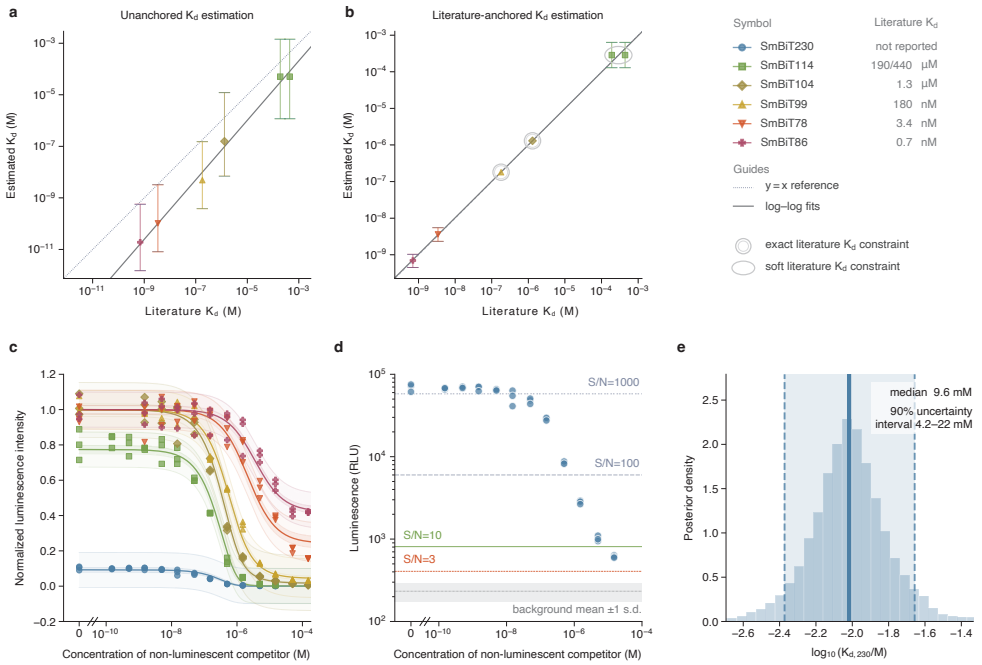


Fig. 5 The volume-based (V) paradigm and the ZEN system extend K_{d} measurements to ultra-weak interactions. SmBiT variants and LgBiT shared a ZEN geometry that fixed accessible volume; DarkBiT **2** (the free DarkBiT) was titrated from bulk, and luminescence reported SmBiT-bound LgBiT. **a**, Unanchored Bayesian fitting. For variants with literature affinities, unanchored K_{d} estimates are plotted against literature values. The tight log-linear relation shows that the fit carries an internal absolute-affinity scale, tracking published values across five orders of magnitude. **b**, Literature-anchored calibration. SmBiT99 and SmBiT104 were fixed at literature K_{d} values (grey halos, no error bars); SmBiT114 was constrained loosely by its two reported values. Other estimates fall on the calibrated line with narrow uncertainty intervals, showing that this approach can predict K_{d} values with high confidence across the series. In **a,b**, dotted lines, $y = x$; grey lines, log–log fits; points/error bars, median estimates/90% uncertainty intervals; duplicate x positions, two literature values. **c**, Normalized DarkBiT **2** titrations and anchored fits. Luminescence was normalized to matched intact-luciferase activity and to the fitted response scale, removing reporter-brightness differences while retaining reconstitution differences. Symbols, replicates ($n = 3$ per point); curves, median fits; dark bands, 95% fitted-response uncertainty intervals; pale bands, 95% prediction intervals. Low-affinity curves start below full signal and retain high-dose luminescence; both features follow quantitatively from the chemistry–geometry crossover and finite local capacity[24]. **d**, Raw SmBiT230 luminescence in relative light units (RLU), plotted logarithmically without fits to show signal-to-noise (S/N) headroom. The competitor-free plateau reaches S/N $= 10^3$. Grey band, background ±1 s.d.; guides, background plus a multiple of s.d.; S/N = 3 and 10, detection and quantification guides[30]. Extrapolating the same readout places S/N = 10 near $K_{\mathrm{d}} \sim 1$ M. **e**, Inferred distribution of $\log_{10}(K_{\mathrm{d,230}}/\mathrm{M})$ under the anchored model. Median $K_{\mathrm{d,230}} = 9.6$ mM; 90% uncertainty interval, 4.2–22 mM. Literature values are from NanoBiT characterization[28]; none has been reported for SmBiT230. Fitting used the companion finite-capacity distribution-averaged inhibition model in its closed-form hypergeometric ($_2F_1$) expression[24].

showed a modest but consistent offset from published K_d values; because its origin remains unresolved, we treated it as a scale difference and used literature anchors only to report values on the published K_d scale. Anchoring changed the scale but not the SmBiT230/SmBiT114 ratio, which shifted by 0.15%: the anchors set the scale, not the relative affinities. We then repeated the fitting with SmBiT99 and SmBiT104 fixed as anchors in the micromolar-to-submicromolar regime, where standard concentration-based assays are most reliable (Fig. 5b). SmBiT114 lies just beyond that regime and its two reported values disagree, so we used them only as a loose constraint. In this anchored fit, SmBiT86 and SmBiT78, whose reported values were withheld, fell close to the $y = x$ line with narrow uncertainty intervals, and the SmBiT114 estimate settled between its two reported values, demonstrating accurate K_d prediction across the panel.

With the literature-anchored model, SmBiT230 yielded a median K_d of 9.6 mM (Fig. 5e). This value lies far beyond the conventional limit for protein–peptide affinity measurement highlighted in Fig. 1, an intrinsic ceiling of the N-paradigm. With one ZEN setup, defined by fixed cavity size, linker lengths and anchor positions, together with the same soluble DarkBiT **2** titration format, the assay covered more than seven orders of magnitude in assigned affinity, from picomolar to millimolar. Part of this range enters the chemistry–geometry crossover regime described in the companion paper, where local geometry can dominate apparent inhibition so strongly that a $\sim 10^4$-fold difference in solution K_d shifts the inhibition midpoint by only $\sim 1\%$[24]. Geometry thereby supplies the matching parameter that conventional bulk competition lacks, allowing interactions separated by orders of magnitude in solution to be evaluated in one measurable local-competition window.

The accessible K_d range still has headroom beyond 10 mM. SmBiT230 produced luminescence at S/N $\sim 10^3$ on a conventional, legacy-generation plate reader from 25 fmol of tethered material per well, totalling under 1 pmol for a complete titration (Fig. 5d). With the same cavity design and sample loading, the fitted response model and measured background noise project a readout above the S/N = 10 guide out to $K_d \sim 1$ M (Fig. 5d). The cavity size, linker lengths and anchor positions used here were chosen to cover a broad picomolar-to-millimolar panel, not to maximize sensitivity at the weakest-binding end. Further headroom could therefore come from higher sample loading, more sensitive detection hardware or ZEN designs tuned for weak binding.

Geometry-guided screening for PPI modulators

The ZEN platform enables a screening mode inaccessible to affinity-based bulk assays: selecting protein–protein-interaction (PPI) modulators by how they reshape local encounters. Affinity-ranked screens are poorly matched to this class of modulators because the primary readout of such screens is how tightly a compound binds, not how it changes the local encounter balance between weak partners[32–38]. The ZEN assay makes that encounter balance the readout by measuring occupancy within a local response landscape jointly set by binding chemistry, K_d, and encounter geometry, w[24]. Candidate compounds can therefore be selected by their ability to shift

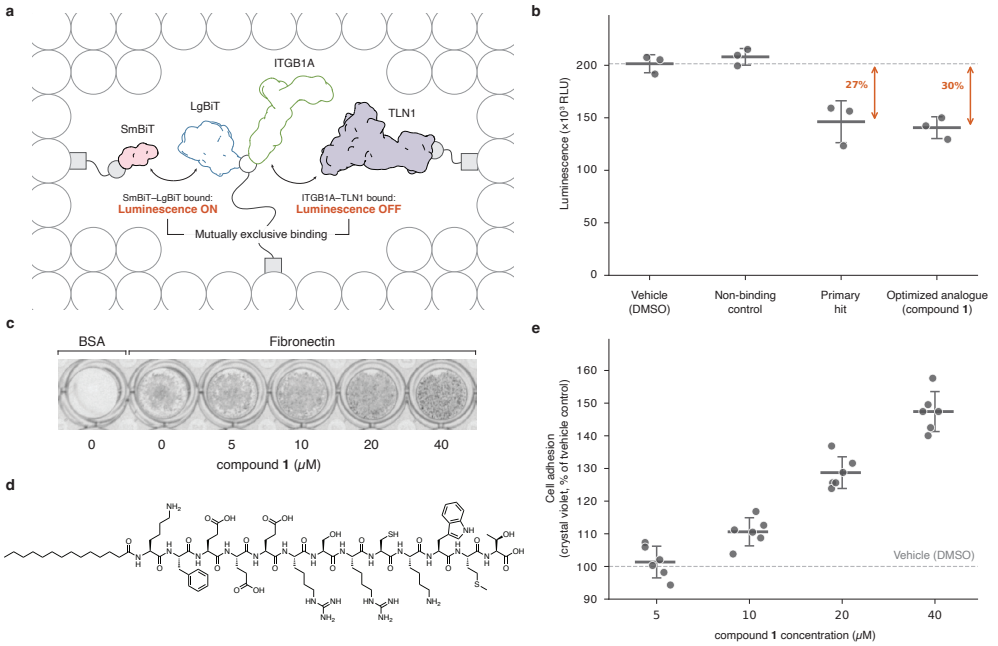


Fig. 6 The ZEN assay makes reporter and target binding mutually exclusive, enabling modulator screening through shifts in local encounters. a, Reporter architecture for the weak interaction between the integrin β1A cytoplasmic tail (ITGB1A) and the talin-1 (TLN1) FERM domain (NMR $K_d = 491 \pm 10$ μM for the talin-1 F3 subdomain[31]). SmBiT–LgBiT binding forms the luminescence-ON reporter state, whereas ITGB1A–TLN1 binding forms a competing luminescence-OFF target state within the same engineered encounter volume. Compounds that shift local occupancy towards ITGB1A–TLN1 engagement therefore reduce reporter luminescence[24]. **b**, Screening readout for a focused peptide library based on the integrin β cytoplasmic tail. Vehicle and a non-binding control maintained luminescence, whereas a primary hit and its optimized analogue, compound **1**, reduced the signal by 27% and 30% at 40 μM, respectively, indicating shifts towards target-state occupancy. Points show replicate wells ($n = 3$); bars, mean ± s.d.; dashed line, vehicle mean. Luminescence is reported in relative light units (RLU). **c**, Enlarged images of crystal-violet-stained wells containing U87MG cells on bovine serum albumin (BSA)- or fibronectin-coated surfaces at the indicated compound **1** concentrations; BSA-coated wells showed minimal staining. **d**, Chemical structure of compound **1**. **e**, Adhesion assay after 5 days. Compound **1** dose-dependently increased blank-subtracted crystal-violet absorbance (A_{595}) to 147±6% of the vehicle control at 40 μM, whereas parallel CellTiter-Glo 3D ATP signals showed no corresponding increase (Supplementary Fig. S19), linking the ZEN screening signal to an adhesion phenotype consistent with enhanced integrin–talin engagement. Points show replicate wells ($n = 6$); bars, mean ± s.d.; dashed line, vehicle mean.

occupancy even when isolated binding is weak or not detectable under standard assay conditions, without requiring a stable ternary-complex readout.

To implement this screen, we configured a mutually exclusive ZEN assay around the interaction between the integrin β1A cytoplasmic tail (ITGB1A) and the talin-1 (TLN1) FERM domain[39], a weak pair with an NMR K_d of 491 ± 10 μM for the talin-1 F3 subdomain (Supplementary Fig. S17)[31]. SmBiT–LgBiT binding formed the luminescent reporter state, whereas ITGB1A–TLN1 binding formed a competing target-PPI state that reduced reporter occupancy and decreased luminescence

(Fig. 6a). A compound that shifts local occupancy towards ITGB1A–TLN1 engagement should therefore reduce the reporter signal. In a peptide-library screen, vehicle treatment and a non-binding control preserved luminescence, whereas a primary hit reduced the signal by 27%. Optimization yielded compound **1**, which reduced the signal by 30% under the same fixed-copy-number and fixed-geometry conditions (Fig. 6b,d). Compound **1** did not show detectable isolated binding by surface plasmon resonance under the tested conditions. As established in the preceding section with the SmBiT affinity series, the reporter pair can be varied independently to tune the assay threshold from sensitive discovery to selective refinement (Supplementary Fig. S18).

Outside the ZEN readout, compound **1** increased fibronectin-dependent cell adhesion in a dose-dependent manner, reaching approximately 150% of the vehicle control at 40 μM, whereas the bovine serum albumin (BSA) control surface showed minimal adhesion (Fig. 6c,e). The cellular response, observed without a detectable proliferation change, is consistent with enhanced integrin–talin engagement[39]. This proof of concept establishes spatial control as a systematic strategy for PPI-modulator discovery, offering a path beyond affinity-ranked or stable-ternary-complex screens towards geometry-aware design of modulators for weak protein–protein interactions.

Summary and outlook

Control of molecular interactions is no longer confined to molecular number: molecular space provides an independent experimental axis. By exploiting the denominator V in N/V, the V-paradigm circumvents the practical concentration ceiling of the conventional N-paradigm. Along this spatial axis, the ZEN architecture inverted a solution-phase binding hierarchy, quantified a K_d of order 10 mM from sub-picomole samples at S/N $\sim 10^3$ and guided the selection of a PPI modulator.

Beyond these experimental gains, the results expose a deeper risk in the routine interpretation of molecular interactions: concentration-based frameworks can mislead when carried unchanged from homogeneous bulk systems into heterogeneous microscopic ones[40]. Equation 1 offers one example. If correct as written, it would make the constant K_d vary with accessible volume. The displayed form is schematic for clarity; strictly, its right-hand side also carries a factor describing the balance between unbound and bound states. In bulk, this balance is folded into the concentration ratio; when local states are resolved, it must remain explicit (Supplementary Section 18). As accessible volume changes, the occupancy balance adjusts so that intrinsic K_d remains constant; volume therefore controls occupancy, not affinity. An interaction classified as weak in bulk can thus become functionally strong within its nanoscale niche. This apparent paradox marks both the danger of unmodified bulk extrapolation and the opening of a spatial control axis. The bulk concentration form is a well-mixed limit; at the opposite single-pair limit realized by the ZEN architecture, a Michaelis–Menten form re-emerges[24].

This spatial control is especially powerful at the nanoscale. At macroscopic scales, practical changes in V fall within the shallow region of the $1/V$ relation; at the nanoscale, small perturbations in geometry or accessible range can produce disproportionately large shifts in encounter probability and occupancy (Fig. 2a). Reshaping a

local environment can require less energy than changing molecular abundance, suggesting that biology may exploit spatial control as an energy-efficient strategy for tuning local equilibria. This view calls for a quantitative reinterpretation of familiar proximity effects: at the nanoscale, local geometry and accessible range can become more influential than intrinsic binding chemistry, as demonstrated by the chemistry–geometry crossover[24, 41–44].

The V-paradigm is not merely a second control axis; it offers a far larger parameter space than the abundance-based N-paradigm. The N-paradigm provides one concentration variable per species, whereas the V-paradigm can encode accessible volumes and pairwise or higher-order overlaps (for X species, X versus up to $2^X - 1$). Even a two-component system gains a third spatial parameter: the overlap of the two components' accessible regions. Placement can therefore generate many local states from the same molecular set, whereas bulk mixing compresses them into a few averages. From this parameter-count perspective, it is unsurprising that simply mixing the right components can fail to reproduce cellular behaviour[45–47].

The ZEN architecture provides a minimal experimental implementation of this expanded space. Its modular design can position additional components, vary cavity geometry and accommodate diverse analytical readouts; the plate-reader assay used here is only one example. Because each implementation retains the same spatial variables, data from functional assays and microscopic observations can be integrated directly with theory and simulation, supporting analyses of interaction networks and regulatory principles across molecular and cellular scales[24]. This modularity enables complex molecular logic to be reconstituted in simplified, controllable models. A few components, precisely placed and balanced, can encode an interaction landscape far richer than their number alone suggests.

References

[1] Sharifi Tabar, M. *et al.* Illuminating the dark protein-protein interactome. *Cell Reports Methods* **2**, 100275 (2022). URL https://www.sciencedirect.com/science/article/pii/S2667237522001527.

[2] Perkins, J. R., Diboun, I., Dessailly, B. H., Lees, J. G. & Orengo, C. Transient protein-protein interactions: Structural, functional, and network properties. *Structure* **18**, 1233–1243 (2010). URL https://www.sciencedirect.com/science/article/pii/S0969212610003035.

[3] Luck, K. *et al.* A reference map of the human binary protein interactome. *Nature* **580**, 402–408 (2020). URL https://doi.org/10.1038/s41586-020-2188-x.

[4] Qin, J. & Gronenborn, A. M. Weak protein complexes: challenging to study but essential for life. *The FEBS Journal* **281**, 1948–1949 (2014). URL https://febs.onlinelibrary.wiley.com/doi/abs/10.1111/febs.12744.

[5] Li, P. *et al.* Phase transitions in the assembly of multivalent signalling proteins. *Nature* **483**, 336–340 (2012). URL https://doi.org/10.1038/nature10879.

[6] Banani, S. F. *et al.* Compositional control of phase-separated cellular bodies. *Cell* **166**, 651–663 (2016). URL https://doi.org/10.1016/j.cell.2016.06.010.

[7] Banani, S. F., Lee, H. O., Hyman, A. A. & Rosen, M. K. Biomolecular condensates: organizers of cellular biochemistry. *Nature Reviews Molecular Cell Biology* **18**, 285–298 (2017). URL https://doi.org/10.1038/nrm.2017.7.

[8] Vaynberg, J. *et al.* Structure of an ultraweak protein-protein complex and its crucial role in regulation of cell morphology and motility. *Molecular Cell* **17**, 513–523 (2005). URL https://doi.org/10.1016/j.molcel.2004.12.031.

[9] Sweetlove, L. J. & Fernie, A. R. The role of dynamic enzyme assemblies and substrate channelling in metabolic regulation. *Nature Communications* **9**, 2136 (2018). URL https://doi.org/10.1038/s41467-018-04543-8.

[10] Pareek, V., Sha, Z., He, J., Wingreen, N. S. & Benkovic, S. J. Metabolic channeling: predictions, deductions, and evidence. *Molecular Cell* **81**, 3775–3785 (2021). URL https://doi.org/10.1016/j.molcel.2021.08.030.

[11] Laursen, T. *et al.* Characterization of a dynamic metabolon producing the defense compound dhurrin in sorghum. *Science* **354**, 890–893 (2016). URL https://www.science.org/doi/abs/10.1126/science.aag2347.

[12] Nakayama, T., Takahashi, S. & Waki, T. Formation of flavonoid metabolons: Functional significance of protein-protein interactions and impact on flavonoid chemodiversity. *Frontiers in Plant Science* **10** (2019). URL https://www.frontiersin.org/journals/plant-science/articles/10.3389/fpls.2019.00821.

[13] Zhang, Y. & Fernie, A. R. Metabolons, enzyme–enzyme assemblies that mediate substrate channeling, and their roles in plant metabolism. *Plant Communications* **2** (2021). URL https://doi.org/10.1016/j.xplc.2020.100081.

[14] Csizmok, V., Follis, A. V., Kriwacki, R. W. & Forman-Kay, J. D. Dynamic protein interaction networks and new structural paradigms in signaling. *Chemical Reviews* **116**, 6424–6462 (2016). URL https://doi.org/10.1021/acs.chemrev.5b00548.

[15] Dueber, J. E., Yeh, B. J., Bhattacharyya, R. P. & Lim, W. A. Rewiring cell signaling: the logic and plasticity of eukaryotic protein circuitry. *Current Opinion in Structural Biology* **14**, 690–699 (2004). URL https://www.sciencedirect.com/science/article/pii/S0959440X04001800.

[16] Chien, P. & Gierasch, L. M. Challenges and dreams: physics of weak interactions essential to life. *Mol. Biol. Cell* **25**, 3474–3477 (2014). URL https://doi.org/10.1091/mbc.e14-06-1035.

[17] McPherson, A. & Gavira, J. A. Introduction to protein crystallization. *Acta Crystallographica Section F: Structural Biology Communications* **70**, 2–20 (2014). URL https://doi.org/10.1107/S2053230X13033141.

[18] McPherson, A. & Cudney, B. Optimization of crystallization conditions for biological macromolecules. *Acta Crystallographica Section F: Structural Biology Communications* **70**, 1445–1467 (2014). URL https://doi.org/10.1107/S2053230X14019670.

[19] Cagney, G., Amiri, S., Premawaradena, T., Lindo, M. & Emili, A. In silico proteome analysis to facilitate proteomics experiments using mass spectrometry. *Proteome Science* **1**, 5 (2003). URL https://doi.org/10.1186/1477-5956-1-5.

[20] Liu, H. *et al.* PPB-Affinity: Protein-protein binding affinity dataset for AI-based protein drug discovery. *Scientific Data* **11**, 1316 (2024). URL https://doi.org/10.1038/s41597-024-03997-4.

[21] Oehler, S. & Müller-Hill, B. High local concentration: A fundamental strategy of life. *Journal of Molecular Biology* **395**, 242–253 (2010). URL https://www.sciencedirect.com/science/article/pii/S0022283609013151.

[22] Scott, J. D. & Pawson, T. Cell signaling in space and time: Where proteins come together and when they're apart. *Science* **326**, 1220–1224 (2009). URL https://www.science.org/doi/abs/10.1126/science.1175668.

[23] Good, M. C., Zalatan, J. G. & Lim, W. A. Scaffold proteins: Hubs for controlling the flow of cellular information. *Science* **332**, 680–686 (2011). URL https://www.science.org/doi/abs/10.1126/science.1198701.

[24] Matsuda, F., Yoshimura, M., Ikeda, S. & Fujita, D. Experimental access to molarity's blind spot in macroscopic assays (2026). Companion paper, submitted to arXiv simultaneously with the present work; arXiv identifier to be added in version 2.

[25] Los, G. V. *et al.* HaloTag: A novel protein labeling technology for cell imaging and protein analysis. *ACS Chemical Biology* **3**, 373–382 (2008). URL https://doi.org/10.1021/cb800025k.

[26] Ong, L. L. *et al.* Programmable self-assembly of three-dimensional nanostructures from 10,000 unique components. *Nature* **552**, 72–77 (2017). URL https://doi.org/10.1038/nature24648.

[27] Ke, Y., Ong, L. L., Shih, W. M. & Yin, P. Three-dimensional structures self-assembled from DNA bricks. *Science* **338**, 1177–1183 (2012). URL https://www.science.org/doi/abs/10.1126/science.1227268.

[28] Dixon, A. S. *et al.* NanoLuc complementation reporter optimized for accurate measurement of protein interactions in cells. *ACS Chemical Biology* **11**, 400–408 (2016). URL https://doi.org/10.1021/acschembio.5b00753.

[29] Gräwe, A. & Merkx, M. Bioluminescence goes dark: Boosting the performance of bioluminescent sensor proteins using complementation inhibitors. *ACS Sensors* **7**, 3800–3808 (2022). URL https://doi.org/10.1021/acssensors.2c01726.

[30] International Council for Harmonisation of Technical Requirements for Pharmaceuticals for Human Use. ICH harmonised guideline: Validation of analytical procedures, Q2(R2). ICH Harmonised Guideline (2023). URL https://database.ich.org/sites/default/files/ICH_Q2(R2)_Guideline_2023_1130.pdf. Final version adopted on 1 November 2023; error correction issued on 30 November 2023.

[31] Anthis, N. J., Wegener, K. L., Critchley, D. R. & Campbell, I. D. Structural diversity in integrin/talin interactions. *Structure* **18**, 1654–1666 (2010). URL https://doi.org/10.1016/j.str.2010.09.018.

[32] Faust, T. B. *et al.* Structural complementarity facilitates E7820-mediated degradation of RBM39 by DCAF15. *Nature Chemical Biology* **16**, 7–14 (2020). URL https://doi.org/10.1038/s41589-019-0378-3.

[33] Würtele, M., Jelich-Ottmann, C., Wittinghofer, A. & Oecking, C. Structural view of a fungal toxin acting on a 14-3-3 regulatory complex. *The EMBO Journal* **22**, 987–994 (2003). URL https://doi.org/10.1093/emboj/cdg104.

[34] Tsai, J. C. *et al.* Structure of the nucleotide exchange factor eIF2B reveals mechanism of memory-enhancing molecule. *Science* **359**, eaaq0939 (2018). URL https://www.science.org/doi/abs/10.1126/science.aaq0939.

[35] Bulawa, C. E. *et al.* Tafamidis, a potent and selective transthyretin kinetic stabilizer that inhibits the amyloid cascade. *Proceedings of the National Academy of Sciences* **109**, 9629–9634 (2012). URL https://www.pnas.org/doi/abs/10.1073/pnas.1121005109.

[36] Słabicki, M. *et al.* Small-molecule-induced polymerization triggers degradation of BCL6. *Nature* **588**, 164–168 (2020). URL https://doi.org/10.1038/s41586-020-2925-1.

[37] Konstantinidou, M. & Arkin, M. R. Molecular glues for protein-protein interactions: Progressing toward a new dream. *Cell Chemical Biology* **31**, 1064–1088 (2024). URL https://doi.org/10.1016/j.chembiol.2024.04.002.

[38] Nada, H. *et al.* New insights into protein–protein interaction modulators in drug discovery and therapeutic advance. *Signal Transduction and Targeted Therapy* **9**, 341 (2024). URL https://doi.org/10.1038/s41392-024-02036-3.

[39] Sun, Z., Costell, M. & Fässler, R. Integrin activation by talin, kindlin and mechanical forces. *Nature Cell Biology* **21**, 25–31 (2019). URL https://doi.org/10.1038/s41556-018-0234-9.

[40] Speer, S. L. *et al.* The intracellular environment affects protein–protein interactions. *Proceedings of the National Academy of Sciences* **118**, e2019918118 (2021). URL https://www.pnas.org/doi/abs/10.1073/pnas.2019918118.

[41] Speltz, E. B. & Zalatan, J. G. The relationship between effective molarity and affinity governs rate enhancements in tethered kinase–substrate reactions. *Biochemistry* **59**, 2182–2193 (2020). URL https://doi.org/10.1021/acs.biochem.0c00205.

[42] Shaw, A. *et al.* Binding to nanopatterned antigens is dominated by the spatial tolerance of antibodies. *Nature Nanotechnology* **14**, 184–190 (2019). URL https://doi.org/10.1038/s41565-018-0336-3.

[43] Rosier, B. J. H. M. *et al.* Proximity-induced caspase-9 activation on a DNA origami-based synthetic apoptosome. *Nature Catalysis* **3**, 295–306 (2020). URL https://doi.org/10.1038/s41929-019-0403-7.

[44] Mugler, A., Tostevin, F. & ten Wolde, P. R. Spatial partitioning improves the reliability of biochemical signaling. *Proceedings of the National Academy of Sciences* **110**, 5927–5932 (2013). URL https://www.pnas.org/doi/abs/10.1073/pnas.1218301110.

[45] Cohen, R. D. & Pielak, G. J. A cell is more than the sum of its (dilute) parts: A brief history of quinary structure. *Protein Science* **26**, 403–413 (2017). URL https://onlinelibrary.wiley.com/doi/abs/10.1002/pro.3092.

[46] Vahey, M. D. & Fletcher, D. A. The biology of boundary conditions: cellular reconstitution in one, two, and three dimensions. *Current Opinion in Cell Biology* **26**, 60–68 (2014). URL https://www.sciencedirect.com/science/article/pii/S0955067413001543.

[47] Ganesh, R. B. & Maerkl, S. J. Towards self-regeneration: Exploring the limits of protein synthesis in the protein synthesis using recombinant elements (PURE) cell-free transcription–translation system. *ACS Synthetic Biology* **13**, 2555–2566 (2024). URL https://doi.org/10.1021/acssynbio.4c00304.

[48] Gruskos, J. J., Zhang, G. & Buccella, D. Visualizing compartmentalized cellular Mg^{2+} on demand with small-molecule fluorescent sensors. *Journal of the American Chemical Society* **138**, 14639–14649 (2016). URL https://doi.org/10.1021/jacs.6b07927.

[49] Strausberg, R. L. *et al.* Generation and initial analysis of more than 15,000 full-length human and mouse cDNA sequences. *Proceedings of the National Academy*

of Sciences of the United States of America **99**, 16899–16903 (2002). URL https://doi.org/10.1073/pnas.242603899.

[50] Shen, B. *et al.* A directional switch of integrin signalling and a new anti-thrombotic strategy. *Nature* **503**, 131–135 (2013). URL https://doi.org/10.1038/nature12613.

[51] Shattil, S. J., Kim, C. & Ginsberg, M. H. The final steps of integrin activation: the end game. *Nature Reviews Molecular Cell Biology* **11**, 288–300 (2010). URL https://doi.org/10.1038/nrm2871.

Acknowledgements The authors thank the iCeMS Analysis Center at Kyoto University for access to the ICP-AES facilities and technical support with sample identification. This work was supported by JSPS KAKENHI (grant No. JP23K26777 to D. F. and grant No. JP23H02776 to Y. I.), AMED (grant No. 22am0401020h0004 to D. F.), JST ACT-X (grant No. JPMJAX20BK to M. Y.), JST FOREST (grant No. JPMJFR203R to D. F. and grant No. JPMJFR220E to M. Y.), JST-Mirai (grant No. JPMJMI22H5), JKA (KEIRIN RACE promotion funds), the Inamori Foundation (InaRIS Fellowship) and the Asian Young Scientist Fellowship.

Author contributions M. Y. designed and performed the chemical synthesis and ZEN binding-affinity experiments. Y. I. designed and performed the modulator screening and cell-adhesion assays. F. M. and D. F. established the theoretical framework and conducted the analysis. M. Y. and D. F. designed the DNA nanostructure, and M. Y. assembled it. C. M., T. Y., M. K., R. M. and Y. N. prepared recombinant proteins. M. Y. and C. N. performed the protein conjugation with AccuLinkers. Y. S. and M. Y. performed cryo-EM analysis. M. T. and M. Y. conducted nsTEM analysis. M. Y., F. M. and D. F. wrote the manuscript. M. Y., Y. I. and D. F. acquired funding. D. F. conceived and supervised the project. All authors critically read and approved the manuscript.

Competing interests The authors declare the following competing interests: Kyoto University is the applicant for a pending international patent application published as WO 2025/079662 A1, covering structures and methods for positioning biomolecules and analysing their interactions as implemented in the ZEN platform described in this work; D. F., M. Y., F. M. and Y. I. are named inventors. D. F. and Y. I. are co-founders of SeedFairing Institute, a Japanese non-profit general incorporated association established to facilitate dissemination of this technology. The remaining authors declare no competing interests.

Data availability The data supporting the findings of this study are available within the paper and its Supplementary Information. Source data underlying the main and Supplementary figures are available from the corresponding author upon reasonable request. The authors plan to make reagents and technical support related to the ZEN platform available through SeedFairing Institute upon reasonable request.

Code availability Code for the Bayesian K_d inference from the ZEN titration assay with DarkBiT **2** (Fig. 5) is available at https://github.com/FujitaG/zen-kd-estimation, and code for the tethered-sphere Monte Carlo overlap calculator (Fig. 4b) at https://

	github.com/FujitaG/zen-spatial-overlap. Both are archived at Zenodo (https://doi.org/10.5281/zenodo.21777953 and https://doi.org/10.5281/zenodo.21777964, respectively). The response-model implementation used by the inference is distributed with the companion paper[24].
Use of large language models	Large language models (Claude, Anthropic; GPT, OpenAI) were used to edit the manuscript text for clarity and concision, and to assist in writing the analysis code listed above.
Correspondence	Correspondence and requests for materials should be addressed to Daishi Fujita (dfujita@icems.kyoto-u.ac.jp).

Supplementary Information

Throughout, bold numerals and letters denote compound names, so DarkBiT **1**, compound **1** and compound **A** are different molecules; the bold numerals in Supplementary Table 9 number the DNA strands. Numerals set close to a name identify sequence variants (for example SmBiT114).

1 Chemicals and reagents

All chemical reagents were purchased from BroadPharm, Tokyo Chemical Industry Co., Ltd. (TCI), Sigma-Aldrich and BLDpharm at the highest commercially available quality, and used without further purification. Synthetic peptides were purchased from Biologica with >95% purity. Synthetic oligonucleotides for DNA bricks were purchased from Eurofins Genomics as oligonucleotide purification cartridge (OPC)-purified grade. Azide- and/or fluorescent-dye-modified oligonucleotides were purchased from Integrated DNA Technologies, Inc. as high-performance liquid chromatography (HPLC)-purified grade. For cell-based assays, human plasma fibronectin (Fibronectin Neosilk, catalogue no. 54071) was purchased from Immuno-Biological Laboratories Co., Ltd. (IBL). High-glucose Dulbecco's modified Eagle's medium (DMEM; catalogue no. 11965118), penicillin/streptomycin (catalogue no. 15140122) and non-treated 96-well Nunc plates (catalogue no. 2674427) were purchased from Thermo Fisher Scientific. Fetal bovine serum (FBS; catalogue no. FB-1003/500; batch no. S00KK; identification no. S00KK10002) was purchased from Biosera. The Nano-Glo Luciferase Assay System (catalogue no. N1110; 10 mL) and the CellTiter-Glo 3D Cell Viability Assay (catalogue no. G9681) were purchased from Promega, and crystal violet (catalogue no. C0428) was purchased from TCI.

2 General chemical reaction

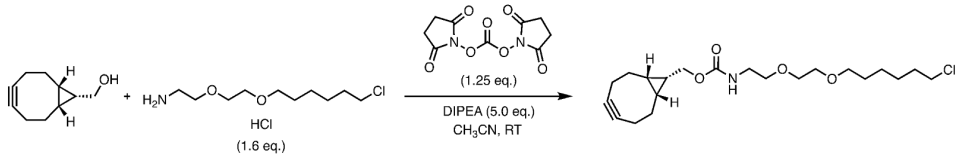
All reactions were carried out under an argon atmosphere with dry solvents unless otherwise noted. Chromatographic purifications were performed on a Teledyne ISCO CombiFlash Rf 200i equipped with standard silica columns (SepaFlash SilicaFlash Cartridge UltraPure irregular Silica Gel, 40–63 µm, 60 Å from Santai Technologies). Thin-layer chromatography (TLC) was performed on precoated silica-gel 60 TLC glass plates with fluorescence indicator UV_{254}. The TLC plates were stained with iodine. ^{1}H and ^{13}C nuclear magnetic resonance (NMR) spectra were recorded on a Bruker spectrometer operating at 500 and 126 MHz, respectively. Chemical shifts are given in ppm and calibrated using residual undeuterated solvent as an internal reference (in $CDCl_3$, $\delta = 7.26$ for ^{1}H NMR and $\delta = 77.1$ for ^{13}C NMR). The following abbreviations describe the multiplets: s, singlet; d, doublet; dd, doublet of doublets; ddd, doublet of doublets of doublets; tdd, triplet of doublets of doublets; t, triplet; dt, doublet of

triplets; q, quartet; tq, triplet of quartets; quin, quintet; sext, sextet; m, multiplet; br, broad. Mass spectra were recorded on a high-resolution mass spectrometer (timsTOF) from Bruker equipped with an electrospray source (polarity: positive, capillary: 3.4 kV, capillary temperature: 200 °C, sheath gas flow rate: 5.0 L/min, mass range: m/z 50 to 1600).

3 Synthesis of molecules

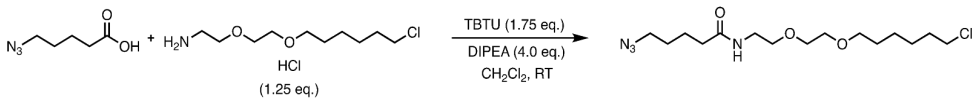
OEG denotes oligo(ethylene glycol); BCN, bicyclo[6.1.0]non-4-yne; NHS, *N*-hydroxysuccinimide. The spacers used throughout are monodisperse oligomers obtained by stepwise synthesis, not by polymerization.

Synthesis of compound A



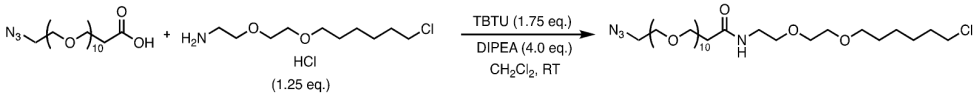
To a solution of BCN-OH (25 mg, 0.16 mmol) and N,N'-disuccinimidyl carbonate (53 mg, 0.21 mmol, 1.25 equiv.) in acetonitrile (0.4 mL, 0.4 M) was added N,N-diisopropylethylamine (DIPEA; 145 µL, 5.0 equiv.). The mixture was stirred at room temperature for 3.5 hours. The reaction was monitored by TLC, which showed complete consumption of BCN-OH. HaloTag ligand amine HCl salt (69 mg, 0.27 mmol, 1.6 equiv.) was added to the reaction solution at room temperature; then the solution was stirred for 16 hours. The reaction mixture was diluted with water and extracted with EtOAc three times. The combined organic phase was washed with saturated $NaHCO_3$ aqueous solution and saturated NH_4Cl aqueous solution. The resulting organic layer was dried over anhydrous $MgSO_4$, filtered and concentrated under reduced pressure. The crude product was purified by chromatography over silica gel with EtOAc and hexane (1:1) to afford the desired carbamate **A** (25 mg, 38% yield) as a colourless oil. ^{1}H NMR (500 MHz, $CDCl_3$) δ = 5.17 (br, 1H), 4.15 (d, J = 8.0 Hz, 2H), 3.60–3.62 (m, 2H), 3.55–3.57 (m, 4H), 3.53 (t, J = 6.5 Hz, 2H), 3.46 (t, J = 6.5 Hz, 2H), 3.38 (q, J = 5.0 Hz, 2H), 2.20–2.29 (m, 5H), 1.78 (quint, J = 6.5 Hz, 2H), 1.59–1.65 (m, 3H), 1.43–1.48 (m, 2H), 1.33–1.41 (m, 3H), 0.93–0.96 (m, 2H), 0.83–0.88 (m, 2H). The obtained ^{1}H NMR signals are consistent with the reported signals[48]. HR-MS: 422.2068 ($C_{21}H_{34}ClNNaO_4^+$, $[M+Na]^+$; calc. 422.2069).

Synthesis of compound B



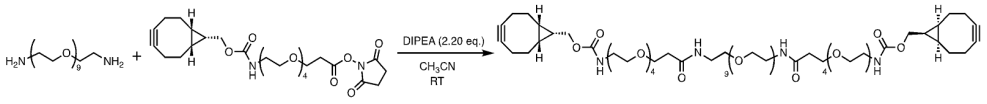
To a solution of 5-azidopentanoic acid (30 mg, 0.21 mmol) in CH_2Cl_2 (0.7 mL, 0.3 M) were added *O*-(benzotriazol-1-yl)-*N*, *N*, *N*′, *N*′-tetramethyluronium tetrafluoroborate (TBTU; 118 mg, 0.37 mmol, 1.75 equiv.) and DIPEA (145 µL, 4.0 equiv.) at room temperature. After adding HaloTag ligand amine HCl salt (68 mg, 0.26 mmol, 1.25 equiv.), the reaction solution was stirred at room temperature for 14 hours. The reaction mixture was diluted with water and extracted with EtOAc three times. The combined organic phase was washed with saturated $NaHCO_3$ aqueous solution and saturated NH_4Cl aqueous solution. The resulting organic layer was dried over anhydrous $MgSO_4$, filtered and concentrated under reduced pressure. The crude product was purified by chromatography over silica gel with EtOAc and hexane (17:3) to afford the desired amide **B** (9.0 mg, 12% yield) as a colourless oil. ^{1}H NMR (500 MHz, $CDCl_3$) δ = 6.00 (br, 1H), 3.60–3.62 (m, 2H), 3.51–3.57 (m, 6H), 3.43–3.47 (m, 4H), 3.29 (t, J = 7.0 Hz, 2H), 2.20 (t, J = 7.5 Hz, 2H), 1.69–1.78 (m, 4H), 1.57–1.65 (m, 4H), 1.42–1.48 (m, 2H), 1.34–1.40 (m, 2H). ^{13}C NMR (126 MHz, $CDCl_3$) δ = 172.32, 71.27, 70.28, 70.04, 69.82, 51.20, 45.04, 39.17, 35.90, 32.53, 29.48, 28.43, 26.69, 25.43, 22.81. HR-MS: 349.2002 ($C_{15}H_{30}ClN_4O_3^+$, $[M+H]^+$; calc. 349.2001), 371.1821 ($C_{15}H_{29}ClN_4NaO_3^+$, $[M+Na]^+$; calc. 371.1820).

Synthesis of compound C



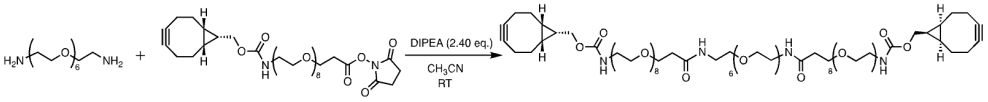
To a solution of azide-OEG10-acid (30 mg, 0.05 mmol) in CH_2Cl_2 (0.18 mL, 0.3 M) were added TBTU (30 mg, 0.09 mmol, 1.75 equiv.) and DIPEA (38 µL, 4.0 equiv.) at room temperature. After adding HaloTag ligand amine HCl salt (17.5 mg, 0.07 mmol, 1.25 equiv.), the reaction solution was stirred at room temperature for 18 hours. The reaction mixture was diluted with water and extracted with EtOAc three times. The combined organic phase was washed with saturated $NaHCO_3$ aqueous solution and saturated NH_4Cl aqueous solution. The resulting organic layer was dried over anhydrous $MgSO_4$, filtered and concentrated under reduced pressure. The crude product was purified by chromatography over silica gel with MeOH and $CHCl_3$ (1:9) to afford the desired amide **C** (24 mg, 58% yield) as a colourless oil. ^{1}H NMR (500 MHz, $CDCl_3$) δ = 6.58 (br, 1H), 3.73 (t, J = 5.0 Hz, 2H), 3.57–3.66 (m, 40H), 3.51–3.55 (m, 6H), 3.40–3.44 (m, 4H), 3.38 (t, J = 5.0 Hz, 2H), 2.46 (t, J = 6.3 Hz, 2H), 1.77 (dt, J = 6.7 Hz, J = 14.8 Hz, 2H), 1.59 (dt, J = 6.5 Hz, J = 15 Hz, 2H), 1.40–1.46 (m, 2H), 1.31–1.38 (m, 2H). ^{13}C NMR (126 MHz, $CDCl_3$) δ = 171.49, 77.41, 77.36, 77.16, 76.90, 71.39, 70.83, 70.80, 70.77, 70.72, 70.70, 70.53, 70.45, 70.41, 70.17, 69.98, 67.41, 50.82, 45.15, 39.25, 37.16, 32.65, 29.59, 26.81, 25.55. The carbon peaks in the repeating units of the oligoethylene glycol moiety overlap. HR-MS: 761.4308 ($C_{33}H_{66}ClN_4O_{13}^+$, $[M+H]^+$; calc. 761.4309), 783.4129 ($C_{33}H_{65}ClN_4NaO_{13}^+$, $[M+Na]^+$; calc. 783.4129).

Synthesis of compound D



To a solution of BCN-OEG4-NHS (11.0 mg, 20 µmol, 2.0 equiv.) in CH_3CN (0.3 mL, 0.033 M) were added amino-OEG9-amine (4.6 mg, 10.2 µmol, 1.0 equiv.) and DIPEA (3.0 mg, 22 µmol, 2.2 equiv.) at room temperature. The reaction solution was stirred for 22 hours. The reaction was monitored by TLC with iodine staining. The reaction solution was diluted with EtOAc, then washed twice with saturated aqueous $NaHCO_3$ to remove *N*-hydroxysuccinimide and the hydrolysed carboxylic acid. The organic layer was subsequently washed twice with saturated aqueous NH_4Cl to remove the unreacted amine starting material and the monoreacted intermediate. The solution was dried over anhydrous $MgSO_4$ for 30 minutes, filtered and concentrated *in vacuo* to afford the desired compound **D** (6.4 mg, 48% yield) as a colourless oil that gave a single spot by TLC with iodine staining. The resulting product was used for the next click reaction with azide-modified single-stranded DNA oligonucleotides (Section 5) without further purification.

Synthesis of compound E



To a solution of BCN-OEG8-NHS (9.5 mg, 13.5 µmol, 2.2 equiv.) in CH_3CN (160 µL, 0.037 M) were added amino-OEG6-amine (2.0 mg, 6.2 µmol, 1.0 equiv.) and DIPEA (2.0 mg, 15 µmol, 2.4 equiv.) at room temperature. The reaction solution was stirred for 24 hours. The reaction was monitored by TLC with iodine staining. The reaction solution was diluted with EtOAc, then washed twice with saturated aqueous $NaHCO_3$ to remove *N*-hydroxysuccinimide and the hydrolysed carboxylic acid. The organic layer was subsequently washed twice with saturated aqueous NH_4Cl to remove the unreacted amine starting material and the monoreacted intermediate. The solution was dried over anhydrous $MgSO_4$ for 30 minutes, filtered and concentrated *in vacuo* to afford the desired compound **E** (1.2 mg, 21% yield) as a colourless oil that gave a single spot by TLC with iodine staining. The resulting product was used for the next click reaction with azide-modified single-stranded DNA oligonucleotides (Section 5) without further purification.

Compound F

Compound **F**, a commercially available BCN dimer, was purchased from BroadPharm and used without further purification.

The ^{1}H and ^{13}C NMR spectra of the synthetic small molecules are collected after the Methods sections.

4 Construct design and protein preparation

Construction of tagged recombinant cDNA plasmids

Genes encoding human integrin β1 cytoplasmic tail (ITGB1A) and talin-1 FERM domain (TLN1) were amplified by polymerase chain reaction (PCR) using human cDNAs from the Mammalian Gene Collection[49] as templates. DNA sequences of HaloTag, LgBiT and the SmBiT variants, which possess different binding affinities for LgBiT, were retrieved from the Promega website (https://www.promega.jp/products/cloning-and-dna-markers/cloning-vectors-and-kits/ph6htn-and-ph6htc-his6halotag-t7-vectors/?catNum=G7971), the Addgene website (https://www.addgene.org/188319/sequences/) and the original report[28], respectively. The DNA sequences were synthesized by Eurofins Genomics. Overlapping sequences were added at the 5′ and 3′ ends for seamless cloning. Amplified ITGB1A and TLN1 were subcloned into the pH6HTN (Promega, catalogue no. G7971) and pET-15b (Novagen, catalogue no. 69661) vectors using Gibson Assembly seamless cloning. The DarkBiT **1** plasmid was derived from the SmBiT104 plasmid using an inverse-PCR point-mutation method. Detailed information on the constructs used in this study is given in **Supplementary Tables 1–4**.

Preparation of recombinant proteins

The recombinant His-tagged-HaloTag-LgBiT, His-tagged-HaloTag-SmBiT, His-tagged-HaloTag-LgBiT-SmBiT and His-tagged-HaloTag-DarkBiT **1** were expressed in the BL21 Star *E. coli* strain. The bacteria were grown in LB medium to an optical density at 600 nm (OD_{600}) of 0.8; isopropyl β-D-1-thiogalactopyranoside (IPTG) was then added to a final concentration of 1 mM, and the cells were grown for a further 2 hours. After collection by centrifugation at 8,000 × g for 20 minutes, the bacterial pellets were resuspended in wash buffer (50 mM 4-(2-hydroxyethyl)-1-piperazineethanesulfonic acid (HEPES), pH 7.5, 150 mM NaCl, 10 mM imidazole) and sonicated. To remove the debris, the samples were centrifuged at 10,000 × g for 30 minutes; then the supernatant was subjected to purification using Ni-NTA agarose resin (QIAGEN, #30210) following the manufacturer's protocol with customized buffers (wash buffer: 50 mM HEPES (pH 7.5), 150 mM NaCl, 10 mM imidazole; elution buffer: 50 mM HEPES (pH 7.5), 150 mM NaCl, 200 mM imidazole). The recombinant His-tagged-LgBiT-HaloTag-ITGB1A and His-tagged-HaloTag-TLN1 were prepared in the same manner from the same strain, using customized buffers (wash buffer: 50 mM HEPES (pH 7.5), 1 M NaCl, 10 mM imidazole; elution buffer: 50 mM HEPES (pH 7.5), 1 M NaCl, 200 mM imidazole). The protein samples were divided into small portions and frozen in liquid nitrogen. The recombinant protein samples were stored at −80 °C until use.

5 Functionalization of oligonucleotides

Synthesis of BCN-conjugated single-stranded DNAs

A 50 µL portion of a 100 µM solution of azide- and/or fluorescent-dye-modified oligonucleotide in Tris-EDTA (TE) buffer (10 mM Tris-HCl, 0.5 mM ethylenediaminetetraacetic acid (EDTA), pH 8.0) was reacted with 5 µL of a 10 mM solution of BCN-modified small molecule (compound **A**, **D**, **E** or **F**) in *N*, *N*-dimethylformamide (DMF), and the reaction solution was then heated at 60 °C for 2 hours. After the reaction, the solution was cooled to room temperature and subjected to 5% native agarose gel electrophoresis at 100 V for 1 hour (gel prepared with PrimeGel agarose PCR-sieve HRS from Takara in Tris/borate/EDTA (TBE) buffer (82 mM Tris-HCl, 81 mM $B(OH)_3$, 1.9 mM EDTA, pH 8.3)). Then, the target gel bands were excised and melted. The target oligonucleotide was purified using a DNA extraction kit (NucleoTrap) from Takara. The concentration of the purified solution containing the target oligonucleotide was determined by A_{260} absorbance.

Synthesis of HaloTag ligand-conjugated single-stranded DNAs (AccuLinkers)

A 30 µL portion of BCN-conjugated oligonucleotide in a 60–80 µM aqueous solution was reacted with 25 equivalents of azide-modified HaloTag ligand (compound **B** or **C**) as a 50 mM solution in DMF, and the reaction solution was then heated at 60 °C for 2 hours. After the reaction, the solution was cooled to room temperature and subjected to 5% native agarose gel electrophoresis at 100 V for 1 hour (gel prepared with PrimeGel agarose PCR-sieve HRS from Takara in TBE buffer). Then, the target gel bands were excised and melted. The target oligonucleotide was purified using a DNA extraction kit (NucleoTrap) from Takara. The concentration of the purified solution containing the target oligonucleotide was determined by A_{260} absorbance. Representative gels are shown in Supplementary Fig. S12.

6 Design and synthesis of DNA brick (DB01)

The DB01 structure was designed using the open-source software NanoBricks[26] (https://nanobricks.software/). To assemble the structures, DNA strands were mixed to a final concentration of 100 nM per strand (DB01 contains 705 strands) in TE (10 mM Tris-HCl, 0.5 mM EDTA, pH 8.0) supplemented with 30 mM $MgCl_2$. The strand mixture was then annealed in a PCR thermal cycler by a linear cooling ramp from 80 °C to 60 °C over 1 hour, followed by a 100-hour ramp from 60 °C to 30 °C. Annealed samples were concentrated in an Amicon Ultra-0.5 device (100 kDa molecular-weight cut-off) from Merck by centrifugation at 3,000 × *g*, then subjected to 1.5% native agarose gel electrophoresis at 100 V for 1 hour (gel prepared in 0.5×TBE buffer supplemented with 6 mM $Mg(OAc)_2$) in a cold room at 4 °C. DNA was stained by incubation

with SYBR Gold (Thermo Fisher Scientific). Then, the target gel bands were excised and placed into a centrifugal filter tube from Merck. The excised gel was crushed into fine pieces by centrifugation at $10{,}000 \times g$ for 10 minutes, and target DNA bricks were extracted in the filtered solution. The buffer was exchanged for 20 mM $MgCl_2$ solution using an Amicon Ultra-0.5 device (100 kDa) by centrifugation at $3{,}000 \times g$, and the concentration of the resulting solution was then determined by A_{260} absorbance. The isolated yield was calculated from that concentration, the recovered volume and a DB01 molecular weight estimated from the average nucleotide mass, relative to the theoretical maximum set by the 100 nM per-strand annealing concentration. The value quoted in the main text is the highest obtained across preparations. The design and the purified product are shown in Supplementary Figs. S1 and S3.

7 HaloTag conjugation with oligonucleotides

AccuLinker (5 µM) was reacted with 3 equivalents of HaloTag-fused recombinant protein (15 µM) in buffer (50 mM Tris-HCl, 100 mM NaCl, pH 7.5) supplemented with 20 mM $MgCl_2$ on ice for 1 hour. The HaloTag conjugation reaction was monitored by polyacrylamide gel electrophoresis (PAGE). The starting material, AccuLinker, was quantitatively converted to the desired protein-conjugated oligonucleotide, and the resulting solution was used for the next protein tethering step without further purification. Conjugation was verified by gel electrophoresis (Supplementary Figs. S7–S9).

8 Protein tethering to DB01

DB01 (30 nM) was reacted with 10 equivalents of protein-conjugated oligonucleotide (300 nM) in buffer (50 mM Tris-HCl, 100 mM NaCl, pH 7.5) supplemented with 20 mM $MgCl_2$ on ice for 2 hours. Excess proteins and protein-conjugated oligonucleotides were removed using an Amicon Ultra-0.5 device (100 kDa) by centrifugation at $3{,}000 \times g$. After five rounds of centrifugation, the concentration of the resulting solution was determined by A_{260} absorbance, and the solution was diluted to 1 nM. Tethering efficiency is shown in Supplementary Fig. S10.

9 Luminescence measurement of the LgBiT-SmBiT complex

In a 96-well white plate (low-binding-surface 1/2-Area OptiPlate, PerkinElmer), 25 µL of protein-immobilized DB01 solution (1 nM) was mixed with 25 µL of NanoBiT

substrate solution (Nano-Glo Luciferase Assay System, Promega) at room temperature. After a 3-minute incubation, the luminescence intensity was measured at room temperature on a plate reader (Infinite F500, Tecan) with an integration time of 200 ms. Background was estimated from 12 wells in plate row H measured on the same plate, and the signal-to-noise ratio was defined as $(I - \bar{B})/s_B$, where $\bar{B}$ and s_B are the mean and sample standard deviation of the background-well signals. The acquired data are summarized and plotted in **Figs. 4 and 5** and **Supplementary Fig. S16**.

10 Peptide regulation of protein-protein interaction in DB01

Protein-immobilized DB01 solution was diluted to 1 nM with an aqueous solution containing the peptide used in each experiment (DarkBiT **2**, one of the screening peptides of Section 12 or the optimized modulator compound **1**), and the solution was incubated on ice for 1 hour. The final aqueous solution contained 50 mM Tris-HCl, 100 mM NaCl and 20 mM $MgCl_2$ (pH 7.5), with a final dimethyl sulfoxide (DMSO) concentration below 1%. In a 96-well white plate, 25 µL of the incubated solution was mixed with 25 µL of NanoBiT substrate solution (Nano-Glo Luciferase Assay System, Promega) at room temperature. After a 3-minute incubation, the luminescence intensity was measured at room temperature on a plate reader (Infinite F500, Tecan) with an integration time of 200 ms. The acquired data are summarized and plotted in **Figs. 5 and 6** and **Supplementary Fig. S18**.

11 Determination of the dissociation constant of DarkBiT 1

To determine the affinity of HaloTag-DarkBiT **1** for HaloTag-LgBiT, recombinant HaloTag-LgBiT (3 µM) was incubated with HaloTag-DarkBiT **1** at concentrations from 0 to 146 µM in 30 µL of reaction buffer (50 mM Tris-HCl, 100 mM NaCl, pH 7.5) in a 96-well white plate. After 30 minutes on ice, intrinsic fluorescence was recorded with excitation at 290 nm and emission from 310 to 400 nm. Tryptophan fluorescence quenching on complex formation, $I = F_a + F_b - F_c$, was obtained at 340 nm from the fluorescence of HaloTag-LgBiT alone (F_a), HaloTag-DarkBiT **1** alone (F_b) and their mixture (F_c). Because I is proportional to the complex concentration, plotting it against the HaloTag-DarkBiT **1** concentration and fitting gave the dissociation constant (K_d) (Supplementary Fig. S15).

12 Protein–protein interaction (PPI) modulator screening

Creation of a focused peptide library and improvement of PPI modulator activity

While designing PPI modulators of integrin–talin binding, we observed that low concentrations of the integrin-β peptide ITGB3 (Supplementary Table 5) slightly promoted integrin–talin complex formation. We therefore prepared a focused peptide library mimicking the cytoplasmic tail of integrin β. Iterative evaluation and refinement of the hit peptides, guided by simulation-based stability scoring in MolDesk Screening (IMSBIO Co., Ltd.; https://www.moldesk.com), yielded the PPI modulator compound **1**.

PPI modulator screening using DB01

Selected peptides were evaluated using the DB01-based switching system (**Fig. 6** and **Supplementary Fig. S18**). The experimental protocol is described in Section 10.

13 Biological evaluation of the PPI modulator

Because integrin–talin complex formation is essential for cell adhesion, we established an integrin-dependent cell-adhesion assay. First, a non-treated 96-well plate was coated with 100 µL of a 10 µg/mL fibronectin solution for 2 hours, then washed twice with 1× PBS(-) (phosphate-buffered saline lacking Ca^{2+} and Mg^{2+}). In parallel, U87MG human glioblastoma cells were cultured at 37 °C in DMEM/10% FBS/1% penicillin/streptomycin (P/S) under 5% CO_2. The cells were trypsinized and collected by centrifugation at 400 × g for 5 minutes, and the medium was changed to DMEM/1% FBS/1% P/S. Then 4×10^3 cells were plated in each well, and two plates were prepared under the same conditions. After incubation at 37 °C for 10 minutes, the peptide compounds were added to the wells at the desired concentrations, and incubation was continued at 37 °C for 5 days. One plate was treated with CellTiter-Glo 3D Cell Viability Assay solution, an adenosine triphosphate (ATP)-based indicator of proliferation, according to the manufacturer's protocol, and luminescence was measured using an EnSpire plate reader (PerkinElmer). These values were analysed independently as a control for viable cell number and were not used to normalize the crystal-violet absorbance. In the other plate, the medium was aspirated and the cells were fixed with 4% paraformaldehyde for 30 minutes, and the wells were washed once with 1× PBS(+) (PBS containing Ca^{2+} and Mg^{2+}). To quantify the cells that remained bound to fibronectin, a stock of 0.2% crystal violet and 2% EtOH was diluted five-fold in PBS(-), and 100 µL of the resulting solution was added and incubated for 30 minutes. The plate was washed three times with 1× PBS(+); it was then inverted and

allowed to dry completely in the dark. Finally, 100 µL of 1% sodium dodecyl sulfate (SDS) solution was added and the plate was incubated for 30 minutes at room temperature with agitation. The absorbance at 595 nm was measured using an EnSpire plate reader (PerkinElmer). Readings were blank-subtracted and then expressed as a percentage of the mean of the vehicle-treated wells on the same plate. These values were used as indicators of cell adhesion. Proliferation and biomass data are shown in Supplementary Fig. S19.

14 Negative-stain transmission electron microscopy (nsTEM)

For imaging, 3.0 µL of agarose-gel-purified DB01 was adsorbed for 30 seconds onto glow-discharged, 2 nm carbon-coated transmission electron microscopy (TEM) grids. The grids were then stained twice, each time for 1 minute, with 25% aqueous EM stainer (Nisshin EM). Imaging was performed using a JEOL Field Emission Transmission Electron Microscope (FE-TEM) JEM-2200FS operated at 200 kV, equipped with an energy filter for high-contrast imaging. Representative images are shown in Supplementary Fig. S4.

15 Cryo-EM analysis

The DB01 sample (30 nM) was applied to glow-discharged Quantifoil R0.6 holey grids and plunge-frozen using a Vitrobot Mark IV (Thermo Fisher Scientific) at 4 °C and 100% humidity. The data were acquired using the EPU software (Thermo Fisher Scientific) on a Glacios cryo-transmission electron microscope operated at 200 kV and equipped with a Falcon 4 direct electron detector, at the Institute for Life and Medical Sciences, Kyoto University. A representative image is shown in Fig. 3c of the main text.

16 Survey of reported protein–protein binding affinities

Figure 1 summarizes the PPB-Affinity dataset[20]. Because multiple mutant records can be associated with the same wild-type complex, the analysis was restricted to wild-type records. Records were further required to have an annotated affinity-measurement method and a parseable affinity-release date. The resulting dataset comprised 1,460 records: 879 measured by surface plasmon resonance or biolayer interferometry (SPR/BLI), 118 by isothermal titration calorimetry (ITC), and 463 by other methods, including records annotated as Unknown. Twelve records with $K_{\mathrm{d}} < 10^{-12}$ M

fell outside the plotted range. The final plot contains 1,448 records: 878 SPR/BLI, 117 ITC, and 453 other-method records.

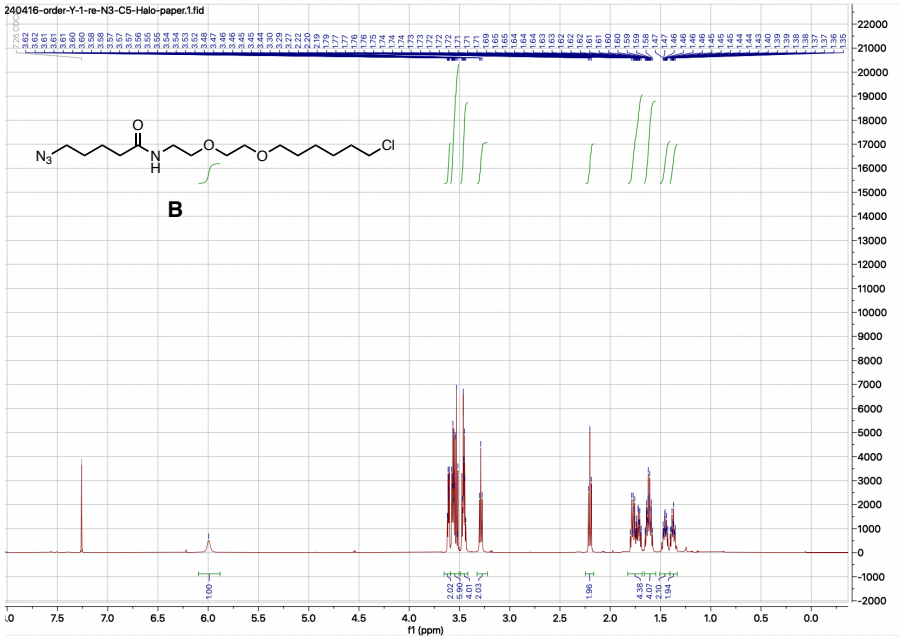
^{1}H and ^{13}C NMR of synthetic small molecules

Compound **A** is a known compound and is shown by ^{1}H NMR only[48]; compounds **D** and **E** were carried into the next step without further purification and are not included.

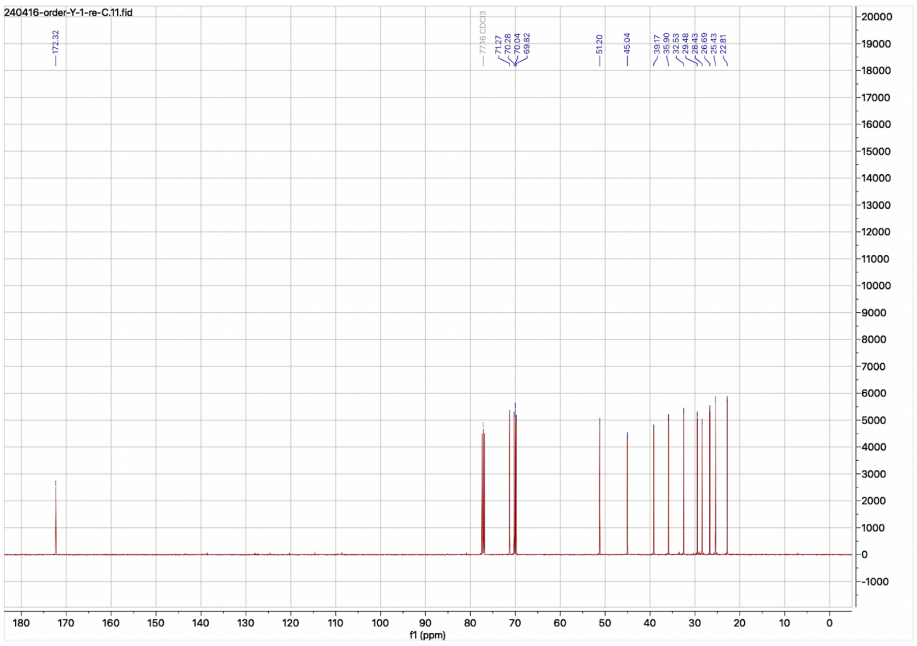
^{1}H NMR of compound **A**



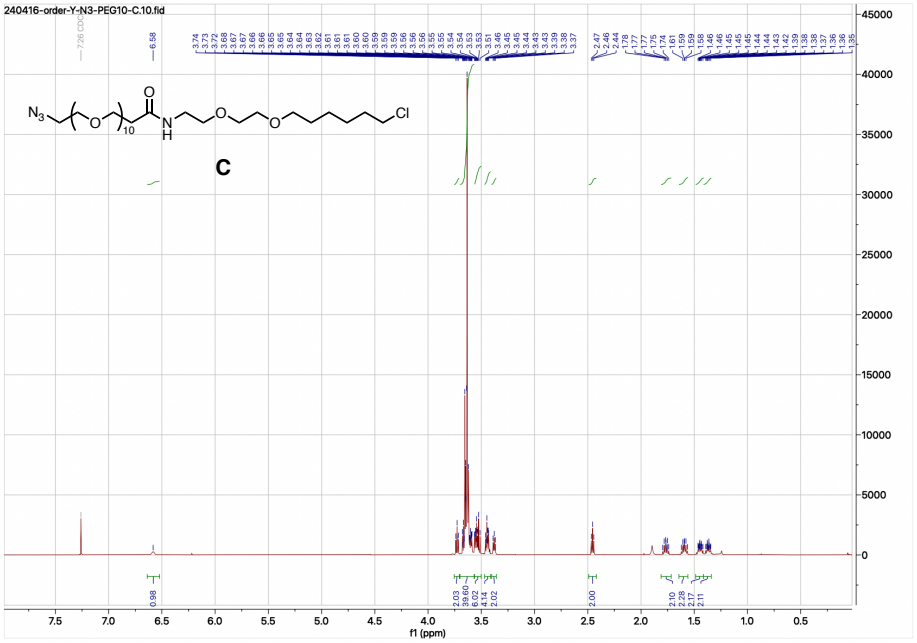
^{1}H NMR of compound **B**



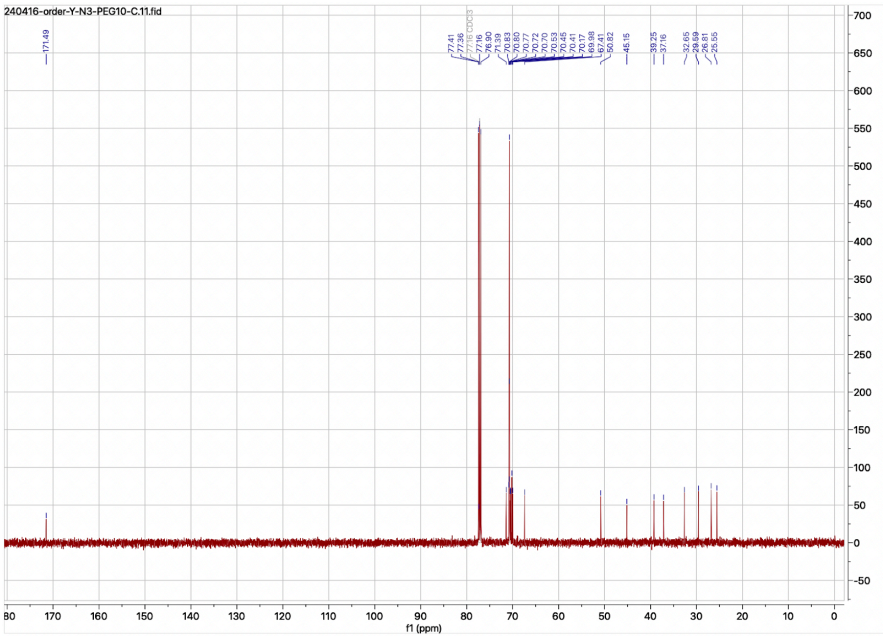
^{13}C NMR of compound **B**



^{1}H NMR of compound **C**



^{13}C NMR of compound **C**



Supplementary Table 1. DNA and amino acid sequences of HaloTag-LgBiT. The His affinity tag is shown in cyan, HaloTag in orange, and LgBiT in blue.

ID	Vector	DNA sequence	Amino acid sequence
HaloTag-LgBiT	pH6HTN	ATGAAACATCATCACCATCACCACGCAGAAATCGGTACTGGCTT TCCATTCGACCCCCATTATGTGGAAGTCCTGGGCGAGCGCATGC ACTACGTCGATGTTGGTCCGCGCGATGGCACCCCTGTGCTGTTC CTGCACGGTAACCCGACCTCCTCCTACGTGTGGCGCAACATCAT CCCGCATGTTGCACCGACCCATCGCTGCATTGCTCCAGACCTGA TCGGTATGGGCAAATCCGACAAACCAGACCTGGGTTATTTCTTC GACGACCACGTCCGCTTCATGGATGCCTTCATCGAAGCCCTGGG TCTGGAAGAGGTCGTCCTGGTCATTCACGACTGGGGCTCCGCTC TGGGTTTCCACTGGGCCAAGCGCAATCCAGAGCGCGTCAAAGGT ATTGCATTTATGGAGTTCATCCGCCCTATCCCGACCTGGGACGA ATGGCCAGAATTTGCCCGCGAGACCTTCCAGGCCTTCCGCACCA CCGACGTCGGCCGCAAGCTGATCATCGATCAGAACGTTTTTATC GAGGGTACGCTGCCGATGGGTGTCGTCCGCCCGCTGACTGAAGT CGAGATGGACCATTACCGCGAGCCGTTCCTGAATCCTGTTGACC GCGAGCCACTGTGGCGCTTCCCAAACGAGCTGCCAATCGCCGGT GAGCCAGCGAACATCGTCGCGCTGGTCGAAGAATACATGGACTG GCTGCACCAGTCCCCTGTCCCGAAGCTGCTGTTCTGGGGCACCC CAGGCGTTCTGATCCCACCGGCCGAAGCCGCTCGCCTGGCCAAA AGCCTGCCTAACTGCAAGGCTGTGGACATCGGCCCGGGTCTGAA TCTGCTGCAAGAAGACAACCCGGACCTGATCGGCAGCGAGATCG CGCGCTGGCTGTCGACGCTCGAGATTTCCGGCAGCGATAACATG GTCTTTACACTGGAGGATTTCGTCGGGGACTGGGAGCAAACGGC GGCCTACAACTTAGATCAAGTCTTAGAACAAGGCGGTGTCAGCA GCTTATTACAAAACCTTGCGGTTTCCGTAACCCCAATCCAACGC ATTGTCCGCTCGGGGGAGAATGCCTTAAAGATTGACATCCACGT CATTATCCCCTATGAGGGACTGTCCGCGGATCAAATGGCACAAA TTGAGGAGGTGTTCAAAGTAGTCTATCCCGTGGATGACCACCAC TTTAAGGTTATCTTACCATATGGAACGCTTGTAATTGACGGTGT AACCCCCAATATGCTGAACTACTTCGGGCGCCCATACGAGGGCA TTGCCGTCTTTGATGGGAAGAAAATTACGGTGACCGGGACCCTG TGGAACGGCAACAAAATCATTGACGAACGTTTAATCACCCCAGA TGGATCCATGTTGTTTCGCGTTACAATCAATTCGTAA	MKHHHHHHAEIGTGF PFDPHYVEVLGERMH YVDVGPRDGTPVLFL HGNPTSSYVWRNIIP HVAPTHRCIAPDLIG MGKSDKPDLGYFFDD HVRFMDAFIEALGLE EVVLVIHDWGSALGF HWAKRNPERVKGIAF MEFIRPIPTWDEWPE FARETFQAFRTTDVG RKLIIDQNVFIEGTL PMGVVRPLTEVEMDH YREPFLNPVDREPLW RFPNELPIAGEPANI VALVEEYMDWLHQSP VPKLLFWGTPGVLIP PAEAARLAKSLPNCK AVDIGPGLNLLQEDN PDLIGSEIARWLSTL EISGSDNMVFTLEDF VGDWEQTAAYNLDQV LEQGGVSSLLQNLAV SVTPIQRIVRSGENA LKIDIHVIIPYEGLS ADQMAQIEEVFKVVY PVDDHHFKVILPYGT LVIDGVTPNMLNYFG RPYEGIAVFDGKKIT VTGTLWNGNKIIDER LITPDGSMLFRVTIN S*

Supplementary Table 2. DNA and amino acid sequences of HaloTag-SmBiT and HaloTag-DarkBiT 1. The His affinity tag is shown in cyan, HaloTag in orange, SmBiT in red, and DarkBiT 1 in grey.

ID	Vector	DNA sequence	Amino acid sequence
HaloTag-SmBiT230	pH6HTN	ATGAAACATCATCACCATCACCACGCAGAAATCGGTACTGGCTT TCCATTCGACCCCCATTATGTGGAAGTCCTGGGCGAGCGCATGC ACTACGTCGATGTTGGTCCGCGCGATGGCACCCCTGTGCTGTTC CTGCACGGTAACCCGACCTCCTCCTACGTGTGGCGCAACATCAT CCCGCATGTTGCACCGACCCATCGCTGCATTGCTCCAGACCTGA TCGGTATGGGCAAATCCGACAAACCAGACCTGGGTTATTTCTTC GACGACCACGTCCGCTTCATGGATGCCTTCATCGAAGCCCTGGG TCTGGAAGAGGTCGTCCTGGTCATTCACGACTGGGGCTCCGCTC TGGGTTTCCACTGGGCCAAGCGCAATCCAGAGCGCGTCAAAGGT ATTGCATTTATGGAGTTCATCCGCCCTATCCCGACCTGGGACGA ATGGCCAGAATTTGCCCGCGAGACCTTCCAGGCCTTCCGCACCA CCGACGTCGGCCGCAAGCTGATCATCGATCAGAACGTTTTTATC GAGGGTACGCTGCCGATGGGTGTCGTCCGCCCGCTGACTGAAGT CGAGATGGACCATTACCGCGAGCCGTTCCTGAATCCTGTTGACC GCGAGCCACTGTGGCGCTTCCCAAACGAGCTGCCAATCGCCGGT GAGCCAGCGAACATCGTCGCGCTGGTCGAAGAATACATGGACTG GCTGCACCAGTCCCCTGTCCCGAAGCTGCTGTTCTGGGGCACCC CAGGCGTTCTGATCCCACCGGCCGAAGCCGCTCGCCTGGCCAAA AGCCTGCCTAACTGCAAGGCTGTGGACATCGGCCCGGGTCTGAA TCTGCTGCAAGAAGACAACCCGGACCTGATCGGCAGCGAGATCG CGCGCTGGCTGTCGACGCTCGAGATTTCCGGCGGTGGTTCAGTC ACCGGATACCGGCTTTTCGAGTAA	MKHHHHHHAEIGTGF PFDPHYVEVLGERMH YVDVGPRDGTPVLFL HGNPTSSYVWRNIIP HVAPTHRCIAPDLIG MGKSDKPDLGYFFDD HVRFMDAFIEALGLE EVVLVIHDWGSALGF HWAKRNPERVKGIAF MEFIRPIPTWDEWPE FARETFQAFRTTDVG RKLIIDQNVFIEGTL PMGVVRPLTEVEMDH YREPFLNPVDREPLW RFPNELPIAGEPANI VALVEEYMDWLHQSP VPKLLFWGTPGVLIP PAEAARLAKSLPNCK AVDIGPGLNLLQEDN PDLIGSEIARWLSTL EISGGGSVTGYRLFE *

ID	Vector	DNA sequence	Amino acid sequence
HaloTag-SmBiT114	pET15b(–)	ATGGGCAGCAGCCATCATCATCATCATCACAGCAGCGGCCTGGT GCCGCGCGGCAGCCATATGCTCGAGGCAGAAATCGGTACTGGCT TTCCATTCGACCCCCATTATGTGGAAGTCCTGGGCGAGCGCATG CACTACGTCGATGTTGGTCCGCGCGATGGCACCCCTGTGCTGTT CCTGCACGGTAACCCGACCTCCTCCTACGTGTGGCGCAACATCA TCCCGCATGTTGCACCGACCCATCGCTGCATTGCTCCAGACCTG ATCGGTATGGGCAAATCCGACAAACCAGACCTGGGTTATTTCTT CGACGACCACGTCCGCTTCATGGATGCCTTCATCGAAGCCCTGG GTCTGGAAGAGGTCGTCCTGGTCATTCACGACTGGGGCTCCGCT CTGGGTTTCCACTGGGCCAAGCGCAATCCAGAGCGCGTCAAAGG TATTGCATTTATGGAGTTCATCCGCCCTATCCCGACCTGGGACG AATGGCCAGAATTTGCCCGCGAGACCTTCCAGGCCTTCCGCACC ACCGACGTCGGCCGCAAGCTGATCATCGATCAGAACGTTTTTAT CGAGGGTACGCTGCCGATGGGTGTCGTCCGCCCGCTGACTGAAG TCGAGATGGACCATTACCGCGAGCCGTTCCTGAATCCTGTTGAC CGCGAGCCACTGTGGCGCTTCCCAAACGAGCTGCCAATCGCCGG TGAGCCAGCGAACATCGTCGCGCTGGTCGAAGAATACATGGACT GGCTGCACCAGTCCCCTGTCCCGAAGCTGCTGTTCTGGGGCACC CCAGGCGTTCTGATCCCACCGGCCGAAGCCGCTCGCCTGGCCAA AAGCCTGCCTAACTGCAAGGCTGTGGACATCGGCCCGGGTCTGA ATCTGCTGCAAGAAGACAACCCGGACCTGATCGGCAGCGAGATC GCGCGCTGGCTGTCGACGCTCGAGATTTCCGGCGGTGGTTCAGT GACCGGCTACCGGCTGTTCGAGGAGATTCTGTAA	MGSSHHHHHHSSGLV PRGSHMLEAEIGTGF PFDPHYVEVLGERMH YVDVGPRDGTPVLFL HGNPTSSYVWRNIIP HVAPTHRCIAPDLIG MGKSDKPDLGYFFDD HVRFMDAFIEALGLE EVVLVIHDWGSALGF HWAKRNPERVKGIAF MEFIRPIPTWDEWPE FARETFQAFRTTDVG RKLIIDQNVFIEGTL PMGVVRPLTEVEMDH YREPFLNPVDREPLW RFPNELPIAGEPANI VALVEEYMDWLHQSP VPKLLFWGTPGVLIP PAEAARLAKSLPNCK AVDIGPGLNLLQEDN PDLIGSEIARWLSTL EISGGGSVTGYRLFE EIL*

ID	Vector	DNA sequence	Amino acid sequence
HaloTag-SmBiT104	pH6HTN	ATGAAACATCATCACCATCACCACGCAGAAATCGGTACTGGCTT TCCATTCGACCCCCATTATGTGGAAGTCCTGGGCGAGCGCATGC ACTACGTCGATGTTGGTCCGCGCGATGGCACCCCTGTGCTGTTC CTGCACGGTAACCCGACCTCCTCCTACGTGTGGCGCAACATCAT CCCGCATGTTGCACCGACCCATCGCTGCATTGCTCCAGACCTGA TCGGTATGGGCAAATCCGACAAACCAGACCTGGGTTATTTCTTC GACGACCACGTCCGCTTCATGGATGCCTTCATCGAAGCCCTGGG TCTGGAAGAGGTCGTCCTGGTCATTCACGACTGGGGCTCCGCTC TGGGTTTCCACTGGGCCAAGCGCAATCCAGAGCGCGTCAAAGGT ATTGCATTTATGGAGTTCATCCGCCCTATCCCGACCTGGGACGA ATGGCCAGAATTTGCCCGCGAGACCTTCCAGGCCTTCCGCACCA CCGACGTCGGCCGCAAGCTGATCATCGATCAGAACGTTTTTATC GAGGGTACGCTGCCGATGGGTGTCGTCCGCCCGCTGACTGAAGT CGAGATGGACCATTACCGCGAGCCGTTCCTGAATCCTGTTGACC GCGAGCCACTGTGGCGCTTCCCAAACGAGCTGCCAATCGCCGGT GAGCCAGCGAACATCGTCGCGCTGGTCGAAGAATACATGGACTG GCTGCACCAGTCCCCTGTCCCGAAGCTGCTGTTCTGGGGCACCC CAGGCGTTCTGATCCCACCGGCCGAAGCCGCTCGCCTGGCCAAA AGCCTGCCTAACTGCAAGGCTGTGGACATCGGCCCGGGTCTGAA TCTGCTGCAAGAAGACAACCCGGACCTGATCGGCAGCGAGATCG CGCGCTGGCTGTCGACGCTCGAGATTTCCGGCGGTGGTTCAGTG GAAGGTTACAGACTGTTCGAAAAAATCTCATAA	MKHHHHHHAEIGTGF PFDPHYVEVLGERMH YVDVGPRDGTPVLFL HGNPTSSYVWRNIIP HVAPTHRCIAPDLIG MGKSDKPDLGYFFDD HVRFMDAFIEALGLE EVVLVIHDWGSALGF HWAKRNPERVKGIAF MEFIRPIPTWDEWPE FARETFQAFRTTDVG RKLIIDQNVFIEGTL PMGVVRPLTEVEMDH YREPFLNPVDREPLW RFPNELPIAGEPANI VALVEEYMDWLHQSP VPKLLFWGTPGVLIP PAEAARLAKSLPNCK AVDIGPGLNLLQEDN PDLIGSEIARWLSTL EISGGGSVEGYRLFE KIS*

ID	Vector	DNA sequence	Amino acid sequence
HaloTag-SmBiT99	pH6HTN	ATGAAACATCATCACCATCACCACGCAGAAATCGGTACTGGCTT TCCATTCGACCCCCATTATGTGGAAGTCCTGGGCGAGCGCATGC ACTACGTCGATGTTGGTCCGCGCGATGGCACCCCTGTGCTGTTC CTGCACGGTAACCCGACCTCCTCCTACGTGTGGCGCAACATCAT CCCGCATGTTGCACCGACCCATCGCTGCATTGCTCCAGACCTGA TCGGTATGGGCAAATCCGACAAACCAGACCTGGGTTATTTCTTC GACGACCACGTCCGCTTCATGGATGCCTTCATCGAAGCCCTGGG TCTGGAAGAGGTCGTCCTGGTCATTCACGACTGGGGCTCCGCTC TGGGTTTCCACTGGGCCAAGCGCAATCCAGAGCGCGTCAAAGGT ATTGCATTTATGGAGTTCATCCGCCCTATCCCGACCTGGGACGA ATGGCCAGAATTTGCCCGCGAGACCTTCCAGGCCTTCCGCACCA CCGACGTCGGCCGCAAGCTGATCATCGATCAGAACGTTTTTATC GAGGGTACGCTGCCGATGGGTGTCGTCCGCCCGCTGACTGAAGT CGAGATGGACCATTACCGCGAGCCGTTCCTGAATCCTGTTGACC GCGAGCCACTGTGGCGCTTCCCAAACGAGCTGCCAATCGCCGGT GAGCCAGCGAACATCGTCGCGCTGGTCGAAGAATACATGGACTG GCTGCACCAGTCCCCTGTCCCGAAGCTGCTGTTCTGGGGCACCC CAGGCGTTCTGATCCCACCGGCCGAAGCCGCTCGCCTGGCCAAA AGCCTGCCTAACTGCAAGGCTGTGGACATCGGCCCGGGTCTGAA TCTGCTGCAAGAAGACAACCCGGACCTGATCGGCAGCGAGATCG CGCGCTGGCTGTCGACGCTCGAGATTTCCGGCGGTGGTTCAGTG ACTGGATACCGCTTATTCGAGAAAATCAGTTAA	MKHHHHHHAEIGTGF PFDPHYVEVLGERMH YVDVGPRDGTPVLFL HGNPTSSYVWRNIIP HVAPTHRCIAPDLIG MGKSDKPDLGYFFDD HVRFMDAFIEALGLE EVVLVIHDWGSALGF HWAKRNPERVKGIAF MEFIRPIPTWDEWPE FARETFQAFRTTDVG RKLIIDQNVFIEGTL PMGVVRPLTEVEMDH YREPFLNPVDREPLW RFPNELPIAGEPANI VALVEEYMDWLHQSP VPKLLFWGTPGVLIP PAEAARLAKSLPNCK AVDIGPGLNLLQEDN PDLIGSEIARWLSTL EISGGGSVTGYRLFE KIS*

ID	Vector	DNA sequence	Amino acid sequence
HaloTag-SmBiT78	pH6HTN	ATGAAACATCATCACCATCACCACGCAGAAATCGGTACTGGCTT TCCATTCGACCCCCATTATGTGGAAGTCCTGGGCGAGCGCATGC ACTACGTCGATGTTGGTCCGCGCGATGGCACCCCTGTGCTGTTC CTGCACGGTAACCCGACCTCCTCCTACGTGTGGCGCAACATCAT CCCGCATGTTGCACCGACCCATCGCTGCATTGCTCCAGACCTGA TCGGTATGGGCAAATCCGACAAACCAGACCTGGGTTATTTCTTC GACGACCACGTCCGCTTCATGGATGCCTTCATCGAAGCCCTGGG TCTGGAAGAGGTCGTCCTGGTCATTCACGACTGGGGCTCCGCTC TGGGTTTCCACTGGGCCAAGCGCAATCCAGAGCGCGTCAAAGGT ATTGCATTTATGGAGTTCATCCGCCCTATCCCGACCTGGGACGA ATGGCCAGAATTTGCCCGCGAGACCTTCCAGGCCTTCCGCACCA CCGACGTCGGCCGCAAGCTGATCATCGATCAGAACGTTTTTATC GAGGGTACGCTGCCGATGGGTGTCGTCCGCCCGCTGACTGAAGT CGAGATGGACCATTACCGCGAGCCGTTCCTGAATCCTGTTGACC GCGAGCCACTGTGGCGCTTCCCAAACGAGCTGCCAATCGCCGGT GAGCCAGCGAACATCGTCGCGCTGGTCGAAGAATACATGGACTG GCTGCACCAGTCCCCTGTCCCGAAGCTGCTGTTCTGGGGCACCC CAGGCGTTCTGATCCCACCGGCCGAAGCCGCTCGCCTGGCCAAA AGCCTGCCTAACTGCAAGGCTGTGGACATCGGCCCGGGTCTGAA TCTGCTGCAAGAAGACAACCCGGACCTGATCGGCAGCGAGATCG CGCGCTGGCTGTCGACGCTCGAGATTTCCGGCGGTGGTTCAAAT GTCAGTGGATGGAGACTGTTCAAGAAAATCTCCAACTAA	MKHHHHHHAEIGTGF PFDPHYVEVLGERMH YVDVGPRDGTPVLFL HGNPTSSYVWRNIIP HVAPTHRCIAPDLIG MGKSDKPDLGYFFDD HVRFMDAFIEALGLE EVVLVIHDWGSALGF HWAKRNPERVKGIAF MEFIRPIPTWDEWPE FARETFQAFRTTDVG RKLIIDQNVFIEGTL PMGVVRPLTEVEMDH YREPFLNPVDREPLW RFPNELPIAGEPANI VALVEEYMDWLHQSP VPKLLFWGTPGVLIP PAEAARLAKSLPNCK AVDIGPGLNLLQEDN PDLIGSEIARWLSTL EISGGGSNVSGWRLF KKISN*

ID	Vector	DNA sequence	Amino acid sequence
HaloTag-SmBiT86	pH6HTN	ATGAAACATCATCACCATCACCACGCAGAAATCGGTACTGGCTT TCCATTCGACCCCCATTATGTGGAAGTCCTGGGCGAGCGCATGC ACTACGTCGATGTTGGTCCGCGCGATGGCACCCCTGTGCTGTTC CTGCACGGTAACCCGACCTCCTCCTACGTGTGGCGCAACATCAT CCCGCATGTTGCACCGACCCATCGCTGCATTGCTCCAGACCTGA TCGGTATGGGCAAATCCGACAAACCAGACCTGGGTTATTTCTTC GACGACCACGTCCGCTTCATGGATGCCTTCATCGAAGCCCTGGG TCTGGAAGAGGTCGTCCTGGTCATTCACGACTGGGGCTCCGCTC TGGGTTTCCACTGGGCCAAGCGCAATCCAGAGCGCGTCAAAGGT ATTGCATTTATGGAGTTCATCCGCCCTATCCCGACCTGGGACGA ATGGCCAGAATTTGCCCGCGAGACCTTCCAGGCCTTCCGCACCA CCGACGTCGGCCGCAAGCTGATCATCGATCAGAACGTTTTTATC GAGGGTACGCTGCCGATGGGTGTCGTCCGCCCGCTGACTGAAGT CGAGATGGACCATTACCGCGAGCCGTTCCTGAATCCTGTTGACC GCGAGCCACTGTGGCGCTTCCCAAACGAGCTGCCAATCGCCGGT GAGCCAGCGAACATCGTCGCGCTGGTCGAAGAATACATGGACTG GCTGCACCAGTCCCCTGTCCCGAAGCTGCTGTTCTGGGGCACCC CAGGCGTTCTGATCCCACCGGCCGAAGCCGCTCGCCTGGCCAAA AGCCTGCCTAACTGCAAGGCTGTGGACATCGGCCCGGGTCTGAA TCTGCTGCAAGAAGACAACCCGGACCTGATCGGCAGCGAGATCG CGCGCTGGCTGTCGACGCTCGAGATTTCCGGCGGTGGTTCAGTA AGCGGGTGGCGGTTGTTCAAGAAGATCAGCTAA	MKHHHHHHAEIGTGF PFDPHYVEVLGERMH YVDVGPRDGTPVLFL HGNPTSSYVWRNIIP HVAPTHRCIAPDLIG MGKSDKPDLGYFFDD HVRFMDAFIEALGLE EVVLVIHDWGSALGF HWAKRNPERVKGIAF MEFIRPIPTWDEWPE FARETFQAFRTTDVG RKLIIDQNVFIEGTL PMGVVRPLTEVEMDH YREPFLNPVDREPLW RFPNELPIAGEPANI VALVEEYMDWLHQSP VPKLLFWGTPGVLIP PAEAARLAKSLPNCK AVDIGPGLNLLQEDN PDLIGSEIARWLSTL EISGGGSVSGWRLFK KIS*

ID	Vector	DNA sequence	Amino acid sequence
HaloTag-DarkBiT 1	pH6HTN	ATGAAACATCATCACCATCACCACGCAGAAATCGGTACTGGCTT TCCATTCGACCCCCATTATGTGGAAGTCCTGGGCGAGCGCATGC ACTACGTCGATGTTGGTCCGCGCGATGGCACCCCTGTGCTGTTC CTGCACGGTAACCCGACCTCCTCCTACGTGTGGCGCAACATCAT CCCGCATGTTGCACCGACCCATCGCTGCATTGCTCCAGACCTGA TCGGTATGGGCAAATCCGACAAACCAGACCTGGGTTATTTCTTC GACGACCACGTCCGCTTCATGGATGCCTTCATCGAAGCCCTGGG TCTGGAAGAGGTCGTCCTGGTCATTCACGACTGGGGCTCCGCTC TGGGTTTCCACTGGGCCAAGCGCAATCCAGAGCGCGTCAAAGGT ATTGCATTTATGGAGTTCATCCGCCCTATCCCGACCTGGGACGA ATGGCCAGAATTTGCCCGCGAGACCTTCCAGGCCTTCCGCACCA CCGACGTCGGCCGCAAGCTGATCATCGATCAGAACGTTTTTATC GAGGGTACGCTGCCGATGGGTGTCGTCCGCCCGCTGACTGAAGT CGAGATGGACCATTACCGCGAGCCGTTCCTGAATCCTGTTGACC GCGAGCCACTGTGGCGCTTCCCAAACGAGCTGCCAATCGCCGGT GAGCCAGCGAACATCGTCGCGCTGGTCGAAGAATACATGGACTG GCTGCACCAGTCCCCTGTCCCGAAGCTGCTGTTCTGGGGCACCC CAGGCGTTCTGATCCCACCGGCCGAAGCCGCTCGCCTGGCCAAA AGCCTGCCTAACTGCAAGGCTGTGGACATCGGCCCGGGTCTGAA TCTGCTGCAAGAAGACAACCCGGACCTGATCGGCAGCGAGATCG CGCGCTGGCTGTCGACGCTCGAGATTTCCGGCGGTGGTTCAGTG GAAGGTTACGCGCTGTTCGAAAAAATCTCATAA	MKHHHHHHAEIGTGF PFDPHYVEVLGERMH YVDVGPRDGTPVLFL HGNPTSSYVWRNIIP HVAPTHRCIAPDLIG MGKSDKPDLGYFFDD HVRFMDAFIEALGLE EVVLVIHDWGSALGF HWAKRNPERVKGIAF MEFIRPIPTWDEWPE FARETFQAFRTTDVG RKLIIDQNVFIEGTL PMGVVRPLTEVEMDH YREPFLNPVDREPLW RFPNELPIAGEPANI VALVEEYMDWLHQSP VPKLLFWGTPGVLIP PAEAARLAKSLPNCK AVDIGPGLNLLQEDN PDLIGSEIARWLSTL EISGGGSVEGYALFE KIS*

Supplementary Table 3. DNA and amino acid sequences of the six single-chain HaloTag-LgBiT-SmBiT fusions, one per SmBiT variant. The His affinity tag is shown in cyan, HaloTag in orange, LgBiT in blue, SmBiT in red.

ID	Vector	DNA sequence	Amino acid sequence
HaloTag-LgBiT-SmBiT230	pH6HTN	ATGAAACATCATCACCATCACCACGCAGAAATCGGTACTGGCTT TCCATTCGACCCCCATTATGTGGAAGTCCTGGGCGAGCGCATGC ACTACGTCGATGTTGGTCCGCGCGATGGCACCCCTGTGCTGTTC CTGCACGGTAACCCGACCTCCTCCTACGTGTGGCGCAACATCAT CCCGCATGTTGCACCGACCCATCGCTGCATTGCTCCAGACCTGA TCGGTATGGGCAAATCCGACAAACCAGACCTGGGTTATTTCTTC GACGACCACGTCCGCTTCATGGATGCCTTCATCGAAGCCCTGGG TCTGGAAGAGGTCGTCCTGGTCATTCACGACTGGGGCTCCGCTC TGGGTTTCCACTGGGCCAAGCGCAATCCAGAGCGCGTCAAAGGT ATTGCATTTATGGAGTTCATCCGCCCTATCCCGACCTGGGACGA ATGGCCAGAATTTGCCCGCGAGACCTTCCAGGCCTTCCGCACCA CCGACGTCGGCCGCAAGCTGATCATCGATCAGAACGTTTTTATC GAGGGTACGCTGCCGATGGGTGTCGTCCGCCCGCTGACTGAAGT CGAGATGGACCATTACCGCGAGCCGTTCCTGAATCCTGTTGACC GCGAGCCACTGTGGCGCTTCCCAAACGAGCTGCCAATCGCCGGT GAGCCAGCGAACATCGTCGCGCTGGTCGAAGAATACATGGACTG GCTGCACCAGTCCCCTGTCCCGAAGCTGCTGTTCTGGGGCACCC CAGGCGTTCTGATCCCACCGGCCGAAGCCGCTCGCCTGGCCAAA AGCCTGCCTAACTGCAAGGCTGTGGACATCGGCCCGGGTCTGAA TCTGCTGCAAGAAGACAACCCGGACCTGATCGGCAGCGAGATCG CGCGCTGGCTGTCGACGCTCGAGATTTCCGGCAGCGATAACATG GTCTTTACACTGGAGGATTTCGTCGGGGACTGGGAGCAAACGGC GGCCTACAACTTAGATCAAGTCTTAGAACAAGGCGGTGTCAGCA GCTTATTACAAAACCTTGCGGTTTCCGTAACCCCAATCCAACGC ATTGTCCGCTCGGGGGAGAATGCCTTAAAGATTGACATCCACGT CATTATCCCCTATGAGGGACTGTCCGCGGATCAAATGGCACAAA TTGAGGAGGTGTTCAAAGTAGTCTATCCCGTGGATGACCACCAC TTTAAGGTTATCTTACCATATGGAACGCTTGTAATTGACGGTGT AACCCCCAATATGCTGAACTACTTCGGGCGCCCATACGAGGGCA TTGCCGTCTTTGATGGGAAGAAAATTACGGTGACCGGGACCCTG TGGAACGGCAACAAAATCATTGACGAACGTTTAATCACCCCAGA TGGATCCATGTTGTTTCGCGTTACAATCAATGTGACTGGTTACA GACTTTTCGAGTAATAA	MKHHHHHHAEIGTGF PFDPHYVEVLGERMH YVDVGPRDGTPVLFL HGNPTSSYVWRNIIP HVAPTHRCIAPDLIG MGKSDKPDLGYFFDD HVRFMDAFIEALGLE EVVLVIHDWGSALGF HWAKRNPERVKGIAF MEFIRPIPTWDEWPE FARETFQAFRTTDVG RKLIIDQNVFIEGTL PMGVVRPLTEVEMDH YREPFLNPVDREPLW RFPNELPIAGEPANI VALVEEYMDWLHQSP VPKLLFWGTPGVLIP PAEAARLAKSLPNCK AVDIGPGLNLLQEDN PDLIGSEIARWLSTL EISGSDNMVFTLEDF VGDWEQTAAYNLDQV LEQGGVSSLLQNLAV SVTPIQRIVRSGENA LKIDIHVIIPYEGLS ADQMAQIEEVFKVVY PVDDHHFKVILPYGT LVIDGVTPNMLNYFG RPYEGIAVFDGKKIT VTGTLWNGNKIIDER LITPDGSMLFRVTIN VTGYRLFE*

ID	Vector	DNA sequence	Amino acid sequence
HaloTag-LgBiT-SmBiT114	pH6HTN	ATGAAACATCATCACCATCACCACGCAGAAATCGGTACTGGCTT TCCATTCGACCCCCATTATGTGGAAGTCCTGGGCGAGCGCATGC ACTACGTCGATGTTGGTCCGCGCGATGGCACCCCTGTGCTGTTC CTGCACGGTAACCCGACCTCCTCCTACGTGTGGCGCAACATCAT CCCGCATGTTGCACCGACCCATCGCTGCATTGCTCCAGACCTGA TCGGTATGGGCAAATCCGACAAACCAGACCTGGGTTATTTCTTC GACGACCACGTCCGCTTCATGGATGCCTTCATCGAAGCCCTGGG TCTGGAAGAGGTCGTCCTGGTCATTCACGACTGGGGCTCCGCTC TGGGTTTCCACTGGGCCAAGCGCAATCCAGAGCGCGTCAAAGGT ATTGCATTTATGGAGTTCATCCGCCCTATCCCGACCTGGGACGA ATGGCCAGAATTTGCCCGCGAGACCTTCCAGGCCTTCCGCACCA CCGACGTCGGCCGCAAGCTGATCATCGATCAGAACGTTTTTATC GAGGGTACGCTGCCGATGGGTGTCGTCCGCCCGCTGACTGAAGT CGAGATGGACCATTACCGCGAGCCGTTCCTGAATCCTGTTGACC GCGAGCCACTGTGGCGCTTCCCAAACGAGCTGCCAATCGCCGGT GAGCCAGCGAACATCGTCGCGCTGGTCGAAGAATACATGGACTG GCTGCACCAGTCCCCTGTCCCGAAGCTGCTGTTCTGGGGCACCC CAGGCGTTCTGATCCCACCGGCCGAAGCCGCTCGCCTGGCCAAA AGCCTGCCTAACTGCAAGGCTGTGGACATCGGCCCGGGTCTGAA TCTGCTGCAAGAAGACAACCCGGACCTGATCGGCAGCGAGATCG CGCGCTGGCTGTCGACGCTCGAGATTTCCGGCAGCGATAACATG GTCTTTACACTGGAGGATTTCGTCGGGGACTGGGAGCAAACGGC GGCCTACAACTTAGATCAAGTCTTAGAACAAGGCGGTGTCAGCA GCTTATTACAAAACCTTGCGGTTTCCGTAACCCCAATCCAACGC ATTGTCCGCTCGGGGGAGAATGCCTTAAAGATTGACATCCACGT CATTATCCCCTATGAGGGACTGTCCGCGGATCAAATGGCACAAA TTGAGGAGGTGTTCAAAGTAGTCTATCCCGTGGATGACCACCAC TTTAAGGTTATCTTACCATATGGAACGCTTGTAATTGACGGTGT AACCCCCAATATGCTGAACTACTTCGGGCGCCCATACGAGGGCA TTGCCGTCTTTGATGGGAAGAAAATTACGGTGACCGGGACCCTG TGGAACGGCAACAAAATCATTGACGAACGTTTAATCACCCCAGA TGGATCCATGTTGTTTCGCGTTACAATCAATGTGACTGGTTACA GACTTTTCGAGGAGATCCTTTAA	MKHHHHHHAEIGTGF PFDPHYVEVLGERMH YVDVGPRDGTPVLFL HGNPTSSYVWRNIIP HVAPTHRCIAPDLIG MGKSDKPDLGYFFDD HVRFMDAFIEALGLE EVVLVIHDWGSALGF HWAKRNPERVKGIAF MEFIRPIPTWDEWPE FARETFQAFRTTDVG RKLIIDQNVFIEGTL PMGVVRPLTEVEMDH YREPFLNPVDREPLW RFPNELPIAGEPANI VALVEEYMDWLHQSP VPKLLFWGTPGVLIP PAEAARLAKSLPNCK AVDIGPGLNLLQEDN PDLIGSEIARWLSTL EISGSDNMVFTLEDF VGDWEQTAAYNLDQV LEQGGVSSLLQNLAV SVTPIQRIVRSGENA LKIDIHVIIPYEGLS ADQMAQIEEVFKVVY PVDDHHFKVILPYGT LVIDGVTPNMLNYFG RPYEGIAVFDGKKIT VTGTLWNGNKIIDER LITPDGSMLFRVTIN VTGYRLFEEIL*
HaloTag-LgBiT-SmBiT104	pH6HTN	ATGAAACATCATCACCATCACCACGCAGAAATCGGTACTGGCTT TCCATTCGACCCCCATTATGTGGAAGTCCTGGGCGAGCGCATGC ACTACGTCGATGTTGGTCCGCGCGATGGCACCCCTGTGCTGTTC CTGCACGGTAACCCGACCTCCTCCTACGTGTGGCGCAACATCAT CCCGCATGTTGCACCGACCCATCGCTGCATTGCTCCAGACCTGA TCGGTATGGGCAAATCCGACAAACCAGACCTGGGTTATTTCTTC GACGACCACGTCCGCTTCATGGATGCCTTCATCGAAGCCCTGGG TCTGGAAGAGGTCGTCCTGGTCATTCACGACTGGGGCTCCGCTC TGGGTTTCCACTGGGCCAAGCGCAATCCAGAGCGCGTCAAAGGT ATTGCATTTATGGAGTTCATCCGCCCTATCCCGACCTGGGACGA ATGGCCAGAATTTGCCCGCGAGACCTTCCAGGCCTTCCGCACCA CCGACGTCGGCCGCAAGCTGATCATCGATCAGAACGTTTTTATC GAGGGTACGCTGCCGATGGGTGTCGTCCGCCCGCTGACTGAAGT CGAGATGGACCATTACCGCGAGCCGTTCCTGAATCCTGTTGACC GCGAGCCACTGTGGCGCTTCCCAAACGAGCTGCCAATCGCCGGT GAGCCAGCGAACATCGTCGCGCTGGTCGAAGAATACATGGACTG GCTGCACCAGTCCCCTGTCCCGAAGCTGCTGTTCTGGGGCACCC CAGGCGTTCTGATCCCACCGGCCGAAGCCGCTCGCCTGGCCAAA AGCCTGCCTAACTGCAAGGCTGTGGACATCGGCCCGGGTCTGAA TCTGCTGCAAGAAGACAACCCGGACCTGATCGGCAGCGAGATCG CGCGCTGGCTGTCGACGCTCGAGATTTCCGGCAGCGATAACATG GTCTTTACACTGGAGGATTTCGTCGGGGACTGGGAGCAAACGGC GGCCTACAACTTAGATCAAGTCTTAGAACAAGGCGGTGTCAGCA GCTTATTACAAAACCTTGCGGTTTCCGTAACCCCAATCCAACGC ATTGTCCGCTCGGGGGAGAATGCCTTAAAGATTGACATCCACGT CATTATCCCCTATGAGGGACTGTCCGCGGATCAAATGGCACAAA TTGAGGAGGTGTTCAAAGTAGTCTATCCCGTGGATGACCACCAC TTTAAGGTTATCTTACCATATGGAACGCTTGTAATTGACGGTGT AACCCCCAATATGCTGAACTACTTCGGGCGCCCATACGAGGGCA TTGCCGTCTTTGATGGGAAGAAAATTACGGTGACCGGGACCCTG TGGAACGGCAACAAAATCATTGACGAACGTTTAATCACCCCAGA TGGATCCATGTTGTTTCGCGTTACAATCAATGTGGAAGGTTACA GACTTTTCGAGAAGATCAGCTAA	MKHHHHHHAEIGTGF PFDPHYVEVLGERMH YVDVGPRDGTPVLFL HGNPTSSYVWRNIIP HVAPTHRCIAPDLIG MGKSDKPDLGYFFDD HVRFMDAFIEALGLE EVVLVIHDWGSALGF HWAKRNPERVKGIAF MEFIRPIPTWDEWPE FARETFQAFRTTDVG RKLIIDQNVFIEGTL PMGVVRPLTEVEMDH YREPFLNPVDREPLW RFPNELPIAGEPANI VALVEEYMDWLHQSP VPKLLFWGTPGVLIP PAEAARLAKSLPNCK AVDIGPGLNLLQEDN PDLIGSEIARWLSTL EISGSDNMVFTLEDF VGDWEQTAAYNLDQV LEQGGVSSLLQNLAV SVTPIQRIVRSGENA LKIDIHVIIPYEGLS ADQMAQIEEVFKVVY PVDDHHFKVILPYGT LVIDGVTPNMLNYFG RPYEGIAVFDGKKIT VTGTLWNGNKIIDER LITPDGSMLFRVTIN VEGYRLFEKIS*

ID	Vector	DNA sequence	Amino acid sequence
HaloTag-LgBiT-SmBiT99	pH6HTN	ATGAAACATCATCACCATCACCACGCAGAAATCGGTACTGGCTT TCCATTCGACCCCCATTATGTGGAAGTCCTGGGCGAGCGCATGC ACTACGTCGATGTTGGTCCGCGCGATGGCACCCCTGTGCTGTTC CTGCACGGTAACCCGACCTCCTCCTACGTGTGGCGCAACATCAT CCCGCATGTTGCACCGACCCATCGCTGCATTGCTCCAGACCTGA TCGGTATGGGCAAATCCGACAAACCAGACCTGGGTTATTTCTTC GACGACCACGTCCGCTTCATGGATGCCTTCATCGAAGCCCTGGG TCTGGAAGAGGTCGTCCTGGTCATTCACGACTGGGGCTCCGCTC TGGGTTTCCACTGGGCCAAGCGCAATCCAGAGCGCGTCAAAGGT ATTGCATTTATGGAGTTCATCCGCCCTATCCCGACCTGGGACGA ATGGCCAGAATTTGCCCGCGAGACCTTCCAGGCCTTCCGCACCA CCGACGTCGGCCGCAAGCTGATCATCGATCAGAACGTTTTTATC GAGGGTACGCTGCCGATGGGTGTCGTCCGCCCGCTGACTGAAGT CGAGATGGACCATTACCGCGAGCCGTTCCTGAATCCTGTTGACC GCGAGCCACTGTGGCGCTTCCCAAACGAGCTGCCAATCGCCGGT GAGCCAGCGAACATCGTCGCGCTGGTCGAAGAATACATGGACTG GCTGCACCAGTCCCCTGTCCCGAAGCTGCTGTTCTGGGGCACCC CAGGCGTTCTGATCCCACCGGCCGAAGCCGCTCGCCTGGCCAAA AGCCTGCCTAACTGCAAGGCTGTGGACATCGGCCCGGGTCTGAA TCTGCTGCAAGAAGACAACCCGGACCTGATCGGCAGCGAGATCG CGCGCTGGCTGTCGACGCTCGAGATTTCCGGCAGCGATAACATG GTCTTTACACTGGAGGATTTCGTCGGGGACTGGGAGCAAACGGC GGCCTACAACTTAGATCAAGTCTTAGAACAAGGCGGTGTCAGCA GCTTATTACAAAACCTTGCGGTTTCCGTAACCCCAATCCAACGC ATTGTCCGCTCGGGGGAGAATGCCTTAAAGATTGACATCCACGT CATTATCCCCTATGAGGGACTGTCCGCGGATCAAATGGCACAAA TTGAGGAGGTGTTCAAAGTAGTCTATCCCGTGGATGACCACCAC TTTAAGGTTATCTTACCATATGGAACGCTTGTAATTGACGGTGT AACCCCCAATATGCTGAACTACTTCGGGCGCCCATACGAGGGCA TTGCCGTCTTTGATGGGAAGAAAATTACGGTGACCGGGACCCTG TGGAACGGCAACAAAATCATTGACGAACGTTTAATCACCCCAGA TGGATCCATGTTGTTTCGCGTTACAATCAATGTGACTGGTTACA GACTTTTCGAGAAGATCAGCTAA	MKHHHHHHAEIGTGF PFDPHYVEVLGERMH YVDVGPRDGTPVLFL HGNPTSSYVWRNIIP HVAPTHRCIAPDLIG MGKSDKPDLGYFFDD HVRFMDAFIEALGLE EVVLVIHDWGSALGF HWAKRNPERVKGIAF MEFIRPIPTWDEWPE FARETFQAFRTTDVG RKLIIDQNVFIEGTL PMGVVRPLTEVEMDH YREPFLNPVDREPLW RFPNELPIAGEPANI VALVEEYMDWLHQSP VPKLLFWGTPGVLIP PAEAARLAKSLPNCK AVDIGPGLNLLQEDN PDLIGSEIARWLSTL EISGSDNMVFTLEDF VGDWEQTAAYNLDQV LEQGGVSSLLQNLAV SVTPIQRIVRSGENA LKIDIHVIIPYEGLS ADQMAQIEEVFKVVY PVDDHHFKVILPYGT LVIDGVTPNMLNYFG RPYEGIAVFDGKKIT VTGTLWNGNKIIDER LITPDGSMLFRVTIN VTGYRLFEKIS*

ID	Vector	DNA sequence	Amino acid sequence
HaloTag-LgBiT-SmBiT78	pH6HTN	ATGAAACATCATCACCATCACCACGCAGAAATCGGTACTGGCTT TCCATTCGACCCCCATTATGTGGAAGTCCTGGGCGAGCGCATGC ACTACGTCGATGTTGGTCCGCGCGATGGCACCCCTGTGCTGTTC CTGCACGGTAACCCGACCTCCTCCTACGTGTGGCGCAACATCAT CCCGCATGTTGCACCGACCCATCGCTGCATTGCTCCAGACCTGA TCGGTATGGGCAAATCCGACAAACCAGACCTGGGTTATTTCTTC GACGACCACGTCCGCTTCATGGATGCCTTCATCGAAGCCCTGGG TCTGGAAGAGGTCGTCCTGGTCATTCACGACTGGGGCTCCGCTC TGGGTTTCCACTGGGCCAAGCGCAATCCAGAGCGCGTCAAAGGT ATTGCATTTATGGAGTTCATCCGCCCTATCCCGACCTGGGACGA ATGGCCAGAATTTGCCCGCGAGACCTTCCAGGCCTTCCGCACCA CCGACGTCGGCCGCAAGCTGATCATCGATCAGAACGTTTTTATC GAGGGTACGCTGCCGATGGGTGTCGTCCGCCCGCTGACTGAAGT CGAGATGGACCATTACCGCGAGCCGTTCCTGAATCCTGTTGACC GCGAGCCACTGTGGCGCTTCCCAAACGAGCTGCCAATCGCCGGT GAGCCAGCGAACATCGTCGCGCTGGTCGAAGAATACATGGACTG GCTGCACCAGTCCCCTGTCCCGAAGCTGCTGTTCTGGGGCACCC CAGGCGTTCTGATCCCACCGGCCGAAGCCGCTCGCCTGGCCAAA AGCCTGCCTAACTGCAAGGCTGTGGACATCGGCCCGGGTCTGAA TCTGCTGCAAGAAGACAACCCGGACCTGATCGGCAGCGAGATCG CGCGCTGGCTGTCGACGCTCGAGATTTCCGGCAGCGATAACATG GTCTTTACACTGGAGGATTTCGTCGGGGACTGGGAGCAAACGGC GGCCTACAACTTAGATCAAGTCTTAGAACAAGGCGGTGTCAGCA GCTTATTACAAAACCTTGCGGTTTCCGTAACCCCAATCCAACGC ATTGTCCGCTCGGGGGAGAATGCCTTAAAGATTGACATCCACGT CATTATCCCCTATGAGGGACTGTCCGCGGATCAAATGGCACAAA TTGAGGAGGTGTTCAAAGTAGTCTATCCCGTGGATGACCACCAC TTTAAGGTTATCTTACCATATGGAACGCTTGTAATTGACGGTGT AACCCCCAATATGCTGAACTACTTCGGGCGCCCATACGAGGGCA TTGCCGTCTTTGATGGGAAGAAAATTACGGTGACCGGGACCCTG TGGAACGGCAACAAAATCATTGACGAACGTTTAATCACCCCAGA TGGATCCATGTTGTTTCGCGTTACAATCAATAATGTGAGTGGTT GGAGACTTTTCAAGAAAATCAGTAATTAA	MKHHHHHHAEIGTGF PFDPHYVEVLGERMH YVDVGPRDGTPVLFL HGNPTSSYVWRNIIP HVAPTHRCIAPDLIG MGKSDKPDLGYFFDD HVRFMDAFIEALGLE EVVLVIHDWGSALGF HWAKRNPERVKGIAF MEFIRPIPTWDEWPE FARETFQAFRTTDVG RKLIIDQNVFIEGTL PMGVVRPLTEVEMDH YREPFLNPVDREPLW RFPNELPIAGEPANI VALVEEYMDWLHQSP VPKLLFWGTPGVLIP PAEAARLAKSLPNCK AVDIGPGLNLLQEDN PDLIGSEIARWLSTL EISGSDNMVFTLEDF VGDWEQTAAYNLDQV LEQGGVSSLLQNLAV SVTPIQRIVRSGENA LKIDIHVIIPYEGLS ADQMAQIEEVFKVVY PVDDHHFKVILPYGT LVIDGVTPNMLNYFG RPYEGIAVFDGKKIT VTGTLWNGNKIIDER LITPDGSMLFRVTIN NVSGWRLFKKISN*

ID	Vector	DNA sequence	Amino acid sequence
HaloTag-LgBiT-SmBiT86	pH6HTN	ATGAAACATCATCACCATCACCACGCAGAAATCGGTACTGGCTT TCCATTCGACCCCCATTATGTGGAAGTCCTGGGCGAGCGCATGC ACTACGTCGATGTTGGTCCGCGCGATGGCACCCCTGTGCTGTTC CTGCACGGTAACCCGACCTCCTCCTACGTGTGGCGCAACATCAT CCCGCATGTTGCACCGACCCATCGCTGCATTGCTCCAGACCTGA TCGGTATGGGCAAATCCGACAAACCAGACCTGGGTTATTTCTTC GACGACCACGTCCGCTTCATGGATGCCTTCATCGAAGCCCTGGG TCTGGAAGAGGTCGTCCTGGTCATTCACGACTGGGGCTCCGCTC TGGGTTTCCACTGGGCCAAGCGCAATCCAGAGCGCGTCAAAGGT ATTGCATTTATGGAGTTCATCCGCCCTATCCCGACCTGGGACGA ATGGCCAGAATTTGCCCGCGAGACCTTCCAGGCCTTCCGCACCA CCGACGTCGGCCGCAAGCTGATCATCGATCAGAACGTTTTTATC GAGGGTACGCTGCCGATGGGTGTCGTCCGCCCGCTGACTGAAGT CGAGATGGACCATTACCGCGAGCCGTTCCTGAATCCTGTTGACC GCGAGCCACTGTGGCGCTTCCCAAACGAGCTGCCAATCGCCGGT GAGCCAGCGAACATCGTCGCGCTGGTCGAAGAATACATGGACTG GCTGCACCAGTCCCCTGTCCCGAAGCTGCTGTTCTGGGGCACCC CAGGCGTTCTGATCCCACCGGCCGAAGCCGCTCGCCTGGCCAAA AGCCTGCCTAACTGCAAGGCTGTGGACATCGGCCCGGGTCTGAA TCTGCTGCAAGAAGACAACCCGGACCTGATCGGCAGCGAGATCG CGCGCTGGCTGTCGACGCTCGAGATTTCCGGCAGCGATAACATG GTCTTTACACTGGAGGATTTCGTCGGGGACTGGGAGCAAACGGC GGCCTACAACTTAGATCAAGTCTTAGAACAAGGCGGTGTCAGCA GCTTATTACAAAACCTTGCGGTTTCCGTAACCCCAATCCAACGC ATTGTCCGCTCGGGGGAGAATGCCTTAAAGATTGACATCCACGT CATTATCCCCTATGAGGGACTGTCCGCGGATCAAATGGCACAAA TTGAGGAGGTGTTCAAAGTAGTCTATCCCGTGGATGACCACCAC TTTAAGGTTATCTTACCATATGGAACGCTTGTAATTGACGGTGT AACCCCCAATATGCTGAACTACTTCGGGCGCCCATACGAGGGCA TTGCCGTCTTTGATGGGAAGAAAATTACGGTGACCGGGACCCTG TGGAACGGCAACAAAATCATTGACGAACGTTTAATCACCCCAGA TGGATCCATGTTGTTTCGCGTTACAATCAATGTGAGTGGTTGGA GACTTTTCAAGAAAATCAGTTAA	MKHHHHHHAEIGTGF PFDPHYVEVLGERMH YVDVGPRDGTPVLFL HGNPTSSYVWRNIP HVAPTHRCIAPDLIG MGKSDKPDLGYFFDD HVRFMDAFIEALGLE EVVLVIHDWGSALGF HWAKRNPERVKGIAF MEFIRPIPTWDEWPE FARETFQAFRTTDVG RKLIIDQNVFIEGTL PMGVVRPLTEVEMDH YREPFLNPVDREPLW RFPNELPIAGEPANI VALVEEYMDWLHQSP VPKLLFWGTPGVLIP PAEAARLAKSLPNCK AVDIGPGLNLLQEDN PDLIGSEIARWLSTL EISGSDNMVFTLEDF VGDWEQTAAYNLDQV LEQGGVSSLLQNLAV SVTPIQRIVRSGENA LKIDIHVIIPYEGLS ADQMAQIEEVFKVVY PVDDHHFKVILPYGT LVIDGVTPNMLNYFG RPYEGIAVFDGKKIT VTGTLWNGNKIIDER LITPDGSMLFRVTIN VSGWRLFKKIS*

Supplementary Table 4. DNA and amino acid sequences of the HaloTag-TLN1 and LgBiT-HaloTag-ITGB1A constructs. The His affinity tag is shown in cyan, HaloTag in orange, LgBiT in blue, ITGB1A in green, and TLN1 in purple.

ID	Vector	DNA sequence	Amino acid sequence
HaloTag-TLN1	t1_405-Bls-Pre_S	ATGGGGGGTTCTCATCATCATCATCATCATGGTTTGAATGATAT TTTCGAAGCACAGAAAATTGAATGGCATGAGGCAGAAATCGGTA CTGGCTTTCCATTCGACCCCCATTATGTGGAAGTCCTGGGCGAG CGCATGCACTACGTCGATGTTGGTCCGCGCGATGGCACCCCTGT GCTGTTCCTGCACGGTAACCCGACCTCCTCCTACGTGTGGCGCA ACATCATCCCGCATGTTGCACCGACCCATCGCTGCATTGCTCCA GACCTGATCGGTATGGGCAAATCCGACAAACCAGACCTGGGTTA TTTCTTCGACGACCACGTCCGCTTCATGGATGCCTTCATCGAAG CCCTGGGTCTGGAAGAGGTCGTCCTGGTCATTCACGACTGGGGC TCCGCTCTGGGTTTCCACTGGGCCAAGCGCAATCCAGAGCGCGT CAAAGGTATTGCATTTATGGAGTTCATCCGCCCTATCCCGACCT GGGACGAATGGCCAGAATTTGCCCGCGAGACCTTCCAGGCCTTC CGCACCACCGACGTCGGCCGCAAGCTGATCATCGATCAGAACGT TTTTATCGAGGGTACGCTGCCGATGGGTGTCGTCCGCCCGCTGA CTGAAGTCGAGATGGACCATTACCGCGAGCCGTTCCTGAATCCT GTTGACCGCGAGCCACTGTGGCGCTTCCCAAACGAGCTGCCAAT CGCCGGTGAGCCAGCGAACATCGTCGCGCTGGTCGAAGAATACA TGGACTGGCTGCACCAGTCCCCTGTCCCGAAGCTGCTGTTCTGG GGCACCCCAGGCGTTCTGATCCCACCGGCCGAAGCCGCTCGCCT GGCCAAAAGCCTGCCTAACTGCAAGGCTGTGGACATCGGCCCGG GTCTGAATCTGCTGCAAGAAGACAACCCGGACCTGATCGGCAGC GAGATCGCGCGCTGGCTGTCGACGCTCGAGATTTCCGGCCGAGC CATGGTTGCACTTTCACTGAAGATCAGCATTGGGAATGTGGTGA AGACGATGCAGTTTGAGCCGTCTACCATGGTGTACGACGCCTGC CGCATCATTCGTGAGCGGATCCCAGAGGCCCCAGCTGGTCCTCC CAGCGACTTTGGGCTCTTTCTGTCAGATGATGACCCCAAAAAGG GTATATGGCTGGAGGCTGGGAAAGCTTTGGACTACTACATGCTC CGAAATGGGGACACTATGGAGTACAGGAAGAAACAGAGACCCCT GAAGATCCGTATGCTGGATGGAACTGTGAAGACGATCATGGTGG ATGACTCTAAGACTGTCACTGACATGCTCATGACCATCTGTGCC CGCATTGGCATCACCAATCATGATGAATATTCATTGGTTCGAGA GCTGATGGAAGAGAAAAAGGAGGAAATAACAGGGACCTTAAGAA AGGACAAGACATTGCTGCGAGATGAAAAGAAGATGGAGAAACTA AAGCAGAAATTGCACACAGATGATGAGTTGAACTGGCTGGACCA TGGTCGGACACTGAGGGAGCAGGGTGTAGAGGAGCACGAGACGC TGCTGCTGCGGAGGAAGTTCTTTTACTCAGACCAGAATGTGGAT TCCCGGGACCCTGTACAGCTGAACCTCCTGTATGTGCAGGCACG AGATGACATCCTGAATGGCTCCCACCCTGTCTCCTTTGACAAGG CCTGTGAGTTTGCTGGCTTCCAATGCCAGATCCAGTTTGGGCCC CACAATGAGCAGAAGCACAAGGCTGGCTTCCTTGACCTGAAGGA CTTCCTGCCCAAGGAGTATGTGAAGCAGAAGGGAGAGCGTAAGA TCTTCCAGGCACACAAGAATTGTGGGCAGATGAGTGAGATTGAG GCCAAGGTCCGCTACGTGAAGCTAGCCCGTTCTCTCAAGACTTA CGGTGTCTCCTTCTTCCTGGTGAAGGAAAAAATGAAAGGGAAGA ACAAGCTAGTGCCCAGGCTTCTGGGCATCACCAAGGAGTGTGTG ATGCGAGTGGATGAGAAGACCAAGGAAGTGATCCAGGAGTGGAA CCTCACCAACATCAAACGCTGGGCTGCGTCTCCCAAAAGCTTCA CCCTGGATTTTGGAGATTACCAAGATGGCTATTACTCAGTACAG ACAACTGAAGGGGAGCAGATTGCACAGCTCATTGCCGGCTACAT CGATATCATCCTGAAGAAGAAAAAAAGCTAATGA	MGGSHHHHHHGLNDI FEAQKIEWHEAEIGT GFPFDPHYVEVLGER MHYVDVGPRDGTPVL FLHGNPTSSYVWRNI IPHVAPTHRCIAPDL IGMGKSDKPDLGYFF DDHVRFMDAFIEALG LEEVVLVIHDWGSAL GFHWAKRNPERVKGI AFMEFIRPIPTWDEW PEFARETFQAFRTTD VGRKLIIDQNVFIEG TLPMGVVRPLTEVEM DHYREPFLNPVDREP LWRFPNELPIAGEPA NIVALVEEYMDWLHQ SPVPKLLFWGTPGVL IPPAEAARLAKSLPN CKAVDIGPGLNLLQE DNPDLIGSEIARWLS TLEISGRAMVALSLK ISIGNVVKTMQFEPS TMVYDACRIIRERIP EAPAGPPSDFGLFLS DDDPKKGIWLEAGKA LDYYMLRNGDTMEYR KKQRPLKIRMLDGTV KTIMVDDSKTVTDML MTICARIGITNHDEY SLVRELMEEKKEEIT GTLRKDKTLLRDEKK MEKLKQKLHTDDELN WLDHGRTLREQGVEE HETLLLRRKFFYSDQ NVDSRDPVQLNLLYV QARDDILNGSHPVSF DKACEFAGFQCQIQF GPHNEQKHKAGFLDL KDFLPKEYVKQKGER KIFQAHKNCGQMSEI EAKVRYVKLARSLKT YGVSFFLVKEKMKGK NKLVPRLLGITKECV MRVDEKTKEVIQEWN LTNIKRWAASPKSFT LDFGDYQDGYYSVQT TEGEQIAQLIAGYID IILKKKKS**

ID	Vector	DNA sequence	Amino acid sequence
LgBiT-HaloTag-ITGB1A	pET15b	ATGGGCAGCAGCCATCATCATCATCATCACAGCAGCGGCGAAGA TTACAAGGATGACGATGACAAGCGTACCGGTATGGTCTTTACAC TGGAGGATTTCGTCGGGGACTGGGAGCAAACGGCGGCCTACAAC TTAGATCAAGTCTTAGAACAAGGCGGTGTCAGCAGCTTATTACA AAACCTTGCGGTTTCCGTAACCCCAATCCAACGCATTGTCCGCT CGGGGGAGAATGCCTTAAAGATTGACATCCACGTCATTATCCCC TATGAGGGACTGTCCGCGGATCAAATGGCACAAATTGAGGAGGT GTTCAAAGTAGTCTATCCCGTGGATGACCACCACTTTAAGGTTA TCTTACCATATGGAACGCTTGTAATTGACGGTGTAACCCCCAAT ATGCTGAACTACTTCGGGCGCCCATACGAGGGCATTGCCGTCTT TGATGGGAAGAAAATTACGGTGACCGGGACCCTGTGGAACGGCA ACAAAATCATTGACGAACGTTTAATCACCCCAGATGGATCCATG TTGTTTCGCGTTACAATCAATTCGAAATGTCTCGAGGCAGAAAT CGGTACTGGCTTTCCATTCGACCCCCATTATGTGGAAGTCCTGG GCGAGCGCATGCACTACGTCGATGTTGGTCCGCGCGATGGCACC CCTGTGCTGTTCCTGCACGGTAACCCGACCTCCTCCTACGTGTG GCGCAACATCATCCCGCATGTTGCACCGACCCATCGCTGCATTG CTCCAGACCTGATCGGTATGGGCAAATCCGACAAACCAGACCTG GGTTATTTCTTCGACGACCACGTCCGCTTCATGGATGCCTTCAT CGAAGCCCTGGGTCTGGAAGAGGTCGTCCTGGTCATTCACGACT GGGGCTCCGCTCTGGGTTTCCACTGGGCCAAGCGCAATCCAGAG CGCGTCAAAGGTATTGCATTTATGGAGTTCATCCGCCCTATCCC GACCTGGGACGAATGGCCAGAATTTGCCCGCGAGACCTTCCAGG CCTTCCGCACCACCGACGTCGGCCGCAAGCTGATCATCGATCAG AACGTTTTTATCGAGGGTACGCTGCCGATGGGTGTCGTCCGCCC GCTGACTGAAGTCGAGATGGACCATTACCGCGAGCCGTTCCTGA ATCCTGTTGACCGCGAGCCACTGTGGCGCTTCCCAAACGAGCTG CCAATCGCCGGTGAGCCAGCGAACATCGTCGCGCTGGTCGAAGA ATACATGGACTGGCTGCACCAGTCCCCTGTCCCGAAGCTGCTGT TCTGGGGCACCCCAGGCGTTCTGATCCCACCGGCCGAAGCCGCT CGCCTGGCCAAAAGCCTGCCTAACTGCAAGGCTGTGGACATCGG CCCGGGTCTGAATCTGCTGCAAGAAGACAACCCGGACCTGATCG GCAGCGAGATCGCGCGCTGGCTGTCGACGCTCGAGATTTCCGGC CTGGTTCCGCGTCCATGGTCGAATCAAACAAGTTTGTACAAAAA AGCTGAACGCCACCCACCACCACCAGGCCTTGCATTACTGCTGA TATGGAAGCTTTTAATGATAATTCATGACAGAAGGGAGTTTGCT AAATTTGAAAAGGAGAAAATGAATGCCAAATGGGACACGGGTGA AAATCCTATTTATAAGAGTGCCGTAACAACTGTGGTCAATCCGA AGTATGAGGGAAAATGA	MGSSHHHHHHSSGED YKDDDDKRTGVFTLE DFVGDWEQTAAYNLD QVLEQGGVSSLLQNL AVSVTPIQRIVRSGE NALKIDIHVIIPYEG LSADQMAQIEEVFKV VYPVDDHHFKVILPY GTLVIDGVTPNMLNY FGRPYEGIAVFDGKK ITVTGTLWNGNKIID ERLITPDGSMLFRVT INSKCLEAEIGTGFP FDPHYVEVLGERMHY VDVGPRDGTPVLFLH GNPTSSYVWRNIIPH VAPTHRCIAPDLIGM GKSDKPDLGYFFDDH VRFMDAFIEALGLEE VVLVIHDWGSALGFH WAKRNPERVKGIAFM EFIRPIPTWDEWPEF ARETFQAFRTTDVGR KLIIDQNVFIEGTLP MGVVRPLTEVEMDHY REPFLNPVDREPLWR FPNELPIAGEPANIV ALVEEYMDWLHQSPV PKLLFWGTPGVLIPP AEAARLAKSLPNCKA VDIGPGLNLLQEDNP DLIGSEIARWLSTLE ISGLVPRPWSNQTSL YKKAERHPPPPGLAL LLIWKLLMIIHDRRE FAKFEKEKMNAKWDT GENPIYKSAVTTVVN PKYEGK*

Supplementary Table 5. Peptide sequences and modifications. Pep1–Pep3 are the screening peptides in Fig. 6b; DarkBiT 2 is the soluble competitor titrated in Fig. 5.

ID	Amino acid sequence	Modification	Article info.
ITGB3	KFEEERARAKWDT	*N*-terminal myristoylation	Ref.[50]
Pep1 (non-binding control)	KAEKEKMNAKADT	*N*-terminal myristoylation	this work
Pep2 (primary screening hit)	KFEEERMRCKWMT	*N*-terminal myristoylation	this work
Pep3 (= compound **1**)	KFEEERSRCKWMT	*N*-terminal myristoylation	this work
DarkBiT **2** (the free DarkBiT)	VTGYALFEKES		Ref.[29]

Supplementary Table 6. DNA sequences of the chemically modified single-stranded DNAs (ssDNAs) used to synthesize the AccuLinkers. The 5′ and 3′ modifications are listed. Cy3 denotes the cyanine 3 dye. Tethering helix denotes the duplex to which the AccuLinker hybridizes; the helix numbering follows Supplementary Fig. S5.

No.	Oligo_sequence (5′ to 3′)	5′ modification	3′ modification	Tethering helix
1	GGTGATGATGGTTTGG	Azide	Cy3	29
2	CTTCTCCATTTTCCAG	Azide	Cy3	45
3	GTGATTTGAAAGTTGC	Cy3	Azide	67
4	CACGTAACAAGATCCC	Azide	Cy3	91
5	TTTTCTACTCTTCACG	Azide	Cy3	175

Supplementary Table 7. Chemical information of synthetic AccuLinkers. 5′ and 3′ indicate 5′ modification and 3′ modification of AccuLinker, respectively. HL, HaloTag ligand; LL, linker length; TH, tethering helix. LL is the maximum distance between the DB01 wall and the tethered HaloTag protein, shown schematically in Supplementary Fig. S13. In the identifier AccuLinker_n_X, n is the number of OEG units and X the tethering helix. The helix numbering follows Supplementary Fig. S5.

ID	Oligo_sequence (5′ to 3′)	5′	3′	OEGn	LL [nm]	TH
AccuLinker_0_29	GGTGATGATGGTTTGG	HL	Cy3	0	1.0	29
AccuLinker_4_29	GGTGATGATGGTTTGG	HL	Cy3	4	4.1	29
AccuLinker_14_29	GGTGATGATGGTTTGG	HL	Cy3	14	7.6	29
AccuLinker_17_29	GGTGATGATGGTTTGG	HL	Cy3	17	9.0	29
AccuLinker_22_29	GGTGATGATGGTTTGG	HL	Cy3	22	10.7	29
AccuLinker_27_29	GGTGATGATGGTTTGG	HL	Cy3	27	12.5	29
AccuLinker_32_29	GGTGATGATGGTTTGG	HL	Cy3	32	14.2	29
AccuLinker_0_45	CTTCTCCATTTTCCAG	HL	Cy3	0	1.0	45
AccuLinker_4_45	CTTCTCCATTTTCCAG	HL	Cy3	4	4.1	45
AccuLinker_14_45	CTTCTCCATTTTCCAG	HL	Cy3	14	7.6	45
AccuLinker_17_45	CTTCTCCATTTTCCAG	HL	Cy3	17	9.0	45
AccuLinker_22_45	CTTCTCCATTTTCCAG	HL	Cy3	22	10.7	45
AccuLinker_27_45	CTTCTCCATTTTCCAG	HL	Cy3	27	12.5	45
AccuLinker_32_45	CTTCTCCATTTTCCAG	HL	Cy3	32	14.2	45

ID	Oligo_sequence (5′ to 3′)	5′	3′	OEGn	LL [nm]	TH
AccuLinker_0_67	GTGATTTGAAAGTTGC	Cy3	HL	0	1.0	67
AccuLinker_4_67	GTGATTTGAAAGTTGC	Cy3	HL	4	4.1	67
AccuLinker_14_67	GTGATTTGAAAGTTGC	Cy3	HL	14	7.6	67
AccuLinker_17_67	GTGATTTGAAAGTTGC	Cy3	HL	17	9.0	67
AccuLinker_22_67	GTGATTTGAAAGTTGC	Cy3	HL	22	10.7	67
AccuLinker_27_67	GTGATTTGAAAGTTGC	Cy3	HL	27	12.5	67
AccuLinker_32_67	GTGATTTGAAAGTTGC	Cy3	HL	32	14.2	67
AccuLinker_0_91	CACGTAACAAGATCCC	HL	Cy3	0	1.0	91
AccuLinker_4_91	CACGTAACAAGATCCC	HL	Cy3	4	4.1	91
AccuLinker_14_91	CACGTAACAAGATCCC	HL	Cy3	14	7.6	91
AccuLinker_17_91	CACGTAACAAGATCCC	HL	Cy3	17	9.0	91
AccuLinker_22_91	CACGTAACAAGATCCC	HL	Cy3	22	10.7	91
AccuLinker_27_91	CACGTAACAAGATCCC	HL	Cy3	27	12.5	91
AccuLinker_32_91	CACGTAACAAGATCCC	HL	Cy3	32	14.2	91
AccuLinker_0_175	TTTTCTACTCTTCACG	HL	Cy3	0	1.0	175
AccuLinker_4_175	TTTTCTACTCTTCACG	HL	Cy3	4	4.1	175
AccuLinker_14_175	TTTTCTACTCTTCACG	HL	Cy3	14	7.6	175
AccuLinker_17_175	TTTTCTACTCTTCACG	HL	Cy3	17	9.0	175
AccuLinker_22_175	TTTTCTACTCTTCACG	HL	Cy3	22	10.7	175
AccuLinker_27_175	TTTTCTACTCTTCACG	HL	Cy3	27	12.5	175
AccuLinker_32_175	TTTTCTACTCTTCACG	HL	Cy3	32	14.2	175

Supplementary Table 8. Sequences of ssDNA overhangs for protein tethering in DB01. The helix numbering follows Supplementary Fig. S5. The 16-nt sequence shown in red is a protein tethering sequence, complementary to the ssDNA end of the AccuLinker, whereas the sequence shown in black is a DB01-folding sequence. Blue text in between is a spacer within the DB01 strand, shown in Supplementary Fig. S5b,c; the supplier part codes denote a C3 (propanediol) spacer (iSpC3), a triethylene glycol spacer (iSp9) and a hexaethylene glycol spacer (iSp18). The side, back, and front positions are illustrated schematically in Supplementary Fig. S5b.

helix	Oligo_sequence (5′ to 3′)	DNA Position
29	CCAAACCATCATCACC(iSp9)GCTAATCGATTATAGTTCTAACC TGATCGTATACATGGCTACGCCTTAACGC	side
45	CTGGAAAATGGAGAAG(iSp18)GAACCGGTCCTTGATACGATTA ATG-TATTCTAAGGAAGCCAAGACCGGTCTA	back
67	ATATTGAGACGTTAGCAGACGGTATG(iSpC3)GCAACTTTCAAA TCAC	front
91	GGGATCTTGTTACGTG(iSp18)CAGTTGTGCCTATAGTAGGCGC GGTT	back
175	CGTGAAGAGTAGAAAA(iSp9)TGCACCTCCGCTCACACCAAGT GCTTCCAGCTACCACACTGTATGTCTGGCA	side

Supplementary Table 9. Sequences of short ssDNAs for folding DB01. The sequence IDs of the five ssDNAs that were chemically modified for tethering proteins are highlighted in red. Detailed information on the sequences and spacers is available in Supplementary Table 8.

ID	Oligo_sequence (5′ to 3′)
1	TTTCAACGCGGTTATC
2	TTTTCAGTCGGCCGTCAACATACAGCATATTT
3	TTTTTGGCTAACAAGCCACTCGTTGAATATTT
4	TTTCCTTACGAACGATATGTTCATGCGGTTTT
5	TTTTAGACCGAGTATCCAAGGATAATGTCTTT
6	TTTTCCGAGAGAGCCATACCAGCAGCTAATTT
7	TTTCTATGCTGTTCAGTATATCTGACGGTTTT
8	TTTAGCTAGGAGTCCTGCTGGCCGTATCCTTT
9	TTTGATCAGCACGCGAGATATCTATTCTATTT
10	TTTTCACTTCTGTCCAGAACGCTAATTACTTT
11	TTTTAGTGTAGCATGAAAGAGCTGCTCCTTTT
12	TTTCTGGAAGTCAATGTTCACTACGGACTTTT
13	TTTAATGTTGGATACGCGCTTACACAGGATTT
14	TTTTCCAAGAGTGTGTTCGTTCTCTAAGGTTT
15	TTTTACTAACACGACAACTCCAACTCGTGTTT
16	GCCACATGCGCCATTT
17	TTTCTTCTAACAACTG
18	TTTGCTCTATACGAATGCGCCAGGACCGTTTT
19	TTTAAGCTTCTGTTACCTTCCTATATGGTTTT
20	TTTAGGATATTGTCGGCTGGCTCGCTTGTTTT
21	TTTCTTGAATAGCAATAACTCAGCTTACATTT
22	TTTAGGATTAGCTTGTAGTAACCAGATATTTT
23	TTTGATTGCCATGAGGGATAAGTACTAAGTTT
24	TTTCCTAATGTGGTACCTAATAGCACGGCTTT
25	TTTGAACCGTTAACCTAGTATGCTCCTTCTTT
26	TTTGTTCCGAGGATTAATGTCGTCCTAATTTT
27	GGCACCAACACGCTTT
28	TTTGAGCCACACTACTAATCGTACACAGGTTT
29	TTTGGTACACAATTAAGTGACTCGACTTATTT
30	GACTGCGCGACACTTT
31	TTTCCATAACCAGTCC
32	TTTATAGTCTGACAATGTAGGTTAGGCTCTTT
33	TTTCCGAACGGCACCG
34	TTTTTACGCAGGTGCAGGACAACCGTCGGTTT
35	TTTAGGCTGGAGAGTCAGGTACGAACGTCTTT
36	TACTCAAGATTGTTTT
37	TTTCATCACGTGATATTAGTTCGGCAGCCTTT
38	GCTTCAGATGTAATTT
39	TTTGGACTTACGAGCC
40	TTTATAGTTCTAACTAGGCAACTGATTGATTT
41	TTTCGGATGTGAACGG
42	TTTTGCGTGGATCGGCGGTCCAACTACTTTTT
43	TTTTCGCGTTCCATATCGTCGTCTGCCAGTTT
44	TTTACCTCAAGGTCGATAACGTTGGACAATTT
45	GTCACGAACCTCGTTT
46	TTTCACCGCCTGAATGATAATCTGTGTACTTT
47	TTTCGACTGAGGCATCGAATCAGATTCCGTTT
48	GCCTGTCACCGGTTTT
49	TTTAAGCCAGTTGTTC
50	TTTCTAGGCTCCATAATATAATAACGAGATTT
51	TTTAGCGCTAGGTCTAGTTAGCAGCAAGCTTT
52	TTTTATGAGCGACTTGTTCAGGACAATTCTTT
53	TTTAGCGATTAACTAAGCAGACCGCGCTTTTT
54	TTTAGACTAGGCGGAAACCAAGTATGGACTTT
55	TTTTTGGAATACCGAACAATACCGTGGAGTTT

56	TTTAGCTTCTTCGGTCCGAAGTAGGTGTGTTT
57	TTTTTGCAACCGGAGTTTCCTCAAGTCGCTTT
58	TTTCCGAAGGTCTGAGAACCAACATCCATTTT
59	TTTGACCGGTGTCCAAGCGAGAGATCAACTTT
60	TTTCCTTGCGGCAATCAAGTGCCACGCGGTTT
61	TTTGTCCAGGCTTCGGTCTCCAGTCGACGTTT
62	TTTGGACCTACCAGTACGCTTCACATAACTTT
63	TTTGTTCGTCCGGTTCCTTCTTGTAAGAGTTT
64	GCTGGATGAGTTGTTT
65	TTTGATTCACTATCGTTATGCTTGTTGGATTT
66	TTTTTCCGGAACAATCCCAGAGCATTGCATTT
67	TTTCCACGCCTGCCAATCAATATGGTGTGTTT
68	TTTGTGTGCGCTAACAGTATGAGCTAGTATTT
69	TTTATGGACCATAAGCCCGTGCTTATACTTTT
70	TTTGACACCATGTAAGCGTGTGCGAGAAGTTT
71	TAGAATAGATATCGTACTATCAATGGACCACGGCCAGAAGATAACCGCGTTG
72	GAAGGAGCATACTTCCAGTGGTTCTAGCACGACTAGTTCCAGTTGTTAGAAG
73	GACGTTCGTACCTTATCACGCATCTGTTAACCAACAAGCGGACTGGTTATGG
74	CTGGCAGACGACGAAGAATTGCCTCGATATAAGACGGTCGGCTCGTAAGTCC
75	GCGACTTGAGGAATTGGTAATATTCGATGACGACATCAAGAACAACTGGCTT
76	TATGCTGTATGTTAATTCCTTGCACG
77	ACGGTCCTGGCGCACCGTGGTCTTCCGCAGTACGATTGATCGCGTGCTGATC
78	GAGCCTAACCTACACTCCACCGGTAAGGCTGTCAGGAGCAGGTTAACGGTTC
79	TCAATCAGTTGCCGCCTCGGTTACGAGGCACCGTGTAGCGACTCTCCAGCCT
80	TCTCGTTATTATAACAAGATTATTCACAGCTTCAGAGCAATATGGAACGCGA
81	AACGAATTCTCTGACTCCGGTTGCAA
82	GTAATTAGCGTTCGAAGCGACCTCAAAGGAATTCCACAGGACGGCCGACTGA
83	ATTAGGACGACATAAGTCGGTTAGTACCTATAGACTCCTATTCGTATAGAGC
84	ACAATCTTGAGTAATCCAGAACCGCAGACGCAAGTTCTCATTGTCAGACTAT
85	TTGTCCAACGTTAATGAATCAAGAACCGTAAGAATGAGATAGTTAGAACTAT
86	ATGGATGTTGGTTCAATCCGCCGCTTGTCCAGGTATGACTTATGGAGCCTAG
87	TATTCAACGAGTGCAGCACAGCAGTATGTGA
88	ACCATATAGGAAGAAGGCTGTATGTTAACACGTGGCACGTGGACAGAAGTGA
89	TAAGTTAGGATTATAATCCTCGGAAC
90	GCTTGCTGCTAACGCAACCTGGATAAACCATTGTATACTTCGACCTTGAGGT
91	TCCAACAAGCATAAGGACCTACGCGATTGACTCTCGGCACTCAGACCTTCGG
92	AGGAGCAGCTCTTAGCAATGTCATAGATTACCAGTACCGGCTTGTTAGCCAA
93	GCGTGTTGGTGCCTGGTCCGGACTCTGCCTTGAACTGTGGTAACAGAAGCTT
94	CGAGGTTCGTGACAACCTAAGACCAG
95	GTTGATCTCTCGCTGCTGGCTTCCTACTAGTTGCGTGCGTAGACCTAGCGCT
96	ATTATCTTACTTCTCTCGACGATAGTGAATC
97	ACCGCATGAACATACCTAATCTCACCTGCAG
98	ACAAGCGAGCCAGGCCAATGGCCGCGGCCGAGCTTCATGTCATGCTACACTA
99	GAATTGTCCTGAATAACATTGTCGAG
100	TGCAATGCTCTGGCCAGCACATACCATGGTATGCAAGGATTGGACACCGGTC
101	AGTCCGTAGTGAATGAGGTCAGTCGGCTAGACGCATCGGATCGTTCGTAAGG
102	GTGACAAGCTCTTCCGACAATATCCT
103	CCGCGTGGCACTTCGGTCGCTTAAGTTTGGACGTTGGCTCAAGTCGCTCATA
104	CGTGAGAATTCGTCGGAGGATTGTTCCGGAA
105	GACATTATCCTTGGATACCATGACATCATTA
106	TGTAAGCTGAGTTCAGTGACTGAGCTGTCGGATGAGCGACATTGACTTCCAG
107	AAGCGCGGTCTGCTCAAGGTTAGGCC
108	CACACCATATTGAAGGCTATCTTGTCACGACGTCGATTCGATTGCCGCAAGG
109	TCCTGTGTAAGCGTCGGCGTTGTTACATGGTGCGCCGTGGATACTCGGTCTA
110	TCATCTTGTGACAATTGCTATTCAAG
111	CGTCGACTGGAGACACGTCTAAGCGGGAGGCTCTAATTCTTAGTTAATCGCT
112	TACACGACGGAGTATAACTTGGCAGGCGTGG
113	TTAGCTGCTGGTAGGCTACCGGTGAGTACCA
114	ATATCTGGTTACTTGCCTGTCAGTTGCACGATAGAACCACGTATCCAACATT
115	GTCCATACTTGGTGCTTAAGGACTGA
116	TACTAGCTCATACACCGAAGGTTCAGAAGAAGGCTACAACCGAAGCCTGGAC

117	CCTTAGAGAACGAATTACGGCGACCGCCATTCTCGACCGTGGCTCTCTCGGA
118	CCTGTGTACGATTAAGAGGAGTACGTATCTCCTCTACGGACAAGCTAATCCT
119	GTACACAGATTATGACCTCGATTGTC
120	GTTATGTGAAGCGATATACAGTTGCACCGTCCTAATGAATTCCGCCTAGTCT
121	CTCTGAACTACTAGGTGATGTTAGCGCACAC
122	ACCGTCAGATATAGGCGCGATGCGTCCTGAG
123	CTTAGTACTTATCCGGTATGTATTCCTAATGACGCCGCCACACACTCTTGGA
124	AATACCTGGCACCAGTAGTGTGGCTC
125	CTCCACGGTATTGGATTGTCCTACTGGTTCGAATACGTCCATTCAGGCGGTG
126	AGTATAAGCACGGAAGATTGTCAGGCTGCATCCTGTAAGTACTGGTAGGTCC
127	CACGAGTTGGAGTATCGCATCAGGCGTGTGCGTATGTCTCTGAACAGCATAG
128	TAAGTCGAGTCACGGATGGATTGTCGCCAGCTCCTCTGGCCTCATGGCAATC
129	GGCTGCCGAACTATCGGCCGACAGCACATGCACAATTGTCGGTGCCGTTCGG
130	CGGAATCTGATTCTGCCAAGTCTAGTTCTCCTGCTGCGGCCGTTCACATCCG
131	CTCTTACAAGAAGAACTCTTATAGGAGAAGCTAATTGGCTTCGGTATTCCAA
132	GGACCAACTGAAGTTGCCGCTTATGGTCCAT
133	GGATACGGCCAGCAGTAACTCCGCATGGCCA
134	GCCGTGCTATTAGGCATTAGCGCTTGCGATATAAGTCGGTGTCGTGTTAGTA
135	CCGACGGTTGTCCATGACCGCGAATCCCAGCTGCATATGTTAATTGTGTACC
136	AAGTAGTTGGACCAAGCACACTACAGGAACAGCTATGGAATATCACGTGATG
137	CACACCTACTTCGTGGCATATGTGCCAAGAGAGCCACTAGATGCCTCAGTCG
138	CTTCTCGCACACGCTTACACTCGGTAAATCTGCAGAGAAGAACCGGACGAAC
139	TGGCGCATGTGGCTCCGACCGCATCCTGCGCTCCGGACAAGGACTCCTAGCT
140	GTGTCGCGCAGTCCAATTGAAGAACTGACTTAGATGCGCGTACCACATTAGG
141	TTACATCTGAAGCGACCGTAGGAGCAATGATCCAACCAATGCACCTGCGTAA
142	ACCGGTGACAGGCTAAGTGCAGCGCCAAGTAATGCTTATGCCGATCCACGCA
143	CAACTCATCCAGCCAATATCGCGAACAGCCTGCCATCAGGACCGAAGAAGCT
144	CCGCTGTTATAACGGATTCTTACATGGTGTC
145	TTCTGGCCGTGGTGCGCGGCGGTCTCGCGGTGTGGTGAACGTGCAAGGAATT
146	CTGTGGAATTCCTCGGACTTGTAAGCGAGGAAGTGTGAATACTGCTGTGCTG
147	CGGTACTGGTAATAAGTCACAGAGGATAGTTCCTGAACAGGTGAGATTAGGT
148	CCGATGCGTCTAGAGGTGCACTACAGTGAGGAAGCACCAATGTCATGGTATC
149	CACGGCGCACCATCATACAACAGGACTAGTGGTGTACTCCTCACCGGTAGCC
150	CGGTCGAGAATGGCCGTATCGAGCATATGCCATACCTGAGACGCATCGCGCC
151	AGACATACGCACAACATCTTCGTTCAAACGTGTGTAGTTATGCGGAGTTACT
152	TGTCCGGAGCGCAAGGTATGATTAGTGCGCT
153	TACCGGCGCGTAAGGCCGCCATTGATAGTAC
154	TCAATCGTACTGCCAATACCTGGTTAATCCTAATTCGTCTTGAGGTCGCTTC
155	CGTGCCACGTGTTGTGGATCCGAGTGAGAGTGCCGTCGACTATGACATTGCT
156	CATGAAGCTCGGCCTGCTCATTCATGTCGTCGTCTCTCTCCGACTGACCTCA
157	TCGCTCATCCGACAGCAACGGAGAGCGTGGAACCTTCACGTAACAACGCCGA
158	TGGTTCTATCGTGCCGGTGTTCAGAGGAGCTATGCCTGACGGTCGCCGTAAT
159	GGCGGCGTCATTATCGCGTGCATCGCTCTCTTACGGCAACGCCTGATGCGAT
160	CCGACTTATATCGCGCTAGTGGCCGAGACTCCACGACCAGGATGCGGTCGGA
161	GAACTAGTCGTGCCAACCAATGAAGGCCTAGAACACGGCGGAAGACCACGGT
162	AGGAGTCTATAGGAATCCGCACTCCTTACGCCTCCTCTCAACATACAGCCTT
163	CACAGTTCAAGGCTGCGTTCTGATTATCTCCTAGGATCACGCGGCCATTGGC
164	AAGAGCTTGTCACTGGATATGGTTATAACGTCTCAATATAGCTCAGTCACTG
165	TGTCACAAGATGATTCTCCTGGTAAGTGCTTCGTTGCTGCAACTGACAGGCA
166	CCGTAGAGGAGATGTTGAGGCGATAAAGACGTAATCGCTGGAATACATACCG
167	CCAGAGGAGCTGGTTCCTGCTTCAACGTGTTGCGCTCAGCAAGCGCTAATGC
168	GCGCATCTAAGTCGTGCGTCGAGTTAAACTC
169	TATCCTAGACGGTGGTCTTAGAACCACTGGA
170	GCTCCTGACAGCCGGTCCGACGGAAGCGGCAGACCTTAATACTAACCGACTT
171	TAATCCTAACTTAACCTCGTCGTTGATTGAGAGCCACTGAGAGTCCGGACCA
172	TTGGCGCACGACTACGTACTCCTCTT
173	GGTGCCAGGTATTGCGTGCGGTCCAATGTCCACCATGGACGACAATCCATCC
174	CATATGCAGCTGGCTAGAGTTCGTACCTCCAGCTATCTAAGTTCTTCAATTG
175	GCTTGTTGGTTAAGCGACTTGCGAGGAGGCTTGTTATTGTTACCGGTGGAGT
176	GAGAACTTGCGTCAACTCCATGCGAG
177	ACAATTGTGCATGAGATATCTCGTATGGAACTCGCTTCGGATTCGCGGTCAT

178	TTGGTTGGATCATTACTGGCCTATCCTTCGA
179	CGCGAAGCGCTGGAGGCTCAGATGCGTGATA
180	GCTACACGGTGCCTATCACACTCTTACCAGCCATAGAGCTGCGGTTCTGGAT
181	TGACATTACAGAATGCTGTCGGCCGA
182	TCCATAGCTGTTCAGGTGAGCAGCTATGAGGTGGTAACATGCTCCTACGGTC
183	GACCGTCTTATATTACGGCTCTCTGGTACTGCTACTGTCTCGTAACCGAGGC
184	TCTCATTCTTACGCGAATGCGGTCCG
185	CCGCAGCAGGAGAGATCCTAGCATTCCGCTGGTGCTTCACTGTAGTGTGCTT
186	ATAAGCATTACTTGTCCTCCGTCATGAGGCC
187	AGTAAATGGAGATGTTAGCGAGGCAATTCTT
188	TGCTCTGAAGCTGAGGTTACCAATGTTTCACCAACTGTCGTTCTTGATTCAT
189	AGTATACAATGGTGGTAGGTGCGTTAATGCGGTTCAAGGCTGGTCTTAGGTT
190	AGAATACAAGGCGGACAATCGAGGTC
191	GACGTATTCGAACCTCACCTGGCCAGGTGGCGGCTACGCACTAGACTTGGCA
192	TAGTGGCTCTCTTCAGAATTCCGTGGTCGGACTTATAATGGCGCTGCACTTA
193	TTGATGTCGTCATAGGCAATCCTCAATCCTTCTCATATATGAATAATCTTGT
194	GTCATACCTGGACCGGATGCTACTTCGACCTACCACACATTATCCAGGTTGC
195	CGCACGCAACTAGCTCTATGTGATACTTCTGTTGGTAACCTCGACAATGTTA
196	AGCCAACGTCCAAGGTCCTCTGTTCAAGACTGCGACGCAGGCCTAACCTTGA
197	GAATTAGAGCCTCCGCGGAGCGGTCTGAGCTCTTCGCGTTCAGTCCTTAAGC
198	TTCATTAGGACGGACTTCACGGTGCGTTGACGGACCATCCAGTAGGACAATC
199	GCCAATTAGCTTCACTGTGCTGCGACATTGCTGTTGATAGGCACATATGCCA
200	CTGATGGCAGGCTGCAGTGGCGACTACGTAG
201	TTCCTCCTTGCACAAGCGCGAATATTACCAA
202	CAGAGAATTCGTTCCTACTTATTCTTACTCGTGCTGGTGAAGCGGCGGATTG
203	TGCCGAGAGTCAAGCCTCGGTCAGGACGGCCGTATTGCTTAGGAAGCCAGCA
204	TCCTTGCATACCATGACCATTGATGGAGGATTCATAAGTACTTAAGCGACCG
205	GAATCGACGTCGTATCTTGGTTACAACAACAGTCCATATCCGCTTAGACGTG
206	TTGTAGCCTTCTTCTACTAGGTTGGCTCACTGACTTGCATGCAACTGTATAT
207	CTTACAGGATGCAACTTAGGTTCTATTATAATTCATGCCTCCTATAAGAGTT
208	TTCTCTGCAGATTCGCATGTCGGCTAGTCTCCAGCATGAGTTCGCGATATTG
209	GCATGCATACTGCTCGCGTAGGTCCT
210	CGAGAGAAGTAAGACTTCAACTTAACCACACAAGATCTATGGTATGTGCTGG
211	CTCCGACGAATTCTAGGATCTGTGGTATTCTCAATGATGGACAAGATAGCCT
212	GTTATACTCCGTCTAGTTCAATAAGTGCCAGCACCTCGCCTGAACCTTCGGT
213	TCACCTAGTAGTTACCGAACACGTGTGATACTTGCCAACGCCTGACAATCTT
214	GGCAACTTCAGTTATGGTGCGCCGAGAGCCACGACATTCTACCGAGTGTAAG
215	AATCCGTTATAACGTTCCAAGGCCTA
216	TATGTGCAGCGGCGAGACCGCCGCGC
217	CGGCCTTACGCGCAAGTCTGGAACCGCCACCGTCCGCCACCTTCATTGGTTG
218	AGACCACCGTCTAAGTCTAGTGAAGGCGTGTGGAAGCAGCCTCGCAAGTCGC
219	AGCCTCCAGCGCTATGGCTGATAACGAGGATCTTGTCCGCCAGAGAGCCGTA
220	CTAACATCTCCATACAGAATGGTTCTGTGTAGGCTCGCCTTGAGGATTGCCT
221	CGCTTGTGCAAGGAACACTCCGTCTG
222	TTCACCACACCGCTGGTACACGAGCGCATCAGCCGGTAATAACCAGGTATTG
223	GCCGTGTTCTAGGAGATTGGCTGCCTAACTTCAATCCTGCTTCCGTCGGACC
224	CAATAACAAGCCTTGGCGCGAAGGCAGAATTCGATAGTCTAAGAGTGTGATA
225	GACAGTAGCAGTACCAGCGGTTAGGAATACCAGTACCTTACATTGGTAACCT
226	TATATGAGAAGGAATGGCTGACCATTTATTATAATCACGAAGAATAAGTAGG
227	CGAACTTAGCATTGCTTACAAGTCCG
228	GACGAATTAGGATCCACCAGATTAAGAATACTCATTCCTAGGAGTGCGGATT
229	TTAAGGTCTGCCGGCGGCAATGAGATTCAGTGATTACATCTCGCATGGAGTT
230	GCTCTATGGCTGGTGAGAACCTTACACTCTCATAGCTCTCGGACCGCATTCG
231	GACAGTTGGTGAAGACGACGAGATCAGTATGCTTAACTCGAAGTAGCATCCG
232	CACCAGCACGAGTAGGCGAACTGCAG
233	TTCACACTTCCTCACCAACAGCGATCCCTATCAGTATCACACTCGGATCCAC
234	GAGAGGAGGCGTATAAGGACTGCGGCGTTAACATTAGCATCAACGACGAGGT
235	TCTTATCCTATTATAACGCACCTACC
236	TGTGTGGTAGGTCCGTCTTATTAATGTCGATCTGGATGTTCCTGACCGAGGC
237	GCAGTATGCATGCATCGTCCAATTCC
238	TCCGCGGATATGTTCCTCTGTGACTT

239	TCGACGGCACTCTGCATTGACCAGCAACACCACACTCGGTAATCAGAACGCA
240	CAGTGGCTCTCAAGGTGTCAACAATT
241	CCTTGAACCGCATGACCTCCGGAGCCGGACACAACTAATGTATCACATAGAG
242	AGCAATACGGCCGTATAACACCTCGGCCGCCGAGCCGTGGTTAAGTTGAAGT
243	TGTTCAGGAACTAGTCCAATATTCGATATCACATGTTGACATGAATGAGCAG
244	TGATCCTAGGAGAAGAGTTAGTTAGC
245	GTTACCAACAGAAGAAGTCTCTACATTTCTGTATCGTGGCCATCAATGGTCA
246	TAGATCTTGTGTGCCGTGGATGAATA
247	GATTGACGATAACCTGTAGTGCACCT
248	AGAGAGACGACGAGCTGGTACGCGTCCAACAATCAGAATATAACCATATCCA
249	ACCTTGATTCGATTGAACAGAGGACC
250	ACTTATGAATCCTAGATTGTATCCTACTCAACCGAAGCCACCACAGATCCTA
251	TGGTGCTTCCTCACACCGTTACGGCACGCGTGGTAAGGCGCTCTCCGTTGCT
252	helix_67 in Supplementary Table 8
253	TGCGTCGCAGTCTTAGAACTAGACTCCCGGTTGACTCTGTTGTAACCAAGAT
254	CATCATTGAGAATCTAGGCTTGGCTG
255	TGTCGCTTCCTAGGTCCTGTTGTATG
256	GTGAAGGTTCCACATAGATCGCCGGTTGGTTGGCCATGACTTACCAGGAGAA
257	GGAAGAATACCTGAGACCGCTCCGCG
258	ATATGGACTGTTGGATTCCAGACAAGCCATTGACGGATAACTTATTGAACTA
259	GAGTACACCACTAGTCATGCGTGCTACAACGAACGCTGACTCTGAACACCGG
260	CAGCAACGAAGCAGGCATGACCATTG
261	ACGCGAAGAGCTCGTCGAGGCTACAAAACTTCGTCCGTGGCCAACCTAGTAG
262	GCGAGGTGCTGGCGGCATTCTAATAA
263	GCAACAGGTGTCTATGCTCGATACGG
264	TCAGGCATAGCTCCGAGGCATACACTTAACACTCTCCTATTATCGCCTCAAC
265	AGTCGTGCGCCAAGCTGTGCGTCATC
266	CGCCTTGTATTCTAGTTAACGTATTCGCTTGTGAACGAACGCACCGTGAAGT
267	TGCAAGTCAGTGAGATGGTCCTCAACTATCGACCTACTAACACGTGTTCGGT
268	TCAGGTATGGCATGTCCAGTAACTGACTGTTCGCGCATTGCGATGCACGCGA
269	AGCGATTACGTCTGGAGAGACCTGTCTGTACGGCCACACTTGGACCGCACGC
270	AACATACACACATCTGGCCAGGTGAG
271	GATGGTCCGTCAACAGAGGTGCAGGTAGATTGCTATGCCATAGAACCTAAGT
272	GTTGGCAAGTATCACGCGAGGCCTCG
273	TGGTAAGTTCTCTTGAACGAAGATGT
274	TTGCCGTAAGAGATTAAGTGATGGACGTCGTATTCTGGAGTTGAAGCAGGAA
275	TCCATGGTGGACAGCGTCGCCACACTATCCTCATCGGTAATACGAGATATCT
276	TTCTGTAATGTCACAAGATCTGGCTAAACGCGTCCACGTGAATGCTAGGATC
277	GCGTAGCCGCCACCATAGCCAGCCATCAGCCGCTCGCCGGTCGCAGCACAGT
278	GGCATGAATTATACTTCCTCTTGCCTTTACGGACCTTGGCTCGGCGCACCAT
279	AACTACACACGTTGGTCTCTCCTTGACCTATAGTGAGCTTCGGCCACTAGCG
280	CTGAGCGCAACACCTTCTATTAAGATGATTGCGCTTACGGTACGAACTCTAG
281	CGAAGCGAGTTCCAACCAGAGAGGACTGCCGATCGACCTTAGCTGCTCACCT
282	TGAAGCACCAGCGCCAACAGTCGCACCGCTAAGGCCAGGCCACGGAATTCTG
283	TATCAACAGCAATAAGGATGCTCCTTGTGAGCAAGTGCATAGCCGACATGCG
284	GAATGTCGTGGCTAGTTGTAATTGAA
285	AACTTACGCCACCACTAATCATACCT
286	TGGTCGTGGAGTCTTGCGGAATGTTCCTTATATAGCACTTAACTCGACGCAC
287	TAGATAGCTGGAGAAGCCTCACCTGTGTGCTTGAATGGTGGATAGGCCAGTA
288	TGTTACCACCTCATGGCAACTATACGTTGATGGAACGGCCATGACGGAGGAC
289	ATTATAAGTCCGAATGAGACTCCATAGCGGCTCGGCTCATAGTCGCCACTGC
290	TCATGCTGGAGACGCGCGCCGCTTCTATTGGCGCTTCAGTAGGCCTTGGAAC
291	GCCGCTGCACATAACTATCTTAGAAC
292	AATGCTAAGTTCGGTCTTACGCTTGCGTCGGCATAATCTCGCTCGTGTACCA
293	ACATATCCGCGGAATAAGATAAGACGATAGAACCATCTGGATCGCTGTTGGT
294	GTTATCGTCAATCGGAGACAAGACCGATTGGTCATAAGATCGAATATTGGAC
295	CTAGGAAGCGACAGGCAGCTAAGGCTTTCAGGCGCCAACTGCCGTAACGGTG
296	AGACACCTGTTGCCGTGCAGAGTAGTGGATACAACTCGTTAGCACGCATGAC
297	AGAGAACTTACCAATCGCAGACTCGTAACTCTCAAGATATCAGTTACTGGAC
298	GGTGGCGTAAGTTCGAACGCCTGGTATACTTGCCAGTGGTCAAGGAGAGACC
299	TTACCGGCTGATGGAGTAGGAGGCGATGCGCGTTCGTTCCGGTTCCAGACTT

300	TGATACTGATAGGTGGTCGCTCCTGATACCTCCAACAACCTTAATCTGGTGG
301	TCAACATGTGATAGATGTCTACCAAGTCAGTTGCCGTGGTGCTGGTCAATGC
302	GCCTTACCACGCGCATCCACACAAGAGTCATCGTACACGGACGCGTACCAGC
303	TCAGCGTTCGTTGTTGTAATGCTAATTACTCTTCCTGAGACCGGCGATCTAT
304	AATGCGCGAACAGGTGGACTTGACCTATTCCAACACGTCAGTGTATGCCTCG
305	AGCTCACTATAGGTATGGTATCAACTCATCACGTGTTCCGTCCATCACTTAA
306	TACTTATGTGAAGGAACATTCCGCAA
307	TGGCGGACGGTGGATGCGAGGACCGC
308	AGGAATGAGTATTACAGCGCAGCTCCAAGAGGTTACAAGAGGCAGCCAATCT
309	CCGAGTGTGGTGTGCGTTAAGGCGTATCTCGATTGGCCAGCCGCAGTCCTTA
310	ATTCTGATTGTTGTATAACCAGATTATTATATTAGGAAGGCTAACTAACTCT
311	TCATGGCCAACCATGCCGAGACATTCTGTTGCGGCTGACCATACCGTCTGCT
312	TAGGAGAGTGTTACCGGTGCCAACGAAGGTATGCCTCTACAATGGTCATGCC
313	TCCAGAATACGACTGTACTTAGTCAGAACAGATTCTGGAGACAGGTCTCTCC
314	AGTGCTATATAAGACACCAGTCGACAGTCAGACAAGGCGATCTTAATAGAAG
315	CAGGATTGAAGTTAGCTCCTGAATTAACCTGTCTATAATCCTTCACTAGACT
316	TGCTAATGTTAACACGGATAGCAACCGCATATAGGAATGATCTCATTGCCGC
317	ATAATCGATTAGCAATTGTTGACACC
318	GTGTGGCCGTACACGGAGACTCAACGCCGGACTAATTCGGATGACGCACAGC
319	CGTAAGCGCAATCCGGAATTAACTAATCTTGTTGCAGAGAGTGTGGCGACGC
320	GAGGATCTGACGGACAGGTGAGGCTT
321	CTGCTTCCACACGTGCCGAACGCTTG
322	ATGTAATCACTGATAGACCGGTCTTGCGCGTTCCAGCTATGCCTTCGCGCCA
323	TACCGATGAGGATTGCCAGACATACA
324	ACCATTCAAGCACCACCATAGTGGTACTTGGTAATCTGAGTCCTCTCTGGTT
325	GACTATCGAATTCAAGGTTGCGGTGCAACGAATGCGTGCCGTTATCAGCCAT
326	CAAGGACCGGTTCTGTAAGGTTCTCA
327	AGGTCGATCGGCATCTGAACGCAACGGAGCGGAGGTGCATAGCCAGATCTTG
328	CATACGGCCATTCCGTATAGTTGCCA
329	CGGACAAGATCCTGACCAGCGCAGAG
330	AGAGCTATGAGAGAGAATATCGGTTAATTCCAGAGTCCGTCCTAACCGCTGG
331	ACGTGGACGCGTTCTAATACTGGTAC
332	GCCGTTCCATCAAGCACTCGCTTGTGAATGATACGATACGTGCGACTGTTGG
333	AAGGTACTGGTATTGGTGAATACCTTATACATCAGTTCAAGAACCATTCTGT
334	TAATAGGATAAGATACGAACCAAGAACTATTACTTCGCTTGATCTCGTCGTC
335	TCGGCTGCCGTGCGGCTCCGGAGGTC
336	ATGTGTGTATGTTGATCGAGGAGGTCCACGTCAAGCCGCGAATACGTTAACT
337	CCTGGCCTTAGCGCCGATGCGTTGGAACGACGCATCCGGATGGCTGGCTATG
338	TCATCATGCAGCCTATGGAGTCTCAT
339	GGCGAGCCTACACAGTGAAGGTGTGG
340	GAGTTAAGCATACTACTTAATCCACCTGCTCTTCATTGGAATGGTCAGCCAT
341	ATTAGTTGTGTCCGTTCGTGTCCACCCGTAGTAACAGGTCATTAATAAGACG
342	ATCGAATCAAGGTTCGGCTTGGTGACAGCGCAGGTCAGTATGTAGAGACTTC
343	CAGGTATTCTTCCGACACGAGAGGTAATAGGCACAACTGGAGTCTAGTTCTA
344	TTCGTTCACAAGCGGAACACGCTCGTACCGAGAGAGGTATTGTAGCCTCGAC
345	CGGCGAGCGGCTGATCAGCTACAATTGTAGAAGTCTTGTACCTGCACCTCTG
346	TGAGCCGAGCCGCTTGTTGTGCATATGTCGTGGCGGCCTAAGGAGCATCCTT
347	CGTGATTATAATAGTGTCCTGTATACTAACTTATAGAGTCAGACGGAGTGTT
348	ACATCCAGATCGATGTGGCCGAATCCTGCGTCACGATGGCTGCAGTTCGCCT
349	CCACGATACAGAACCAGTCCGGCCAAATCATATATCGGACCGAGGTGTTATA
350	CAGAGTCAACCGGCTCAATGGATCGTCACTTAGGAACAATAGGATACAATCT
351	CACGGACGAAGTTAATTACAATAATACTGGTACCTCAAGCTTGTCTGGAATC
352	GGCATAGCAATCTCCTTATTACCGGTTTACAGCACGATTGTTGAGGACCATC
353	TGCACTTGCTCACTCAAGTCGGTTGGTATGTTGGAATCAAGGCAAGAGGAAG
354	CCTCGGAGTATATAGAAGCGGCGCGC
355	CACGGCTCGGCGGAGCCTTATAGGACGGACAATTACGGAGGAATTGGACGAT
356	GGCTTCGGTTGAGGCGACCACGTCAACACATAACCGTAGTATTCATCCACGG
357	TATCCGTCAATGGAACAACGTATGTCGTCTCGCTAACAACAGCCAAGCCTAG
358	TAGTAGGTCGATATAAGGAGGTGACTATCCTGGACAGAATTATTAGAATGCC
359	CCAAGGTCCGTAAGCCAGATAGGCGAGCCTGCCGTTATCCGAGGCCTCGCGT
360	CTGAAGCGCCAATATTCGTGTGTCCTTCACCAGGATACCTTCAATTACAACT

361	GAACGAACGCGCAGCTAGATCTTGGAATCTAAGGTTAAGGTTCTAAGATAGT
362	ATTATAGACAGGTAACGTGCTAATTCTTGATTCTGCTAGGCGGTCCTCGCAT
363	GCACGCATTCGTTGTTATCGACGAAGCTGTGATGTGGCGCAAGCGTTCGGCA
364	TGAACTGATGTATCGCGTTCCTTAACTAGCCGCTAACCGCTCTGCGCTGGTC
365	ACTCTATAAGTTATTATGCGAGCTTGAGCGATATCTCCGCCACACCTTCACT
366	AGATTATGCCGACCAGATCCTCCACC
367	CTTGTAACCTCTTATTAGAGCAATCAGCGAGGTTACCGATCGCCTCCTACTC
368	TAGCTGGAACGCGGCGGAGCCTATCCCCGACTTCATCATTAATTCAGGAGCT
369	CGGACTCTGGAATTAAGTTCGGCGACACTGGCTATTCACGCACCGCAACCTT
370	CCAATGAAGAGCATCAACGTCATGATGTCTCTTACTAGGAAGGTATTCACCA
371	CAACTCTGTCATCGTATACAGGACAC
372	GTTGTTGGAGGTACCATTGAATTGCAACCGTAGGTTACGGCAAGCGTAAGAC
373	CATTCCTATATGCTATGTACGGTTAGAAGGTAAGCAACCGGAGCTGCGCTGT
374	helix_45 in Supplementary Table 8
375	AGCGAAGTAATAGAGGATTCTATTAAAGGATGCGGTAGCTAACCGATATTCT
376	CCATCGTGACGCACGCTCTACAACGGCGCTTAGAGCAATGGTGGATTAAGTA
377	CAGATGGTTCTATACCATGACCGGAAATTAA
378	TGGCCAATCGAGAGGATGCAATTGCGAACCGTTCTCAACTCAGGAGCGACCA
379	CAGATATAATTGTGGTTGCTATCCGT
380	ACCTGTTACTACGCGGAGGACTCACTATGATCGTGGCCGTTCTTGGTTCGTA
381	TCCGTAATTGTCCATGGCGGATGGTAATTGGCAAGGCGTGGATTCGGCCACA
382	CCACGGCAACTGAACTCAAGGATCATTCGCGTCTTAGTACGTCTTATCTTAT
383	helix_29 in Supplementary Table 8
384	GCACGGCAGCCGACTAGCTCGTTAGG
385	TCCGATATATGATAGGTTAGAGATACTTCCTACCGAATAGGTGGACACGAAC
386	AAGTCGCCACGCCAGAATGTCCTATAAGGCT
387	TCTTATGACCAATTGGCATACATTGGTCCGA
388	CTTCCTAATATAAGGCCTTCTCAAGACTTCAGTACAGGACTTGGTAGACATC
389	ACTGACCTGCGCTACAGATCGACCAA
390	CTACGGTTATGTGAAGCGCAACAGCCCAACACCTCTCGATTGGCCGGACTGG
391	CGTGTACGATGACGGACTGGCCGCGGGTATAATTACAGTCGGTCTTGTCTCC
392	GAGATAATCGATCTAATCTGGTTATA
393	TTGTTCCTAAGTGGTCTCAGGCGTCGCGAATCGTTCAGAGTCACCAAGCCGA
394	GAGGATCATGCCTCACTCTTGACGTGGTCGC
395	GTTGGCGCCTGAATCATCTTCCTCGTGTTCG
396	GTCAGCCGCAACATGATCCTAGACCATCTTACGTTCTAATCTTGTGTGGATG
397	helix_91 in Supplementary Table 8
398	TTGTTAGCGAGACAATACCGCCTTGTTGGTCGCTAGCGCACGATCCATTGAG
399	CTCAGGAAGAGTAGCGAGAGTGGACGACACGAAGGACCAAGCCTTAGCTGCC
400	ACGAATTGCACACGAATGTCTCGGCA
401	CTTGAGGTACCAGTTAGGCAATTGAATATCGTTCGCTCATACCTCTCGTGTC
402	CATTAGCCGGTGTTCTTCGACATACGTTGTT
403	ACGAGTTGTATCCGAACGATCCACTCAATTA
404	TAGAGGCATACCTAGCGTTCCAGCTCCTAGACACCGGCTATTAGCATTACAA
405	TACCTCTCTCGGTACGAATTGGAATA
406	TTCTGTCCAGGATAAGCAATGGCTTACAGTCTTGTTAGTTATTATTGTAATT
407	GACGTGTTGGAATGTACCGGAACAAGTGCCTATGTTAACACTACTCTGCACG
408	CGAATTAGTCCGGTTGGCCTAGGTACATATATTACAACTTCGTTGGCACCGG
409	GCGGCTTGACGTGGTCAGTAGAGGCA
410	AATCGTGCTGTAACCGTTAAGTTGCAGGAACTGAGAACAACGAGCGTGTTCC
411	TGTTCCGAGTTGCTAAGAAGTCACCTCCTTA
412	TATCTTGAGAGTTGCACTAGGAACACATAAG
413	TCCAGAATCTGTTGCAGGTTCACGGCATACCATGCAGCAAGGTCAAGTCCAC
414	TCCAATAGGTTGACGTTGAGTCTCCG
415	ACAAGACTTCTACATCTTACACCGTATTAGAGCTTGTTCGACCTCCTCGATC
416	GATAACGGCAGGCTACGAGAGCCGGTCCTCGTGGACATTACCGGTAATAAGG
417	GGAACACGTGATGCAATTGCTTGAAGAACTAGTGGTATAACGAGTCTGCGAT
418	CTCTGCAACAAGACCAACTTGGTTCGGTAACTGGTCGACCTGACTAAGTACA
419	helix_175 in Supplementary Table 8
420	CCGGATGCGTCGTTACCTAGCCTCACTTGCAAGTATGTCGTACCAGTATTAG
421	TGATTCCAACATACAGTTCGTTCCTCCGTTATAACTGTCAATTGTAGCTGAT

422	GGTAGAACATGTCTAGTATCGCCTATCTGGC
423	CCACTGGCAAGTACGCAATGTGATGCGTGTT
424	CGCCTTGTCTGACGTGCGAGTGGAACTCTTCCGCGGAACAGTTGATACCATA
425	TCAGATTACCAAGGACCTTCCATGTATTACGCATTGAACTTAGTTAATTCCG
426	GTATCGTATCATTAGCTTACCTTAGATAAGCGTTATATGCGTTGCGTTCAGA
427	AGGCCGCCACGACTTGCAACATACACATACTCTAGGTCGTCCAACGCATCGG
428	GGTATCCTGGTGAACAGAGTGAGCCAGACGCCAACCGGTCCAACCGACTTGA
429	CTTCACATAAGTATGGCCTTCGCCTGCGTAGACCGTTATTACCAGGCGTTCG
430	CCGTCAGATCCTCGAGACTTCTTACCGATGCGGCCAGGATGTCGACTGGTGT
431	GAATGGCCGTATGAATCACGAACTCACAAGTGTTCGTCATACCACTATGGTG
432	GGCTGCATGATGATATTAATATGACCTAATCTACCGATTCACAAGCGAGTGC
433	ATATACTCCGAGGAATTAGTCCGGCTGCTCGGACCAGCCATATGCACAACAA
434	AATTCATTACGATGAGATAGGACACACGAAT
435	CTTAACCTTAGATTAACACCGACGACGGATCTTACGATAGGTGGAGGATCTG
436	CGTAACCTACGGTGGTCGGATGGTGCCTCCACCTGAGAATTCCGGTCATGGT
437	TACTAAGACGCGAATGTCTTGGCAATGGACGTGTGATGGCCAATGTATGCCA
438	ACTGTAATTATACCATATCATGGCTTAAGGCAAGCTGACACGAGGAAGATGA
439	TGGTCCTTCGTGTATACGCTCTGGCTCCTTAGTAGTCACGAGTGGATCGTTC
440	GTTAACATAGGCACAAGCTTAACAATGAATTGTCCAGCTGTGTTCCTAGTGC
441	TATACCACTAGTTACGACGGTCCTTCTTAGATCTGAGCAGCATCACATTGCG
442	ATAACGGTCTACGCTAACACAATTATTATCG
443	ATATCTAACGCGCAGCCATCCAAGATCTAGC
444	TCGGTAACCTCGCCGGCGGTGGCGCCCACGGTAATTCGGTGCAATTCAATGG
445	GTTGAGAACGGTTCCGAACTTCATTCAGTTATGTCGACAATGATCCTTGAGT
446	TCCTGTACTGAAGGCAGCGGCTTGACTGCTGCACATTCGCCGCGGCCAGTCC
447	TTAGAACGTAAGATGCTACGTCGACTATTCCTGTTAACGCGTCCACTCTCGC
448	AGCCGGTGTCTAGTGTTCATGGTACCTGCGTCGGTCTCTCTTGTTCCGGTAC
449	TGCTGCATGGTATTAAGGATTATTCATGTTACCACGGTTCTTCAAGCAATTG
450	GTTCCGCGGAAGAGGACCAGCCGCTAGTGATAACTAATCCAGGCGAAGGCCA
451	CTAGCAGAATCAACCAATTATCCTTCCCAGGTTGCTGGCTGATTGCTCTAAT
452	GGTTGCTTACCTTAATACTACCATGGAGGTGCTACTCATCGCAATTGCATCC
453	GCCATGTATACGATTAGCGGACTCCACAAGACACAATTGTCTTGAGAAGGCC
454	GATCGATTATCTCCTTACAATTCCATGTGTGTAGCTCAATGGTCTAGGATCA
455	GTGTGCAATTCGTCAAGAGCTTCCAGCTGGCGGCCACTTGAGCTGGAACGCT
456	AGTTGTAATATATTAGGAAGCAAGGTCTAACGCGTTCGAGCCGTGAACCTGC
457	GTCGACCAGTTACCTGTAACCTTCCAGCAGGTAGCCAAGGTTCCACTCGCAC
458	TCCTGGCCGCATCACTATCTCGCGTGAGCCA
459	ATTGTCGATCACGCTACTGAATTAGCACGTT
460	ATGATGAAGTCGGACACAATCACATGGTCAACTGGTGTCCTAACCGTACATA
461	ACAATTATATCTGCAGATTACTGTAGGTCCTCTCGAGCGTCAGGTTAGAACT
462	TCGCCTACCACTAGTACCTAGGCCAA
463	TCAACCTATTGGACATGGTAATCCATCGGACTAGCCTTGCGAACCAAGTTGG
464	GTTCAATGCGTAAGGACTTGCAAGGAGCATTAAGCTCAAGGTAAGAAGTCTC
465	CGCCACATCACAGTCTGTCGTAGCTTTGTCATTGGCCGAGGATAGGCTCCGC
466	GCTTCCTTAGAATCGTGGACGTCCAT
467	GTGTGGTAGCTGGAGCCGGATAACTTATGCCTGACCTAATACATGGAAGGTC
468	TGACGAACACTTGAGTAGCTGTTAAGGAAGT
469	ATGCATTCCACAATGTGTCTTCGTCGATAAC
470	GTGAATAGCCAGTCGGCCATACGCAGGACGTTACCGCCTACATTAATCGTAT
471	CACTCCGCCGGTGAAGCACTTGGTGT
472	CATATAACGCTTACCGTCCGGCCGTTCATTAACACCAACTGAGTTCGTGATT
473	CGGTTAGCGGCTAATCACTCATCAGCAATGAGACCATAAGTCGCCGAACTTA
474	GCTACCGCATCCTTCCATGGTCTAAT
475	GACATACTTGCAAGCACCTCCTCACCCCTCAAGGTTAGATCTAAGGTAAGCT
476	AATCGGTAGATTAAGGACTATGGACGACATG
477	GCAGTAGGAGGCGGCTTCGTTAAGGAACGCG
478	CCTAGTAAGAGACGTGAGAGTCGAGCCTACGGCCTGCCATTAATAGAATCCT
479	CGGCCACGATCATGTGCCTCGATGGTGAGAAGTGCTACGCCTAACGAGCTAG
480	CAGGACAGGCCATTGCCTCTACTGAC
481	GAACAAGCTCTAACCTACGCGGTTCAAGGATCAAGATGAGTGAGGCTAGGTA
482	CGACCTAGAGTATCTACCGACCACAGTCTCGTCAGAGTTGGTCATATTAATA

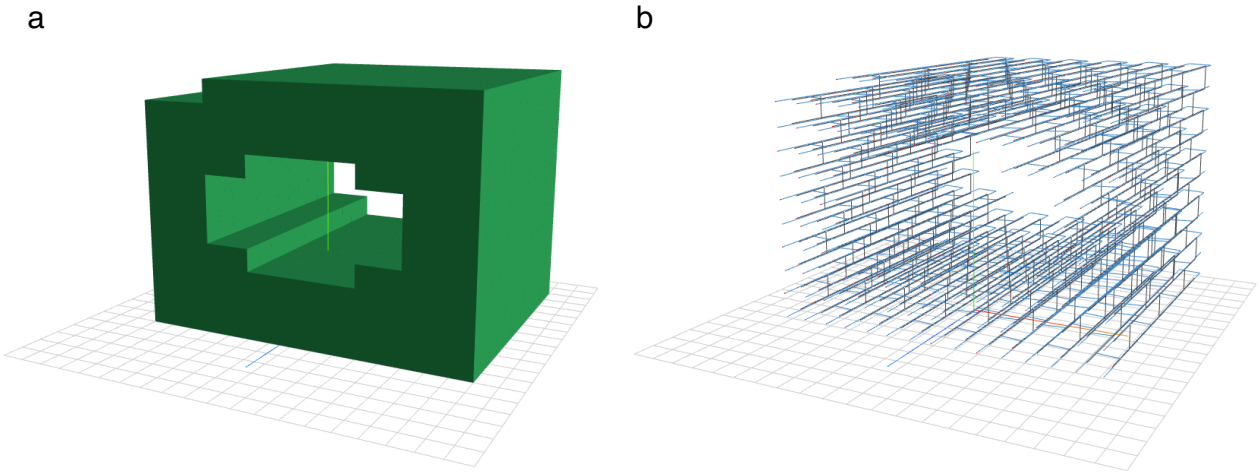
483	CGGAGATATCGCTTCGCACTCCTTACAAGCTACAATCACATCATGACGTTGA
484	ATTGCTCTAAGCGTATAGGACGAATTACCTTAGAATGACAGTGAGTCCTCCG
485	TATTCGGTAGGAATTCTGAAGAGCACCAACCTCATGTTGTTGGTCGATCTGT
486	TCTGAACGATTCGATGCTGGCAACCGGTCGGCAATCTAGAACCGCGCCTACT
487	TGAGCGAACGATATAACGTGGTAGTGTGACCTATAATACTATTCCAATTCGT
488	TGTTCTCAGTTCCTATTGCGAGCCTAACTGTCACTTGCTTACGGTGTAAGAT
489	GACAGTTATAACGTGTTCTAGCTTCACAGATCTTCAATTGTGTATGTTGCAA
490	GGCTGGTCCGAGCTTGAATCACCGTCTCTTA
491	CTATAAGCTTCTTGTAATCAAGCTCGCATAA
492	GATGACAGAGTTGCACGGCGCGACCAACTCATTGCGGTGCCGTTGTAGAGCG
493	ACGCCTTGCCAATCATCCTCGCGATAAGGATATCTGTTAGTATCTCTAACCT
494	TCGAGAGGTGTTGAACGGACCAATAGCCGGCCGACACAACGACGCCTGAGAC
495	GCGCTAGCGACCAGGCCACTCGGTGTCGCAGGCAGGAGGTTCAATTGCCTAA
496	ACTAACAAGACTGGCGTCTTGGCTTGAGAATACCGAGCGTGCAACTTAACGG
497	AATGTCCACGAGGTCATATGTAATAAAGTAACACCAGGTGAGGAACGAACTG
498	ACCGGTTGGCGTCCTTGTCCGGATAGGCATACATAATCCAGCCGGACTAATT
499	TATAACTACTAATTACCATCCGCCAT
500	ATTCTGGCGTGGCTAGGAACGGTGGATATCCATCTGCTCGGCTGTTGCGCTT
501	GAGTGAGGCATGACGTAGAATCAGGCAGGATGCCGTACGACAAGGCGGTATT
502	GAAGAACACCGGCCTGGTGGCCACAGGAACGGTGACTTCTAAGCCATTGCTT
503	TCTTAGCAACTCGGTCACCTAGTAAGGTAGCAAGTGACCACCGGCTCTCGTA
504	TACTAGACATGTTCAATCCATCGCCAATCCTGGAGCTTCTGGCTCACTCTGT
505	ATCTCATCGTAATACAATTAGTTACC
506	GCCACTTGTACACGTCGTCGGTGTTA
507	TGGCTGCGCGTTATTAGTCCATGCCTATCGCACCGAATGGAAGGATAATTGG
508	AGTAGCGTGATCGGCACAATCGTTACAGCCTAACCTCCGAAGCTACGACAGA
509	ACACATTGTGGAATTCATAGAACACTATCCGACGCAGGCGCTGATGAGTGAT
510	GAAGCCGCCTCCTTAGCTGGAGGTGGTGTCTGATTGTCCGTAAGGAGTGCGA
511	ATTACAAGAAGCTCACACCTCCAGGA
512	TATCGTAAGATCCGGTAAGCTTGATGTATCTGACCGGCAGGCGCCACCGCCG
513	GCCAGCAACCTGGTTCAGTTCGTCGTTATCGATGATTAGCATGTGATTGTGT
514	TCGGCCAATGACAATTAAGCATGAATTAGGTAATTCGGTCTGCGTATGGCCG
515	TTATGGTCTCATTCATTGAGCGTGGAGCTATCCGCAACGGCTCGACTCTCAC
516	GTGATTGTAGCTTAACTCAGCTAACCTTAAGGTCATTCGTGGTCGCGCCGTG
517	TGTTCTTCTCACCGCACCATCCGACC
518	CCGAATTACCGTGTGTTCTTGGAGAAGGACGGTGCACGGCCATGGTAGTATT
519	GACACCAGTTGACTTGACTGATCTCGCGATTATTCGCGAATGGACGTCCACG
520	AGGCGGTAACGTCCGTGAGAGATTAATGCCACAATCTTAATTAGACCATGGA
521	TGGCAGGCCGTAGAATAATAGTAGCGACCGGAAGTGAGCAATTCGTCCTATA
522	CACCGCAATGAGTATTGCGGATGCTT
523	TTCTCAGGTGGAGTTGCTCAGACTTCGTCCAGGTGGTGTGAATGAAGTTCGG
524	ATGAGTAGCACCTCCAACTATCGTCCTAGGAGTCGAATCCTACAGTAATCTG
525	GCAGAATTCCGCTACCATCGAGGCAC
526	GTCATTCTAAGGTCGGCTACGTAGAAGTTCTTGTCCGCCTATCGCGAGGATG
527	ATTAGTAGTTATAGGCCATGTGGTGT
528	ACCGGATGACATTATTGCCAAGACAT
529	TGTCGACATAACTTGGATCCAGTCGTGATACTACCGCTGTGGAGTCCGCTAA
530	CGCTCGAGAGGACGTTCGGACTGAGT
531	CGTAGCACTTCTCGGTGTGACTTACGAATTGCGCATCGCGTGCTCTTCAGAA
532	TAACAGATATCCTCTACCGCGAATGTTCTTGTAACAACTTCCACCGTTCCTA
533	CCATCACACGTCCTCACGAGTACCAGCCTGTATGAATAGGTCAAGCCGCTGC
534	CAATTGTGTCTTGTCCGCAGTGCAGA
535	CAACATGAGGTTGTTGAGGTCGGTGGATGGCGCTGTAAGCTATTGGTCCGTT
536	GAGCAGATGGATATTCCAGTGCCTTC
537	CGTAGCATGCGGTAAGCCATGATATG
538	CGAATGTGCAGCACACACGAGTCCAGTCCGGAGTACTGCATGGAATTGTAAG
539	GCAAGTGAGGAGTCGGTTGCCAGCAT
540	TTGTGTCGGCCGGACGTCGCAGCACTAGGACGCTCTACAGCCTGATTCTACG
541	GTCAGCTTGCCTTCACCTGGACACTGTACCGATCTTAACAGTCGACGTAGCA
542	TTGAGCTACACACTATGAAGCCAAGG
543	CTAGATTGCCGACCATAAGTTCATACACTGGACAAGGACACACCGAGTGGCC

544	CGTACGGCATCCTAGCGGCCGCCTTC
545	CGGTGAATGGATTAGCCAGAGCGTAT
546	CGTTAACAGGAATGGAACCGTTGGTACGCTTGGTTGTGTCTGGAAGCTCTTG
547	CGATCCGTACCTCCACTACCACGTTA
548	CCTCCTGCCTGCGAGTCAATGACCTATGAGATGTCATATCTGTGGCCACCAG
549	GTGACTACTAAGGACTCGTCCATCCGAGATCTTAACAACGGTACCATGAACA
550	AAGTGGCCGCCAGGCGTTGGAAGACT
551	GTATTATAGGTCACTTAACATGTATCGTCACTAATTACACAAGCCAAGACGC
552	GAAGTCACCGTTCCGAATCATCTCAG
553	TATCAGTGCCTGGATTGTTAAGCTTG
554	AGAGACCGACGCATGATCTAAGCTCGACGAGCTCACGAGACCTTGCTTCCTA
555	TAGTGGTAGGCGAAGAATCGTAACGT
556	ATGGCCTGTCCTGACGTACAAGTGAGTAAGCACCGCTTATAGGCTCGCAATA
557	CGCTCGGTATTCTATGTGTCAAGTAATCAAGTGTCTTCGCTTACTAGGTGAC
558	AGCTGGACAATTCACTCAGGTTGGCCCCACCATTATGATTGAATAATCCTTA
559	TCGAACGCGTTAGCCACGGTTGTGACAGTACCTCCTAAGATGGATTACCATG
560	AGGATAATAAGCCTGAACCGCGTAGG
561	AGCAAGTGACAGTTGATGAGGTAATCTGGTCATATGACATTATTACATATGA
562	GGTCACTTGCTACTCGGCCTTGTTCA
563	TGTTATCAATCTGGAAGGACCGTCGT
564	AACCGTGGTAACAATTCACAATGGATCGGAACGCACGACTGGAAGGTTACAG
565	CAAGGCTAGTCCGCGCGTAGTAAGGAGTCCGGCTTGTGGAAGTTATCCGGCT
566	CACCGGCGGAGTGCCTAAGATCGGTAGCATTGCGATCCAGGTGAGGAGGTGC
567	TCATCTTGATCCTAAGAGAATAGCGGCTAGCAGAGAACTTGAAGCTAGAACA
568	ACCTGGTGTTACTGTGCCATTATACTTTGGTTACTACCATGGCGATGGATTG
569	TGCTCAGATCTAATTCAGAGCAATCATGACGTTGTCACTTAGCGGCTGGTCC
570	CTTGGCTACCTGCAATCGGTGCCTGTCATCTGGTATACTTCCTTGCAAGTCC
571	TTAGGTCAGGCATATCACGAGAGGAACGGTGCCGATCCGAACGGCCGGACGG
572	TCTAACCTTGAGGCTAGGATCGGAACATTGGTCATTCAGCTGTGGTCGGTAG
573	AATTGAAGATCTGTGTGAAGCTCCTGCGAGGATGCGCGCCTATCCGGACAAG
574	GAAGCTCCAGGATTCTGTGCCTTGGA
575	CCAGATTATCAAGATAATTGTGTTAG
576	GATTAGTTATCACACGTATCTGACAAATGCCGAAGCACGCACGCGAGATAGT
577	TTGAGCTTAATGCGACAGCGATAATTTCAATTCCTATTCCTTAACAGCTACT
578	GTTGGTGTTAATGTCCTAATCCTCGTTATACCATACAACCGTCCATAGTCCT
579	AACTCTGACGAGAAGCCGAACTTACTGCGAGTCGAGTAGGACGGTGATTCAA
580	GGATTATGTATGCCATGTTGAACAGTCACTAATCTTGGAGGTAACTAATTGT
581	GTGTACAAGTGGCTTT
582	TTTAGGCATGGACTAA
583	CATTCGGTGCGATTTT
584	TTTGTAACGATTGTGC
585	CGGAGGTTAGGCTTTT
586	TTTAGTGTTCTATGAA
587	GCCTGCGTCGGATTTT
588	TTTCCACCTCCAGCTA
589	GGACAATCAGACATTT
590	TTTTCCTGGAGGTGTG
591	TTTCATCAAGCTTACC
592	TGCCGGTCAGATATTT
593	TTTACGACGAACTGAA
594	CTAATCATCGATATTT
595	TTTATTCATGCTTAAT
596	ACCGAATTACCTATTT
597	TTTTCCACGCTCAATG
598	CGTTGCGGATAGCTTT
599	TTTGGTTAGCTGAGTT
600	CGAATGACCTTAATTT
601	GGTGAGAAGAACATTT
602	TTTTTCTCCAAGAACA
603	CCGTGCACCGTCCTTT
604	TTTCGAGATCAGTCAA

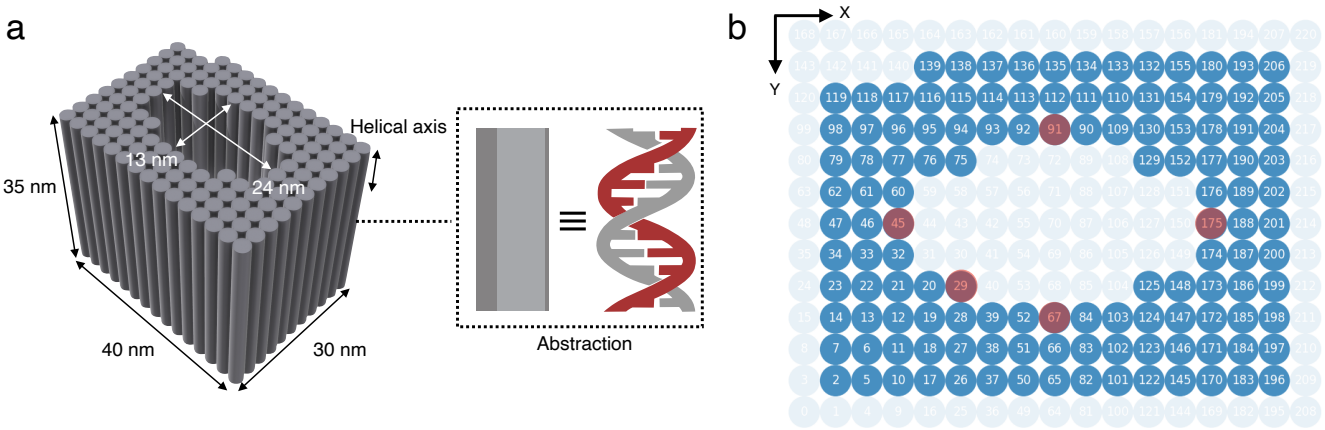
605	TCGCGAATAATCGTTT
606	TTTTTAATCTCTCACG
607	TAAGATTGTGGCATTT
608	TTTCGCTACTATTATT
609	GCTCACTTCCGGTTTT
610	TTTAAGCATCCGCAAT
611	TTTGAAGTCTGAGCAA
612	ACACCACCTGGACTTT
613	TTTGGACGATAGTTGG
614	GATTCGACTCCTATTT
615	AGCGGAATTCTGCTTT
616	TTTTTCTACGTAGCCG
617	GGCGGACAAGAACTTT
618	TTTACACCACATGGCC
619	AATGTCATCCGGTTTT
620	TTTACGACTGGATCCA
621	CAGCGGTAGTATCTTT
622	TTTACTCAGTCCGAAC
623	TTTCGTAAGTCACACC
624	GCGATGCGCAATTTTT
625	TTTACATTCGCGGTAG
626	AGTTGTTACAAGATTT
627	TTTCTGGTACTCGTGA
628	CTATTCATACAGGTTT
629	TTTTCTGCACTGCGGA
630	TTTCCACCGACCTCAA
631	CTTACAGCGCCATTTT
632	TTTGAAGGCACTGGAA
633	ACCGCATGCTACGTTT
634	TTTCTGGACTCGTGTG
635	GCAGTACTCCGGATTT
636	ACTCCTCACTTGCTTT
637	TTTAGTGCTGCGACGT
638	TGTAGAGCGTCCTTTT
639	TTTCAGTGTCCAGGTG
640	GTTAAGATCGGTATTT
641	TTTCCTTGGCTTCATA
642	TTTGTATGAACTTATG
643	GTCCTTGTCCAGTTTT
644	TTTGAAGGCGGCCGCT
645	AATCCATTCACCGTTT
646	TTTTACCAACGGTTCC
647	ACACAACCAAGCGTTT
648	GAGGTACGGATCGTTT
649	TTTTAGGTCATTGACT
650	ATATGACATCTCATTT
651	TTTCGGATGGACGAGT
652	GTTGTTAAGATCTTTT
653	TTTAGTCTTCCAACGC
654	TTTGATACATGTTAAG
655	TGTAATTAGTGACTTT
656	TTTCTGAGATGATTCG
657	CCAGGCACTGATATTT
658	TTTCGAGCTTAGATCA
659	CTCGTGAGCTCGTTTT
660	TTTACGTTACGATTCT
661	TTTCTCACTTGTACGT
662	TAAGCGGTGCTTATTT
663	TTTTTACTTGACACAT
664	CGAAGACACTTGATTT
665	TTTGGCCAACCTGAGT

666	ATCATAATGGTGGTTT
667	TTTGTCACAACCGTGG
668	CTTAGGAGGTACTTTT
669	GGCTTATTATCCTTTT
670	TTTGATTACCTCATCA
671	TGTCATATGACCATTT
672	TTTTGAACAAGGCCGA
673	CAGATTGATAACATTT
674	TTTATCCATTGTGAAT
675	GTCGTGCGTTCCGTTT
676	TTTTCCTTACTACGCG
677	CCACAAGCCGGACTTT
678	TTTTACCGATCTTAGG
679	TGGATCGCAATGCTTT
680	TTTCCGCTATTCTCTT
681	AGTTCTCTGCTAGTTT
682	TTTAGTATAATGGCAC
683	TGGTAGTAACCAATTT
684	TTTTGATTGCTCTGAA
685	AGTGACAACGTCATTT
686	TTTACAGGCACCGATT
687	AGTATACCAGATGTTT
688	TTTTTCCTCTCGTGAT
689	CGGATCGGCACCGTTT
690	TTTGTTCCGATCCTAG
691	CTGAATGACCAATTTT
692	TTTCAGGAGCTTCACA
693	GCGCGCATCCTCGTTT
694	TTTTCCAAGGCACAGA
695	CTTGATAATCTGGTTT
696	TTTTTGTCAGATACGT
697	CGTGCTTCGGCATTTT
698	TTTAATTATCGCTGTC
699	GAATAGGAATTGATTT
700	TTTACGAGGATTAGGA
701	GTTGTATGGTATATTT
702	TTTAGTAAGTTCGGCT
703	CTACTCGACTCGCTTT
704	TTTACTGTTCAACATG
705	TCCAAGATTAGTGTTT

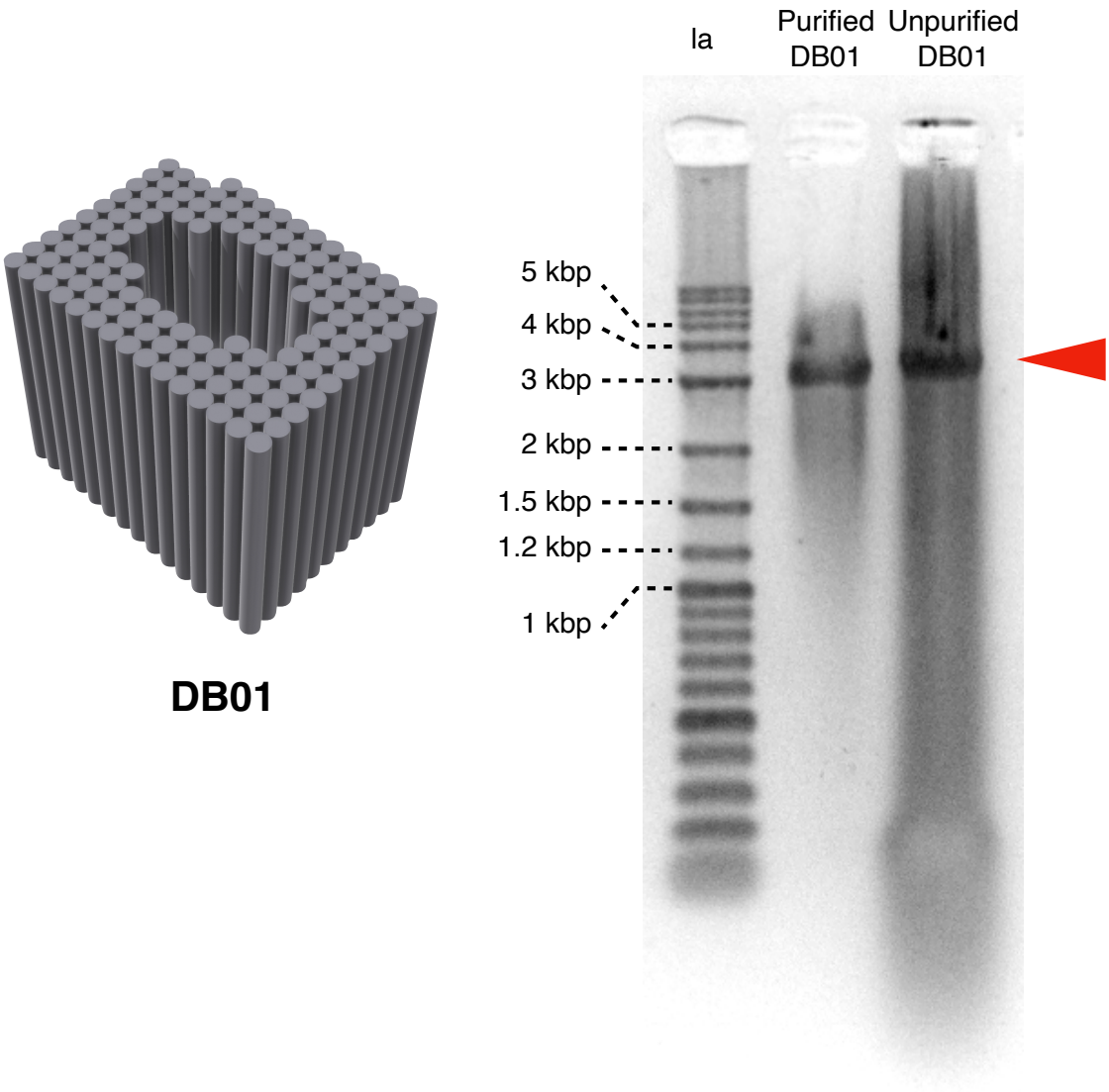
Unless stated otherwise, the following symbols are used throughout the Supplementary Figures: grey sphere, HaloTag; black wavy line, oligo(ethylene glycol) (OEG) chain; dark red helix, single-stranded DNA; yellow star, Cy3.



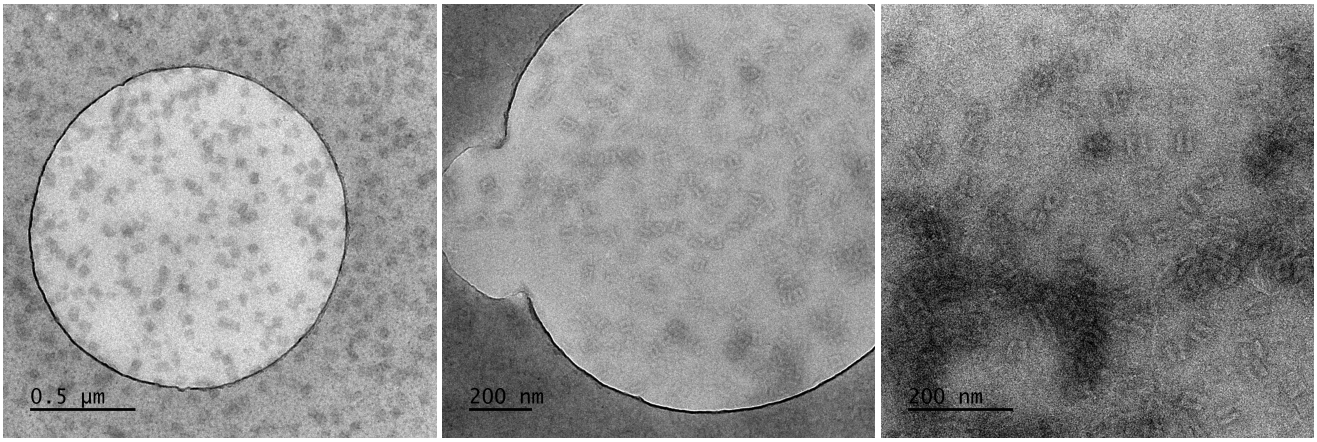
Supplementary Fig. S1 NanoBricks design of DB01. a. Voxelized image of DB01. b. Image of the voxelized DB01 converted into a set of DNA strands. The images were created with NanoBricks[26].



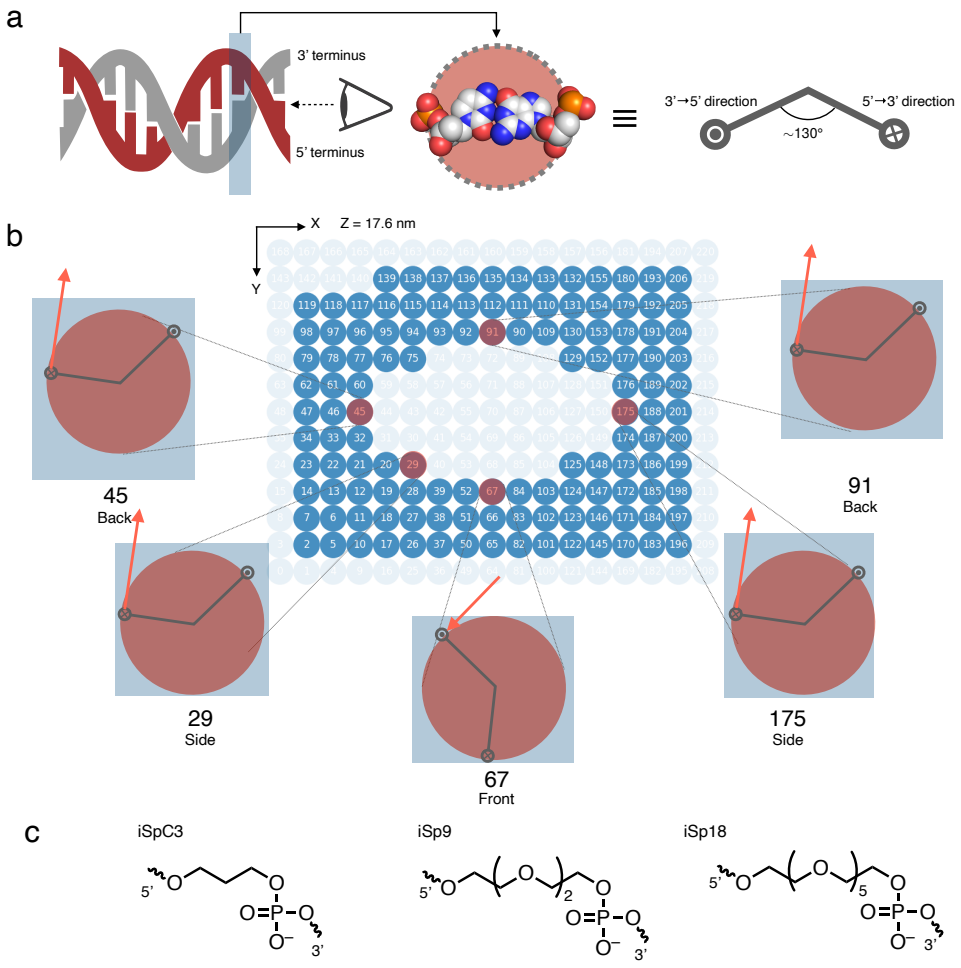
Supplementary Fig. S2 Overview of structural features of the DNA-brick structure DB01. a. DB01 is built by folding 705 short single-stranded DNA oligonucleotides into a 125-helix, 40×30×35 nm^3 cuboid (W × D × H, corresponding to X, Y and Z) containing an elliptical through-hole cavity that spans 24 nm in X and 13 nm in Y over the full height. DNA duplexes are abstracted to cylinders, indicated in grey. b. The X-Y cross-section looking down the Z+ direction. The five helices highlighted in red carry single-stranded DNA overhangs for protein tethering, 17.6 nm from the top face along Z.



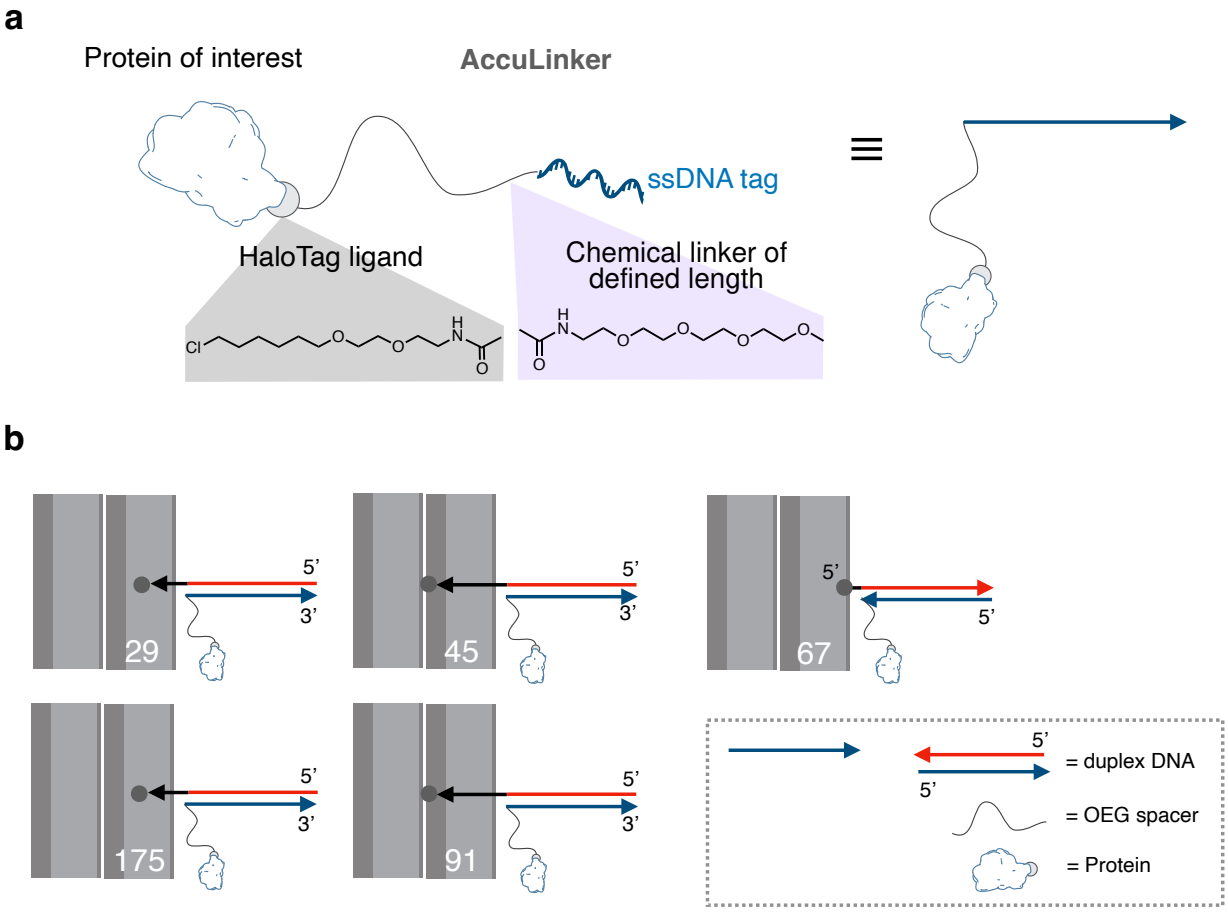
Supplementary Fig. S3 Design and gel analysis of DB01. Left, cylinder model of the DB01 structure, in which each cylinder is a DNA duplex. Right, 1.5% agarose gel of purified and unpurified DB01, stained for DNA with SYBR Gold; la, DNA ladder with the indicated sizes. The red arrow marks the DB01 band.



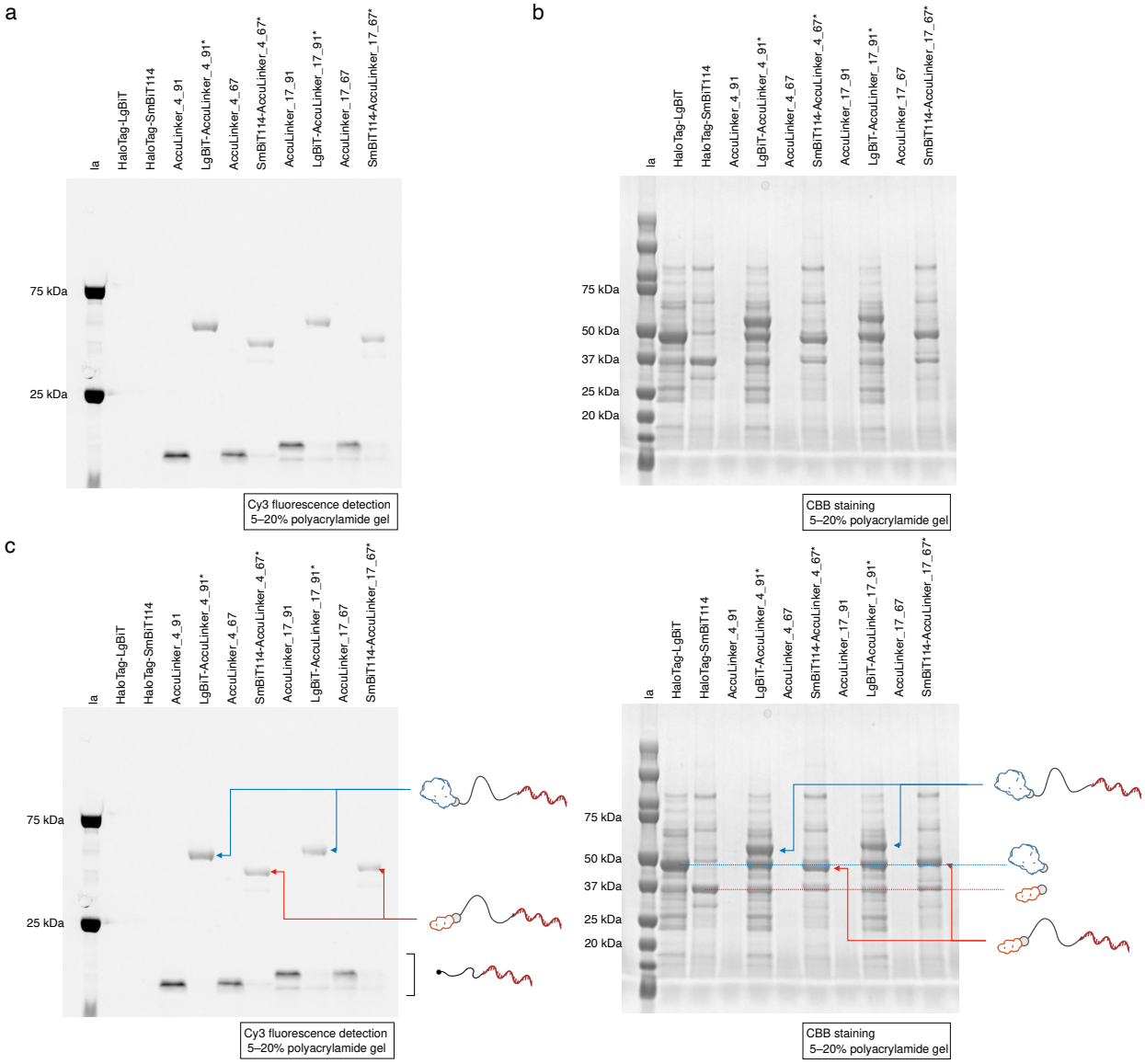
Supplementary Fig. S4 Negative-stain TEM analysis of DB01, purified from the band indicated by the red arrow in Supplementary Fig. S3. Left, overview field; centre and right, higher-magnification fields. Scale bars, 0.5 µm (left) and 200 nm (centre, right).



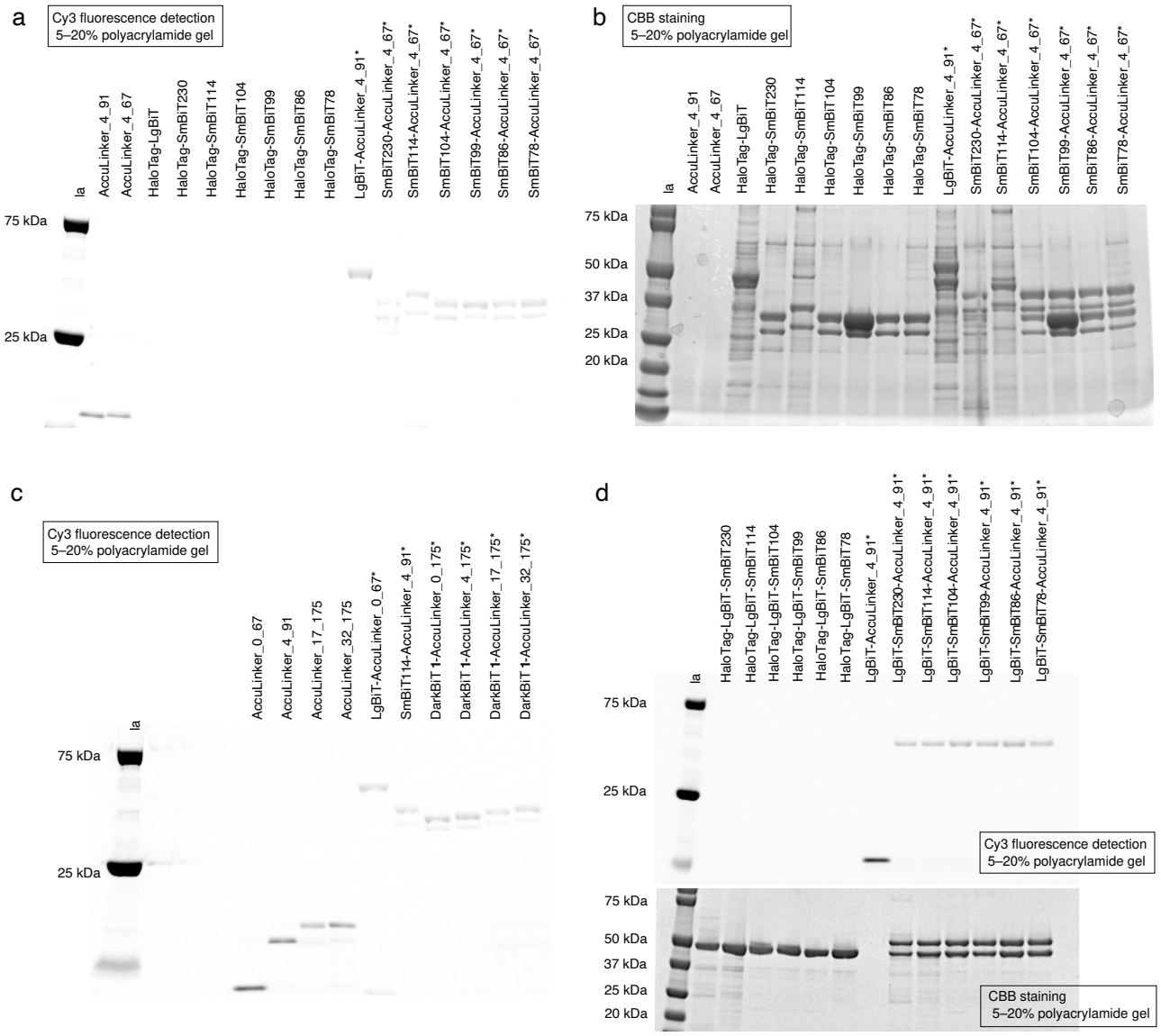
Supplementary Fig. S5 Helix information and chemical modification of the protein tethering helices. a. Schematic illustration of the phase of the DNA bases within the double helix at a particular Z-slice. ⊙ indicates the 5′ to 3′ direction from the back to front. ⊗ indicates the 5′ to 3′ direction from the front to back. b. The phase of the DNA bases within the protein tethering helices, highlighted by red circles, at Z = 17.6 nm. Red arrows indicate the single-stranded DNAs for the protein tethering. In helix 67, a single-stranded DNA extends from the front of the helix towards the inner cavity. In helices 45 and 91, a single-stranded DNA extends from the back of the helix towards the inner cavity. In helices 29 and 175, a single-stranded DNA extends from the side of helix towards the inner cavity. To extend the single-stranded DNA for protein tethering (complementary to the ssDNA end of the AccuLinker) from the front surface of the helix towards the inner cavity, a chemical spacer of appropriate length was incorporated. Specifically, an iSpC3 spacer (three carbons, ca. 0.4–0.5 nm) was used for helix 67, an iSp18 spacer (hexaethylene glycol, ca. 2 nm) for helices 45 and 91, and an iSp9 spacer (triethylene glycol, ca. 1 nm) for helices 29 and 175. c. Chemical structures of the iSpC3, iSp18 and iSp9 spacers.



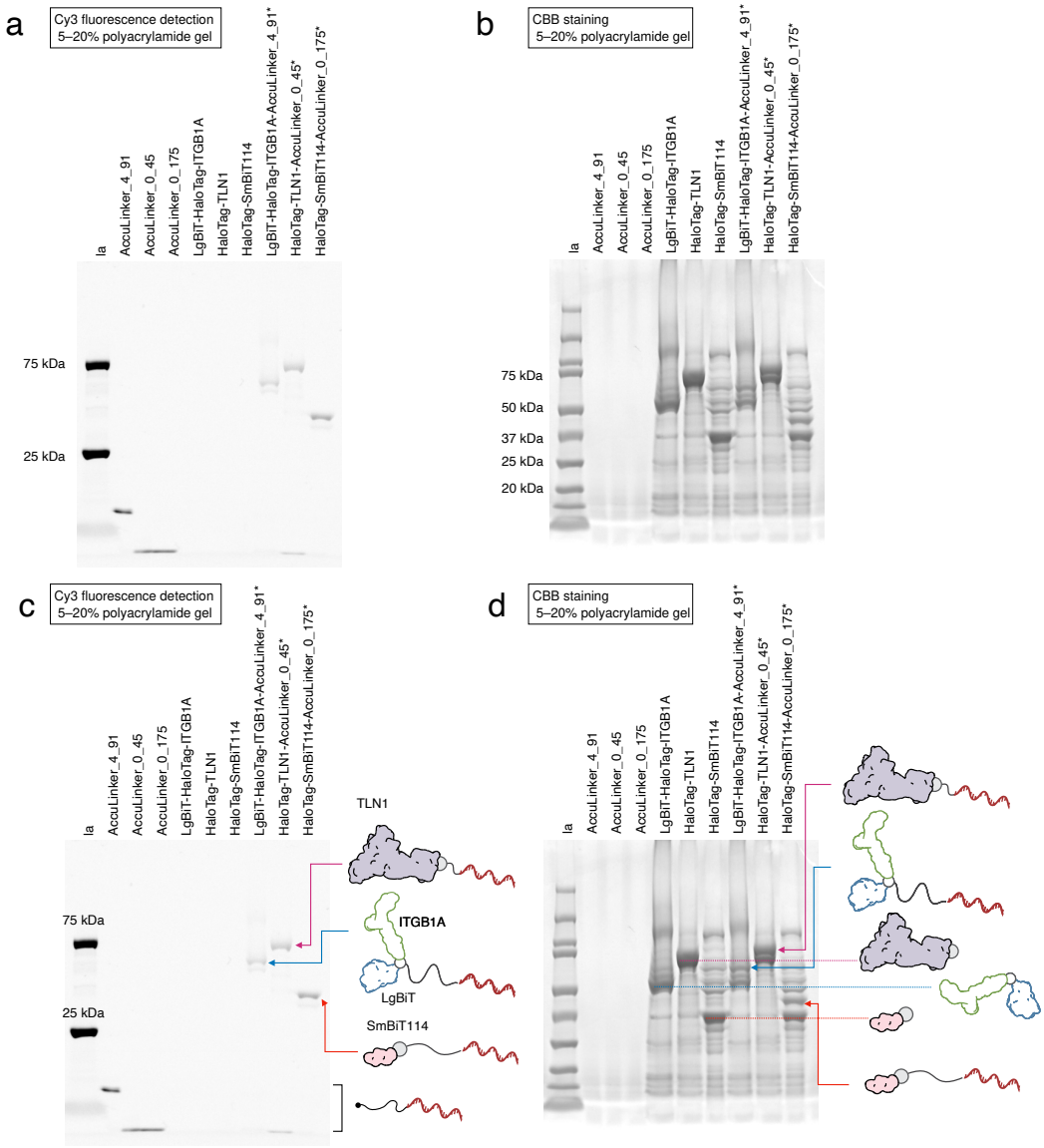
Supplementary Fig. S6 AccuLinker and protein confinement in DB01. a. Schematic illustration of AccuLinker. Each AccuLinker is a chemical linker of defined length, carrying a specific tag at one end that binds the protein of interest and a single-stranded DNA (ssDNA) at the other. b. Schematic image of protein confinement. The red and blue arrows, shown in the 5′-to-3′ direction, indicate the 16-nt ssDNA. The ssDNA of the AccuLinker (blue arrow) binds to pre-installed ssDNA (red arrow) overhangs on the inner surface of DB01. DNA duplexes of DB01 are abstracted to cylinders, indicated in grey. The numbers correspond to the helix numbers in Supplementary Fig. S5.



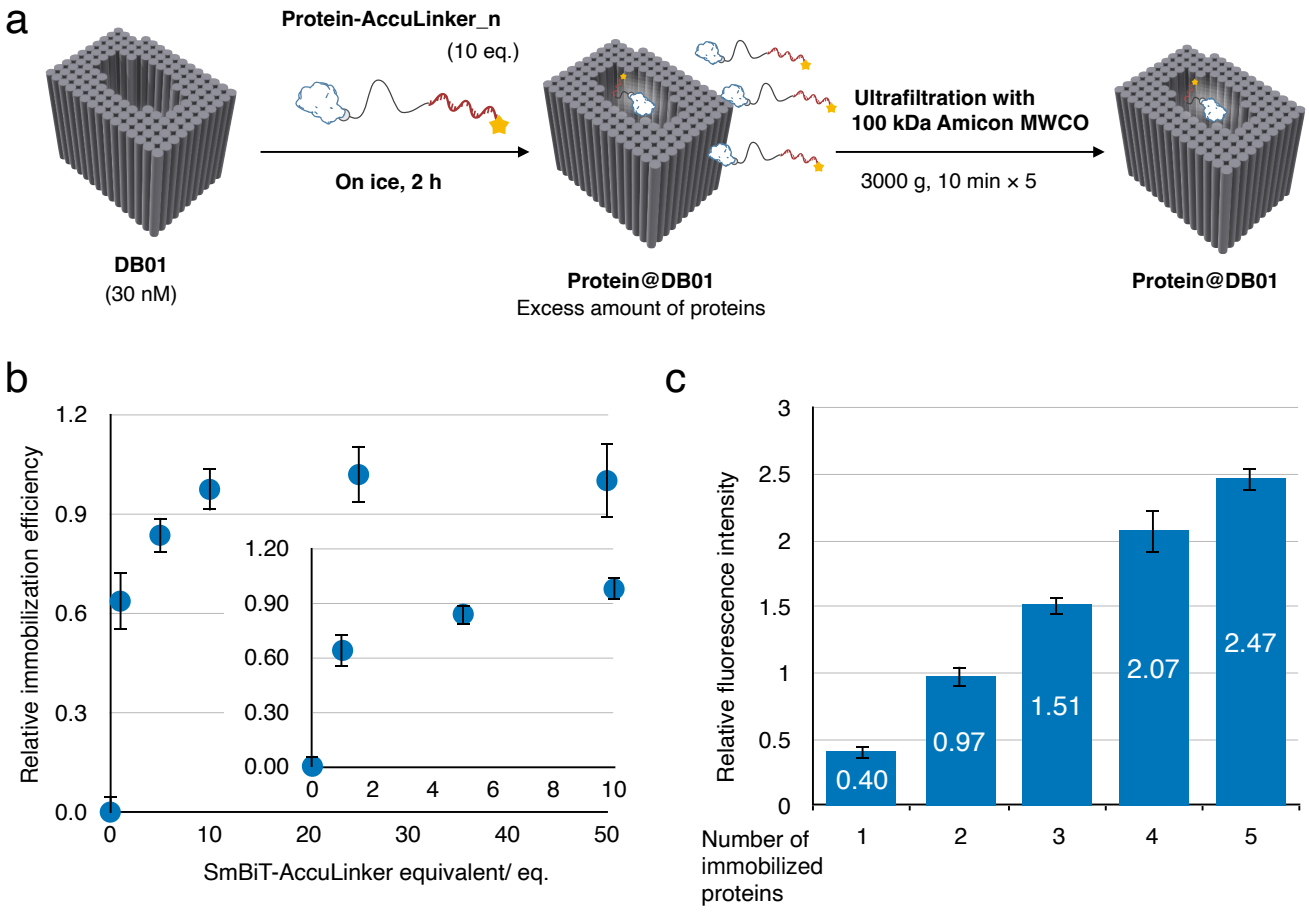
Supplementary Fig. S7 HaloTag-mediated conjugation of AccuLinker to HaloTag-LgBiT and HaloTag-SmBiT114. a. Cy3 fluorescence image of the PAGE gel. b. Coomassie Brilliant Blue (CBB) staining image of the PAGE gel. c. Molecular annotation of the bands in a and b. la, molecular-weight marker. The gel electrophoresis was conducted on a 5–20% gradient polyacrylamide gel. The gel shown is representative of independent preparations. *The samples are unpurified reaction mixtures. AccuLinker_n_X: n indicates the number of OEG units and X indicates the helix number for the protein tethering. The numbering corresponds to the helix numbers in Supplementary Fig. S5.



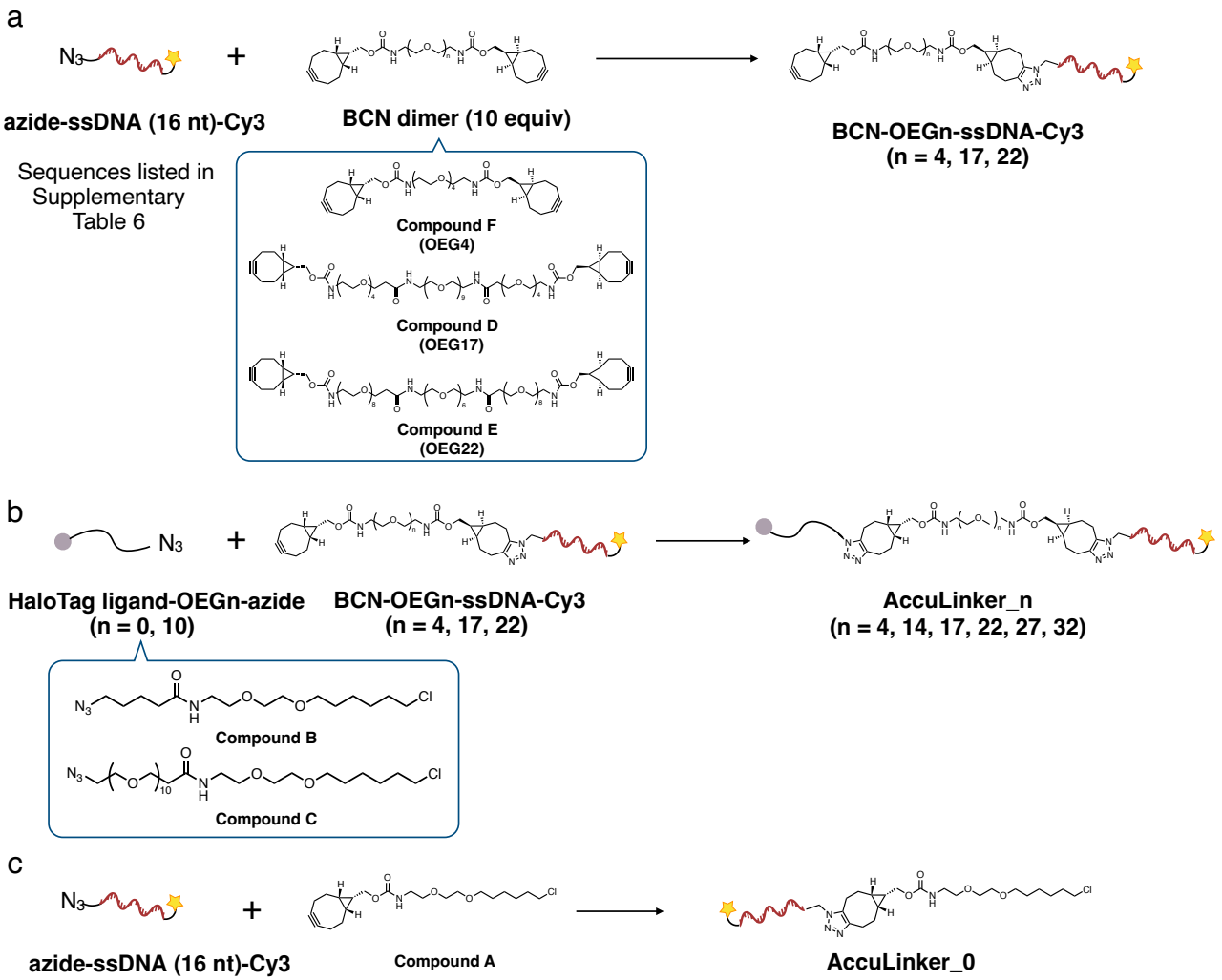
Supplementary Fig. S8 HaloTag-mediated conjugation of AccuLinker to a series of HaloTag-fused LgBiT, SmBiT, DarkBiT **1** and single-chain LgBiT-SmBiT constructs. a. Cy3 fluorescence image of the LgBiT and SmBiT gel. b. CBB staining of the same gel. c. Cy3 fluorescence image of the DarkBiT **1** gel. d. Cy3 fluorescence (upper) and CBB staining (lower) of the gel for the six single-chain HaloTag-LgBiT-SmBiT fusions. la, molecular-weight marker. The gel electrophoresis was conducted on a 5–20% gradient polyacrylamide gel. The gel shown is representative of independent preparations. *The samples are unpurified reaction mixtures. AccuLinker_n_X: n indicates the number of OEG units and X indicates the helix number for the protein tethering. The numbering corresponds to the helix numbers in Supplementary Fig. S5.



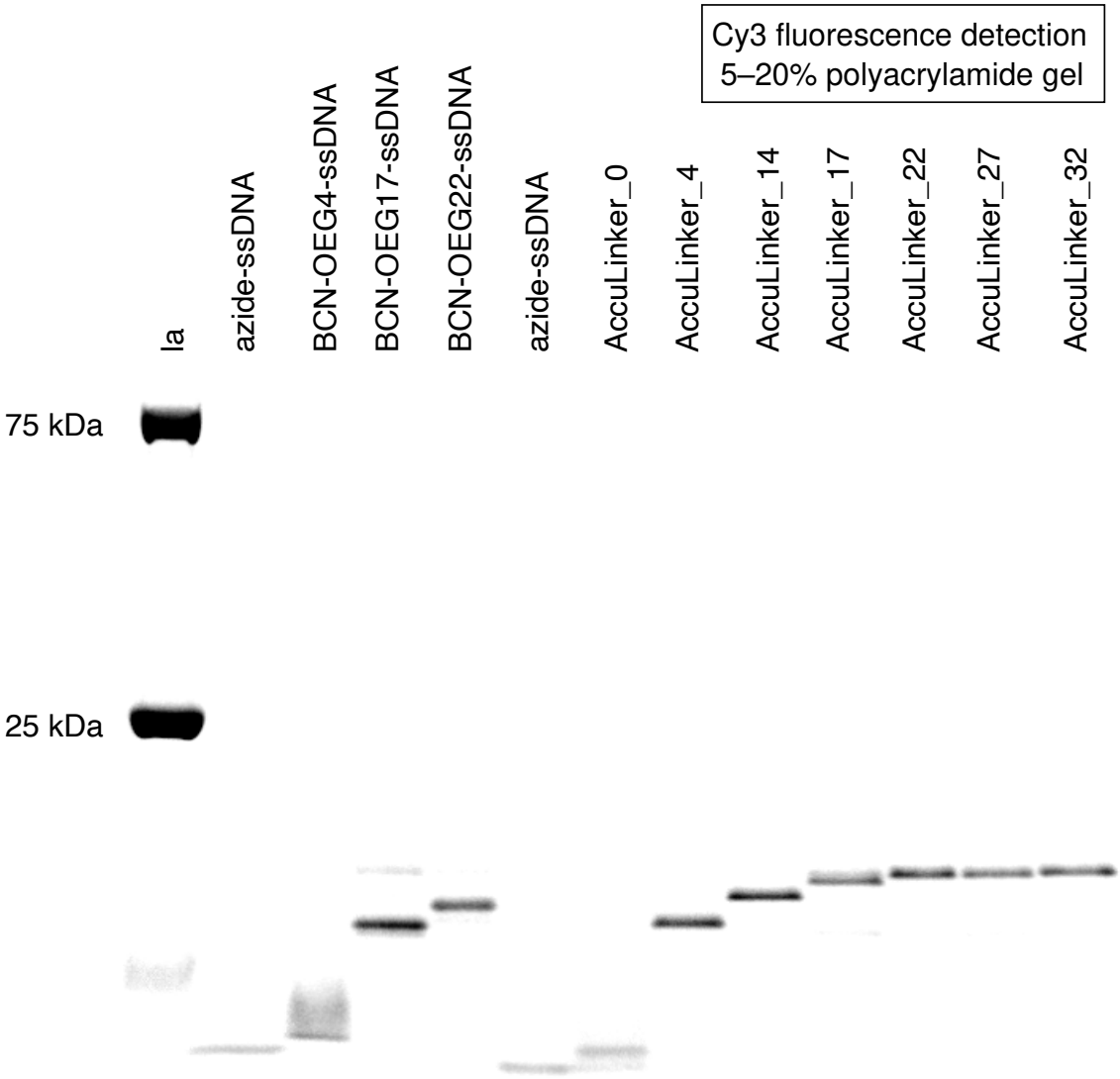
Supplementary Fig. S9 HaloTag-mediated conjugation of AccuLinker to the ITGB1A, TLN1 and SmBiT114 constructs used in the modulator screen. a. Cy3 fluorescence image of the PAGE gel. b. CBB staining image of the PAGE gel. c, d. Molecular annotation of the bands in a and b, respectively. la, molecular-weight marker. The gel electrophoresis was conducted on a 5–20% gradient polyacrylamide gel. The gel shown is representative of independent preparations. *The samples are unpurified reaction mixtures. AccuLinker_n_X: n indicates the number of OEG units and X indicates the helix number for the protein tethering. The numbering corresponds to the helix numbers in Supplementary Fig. S5.



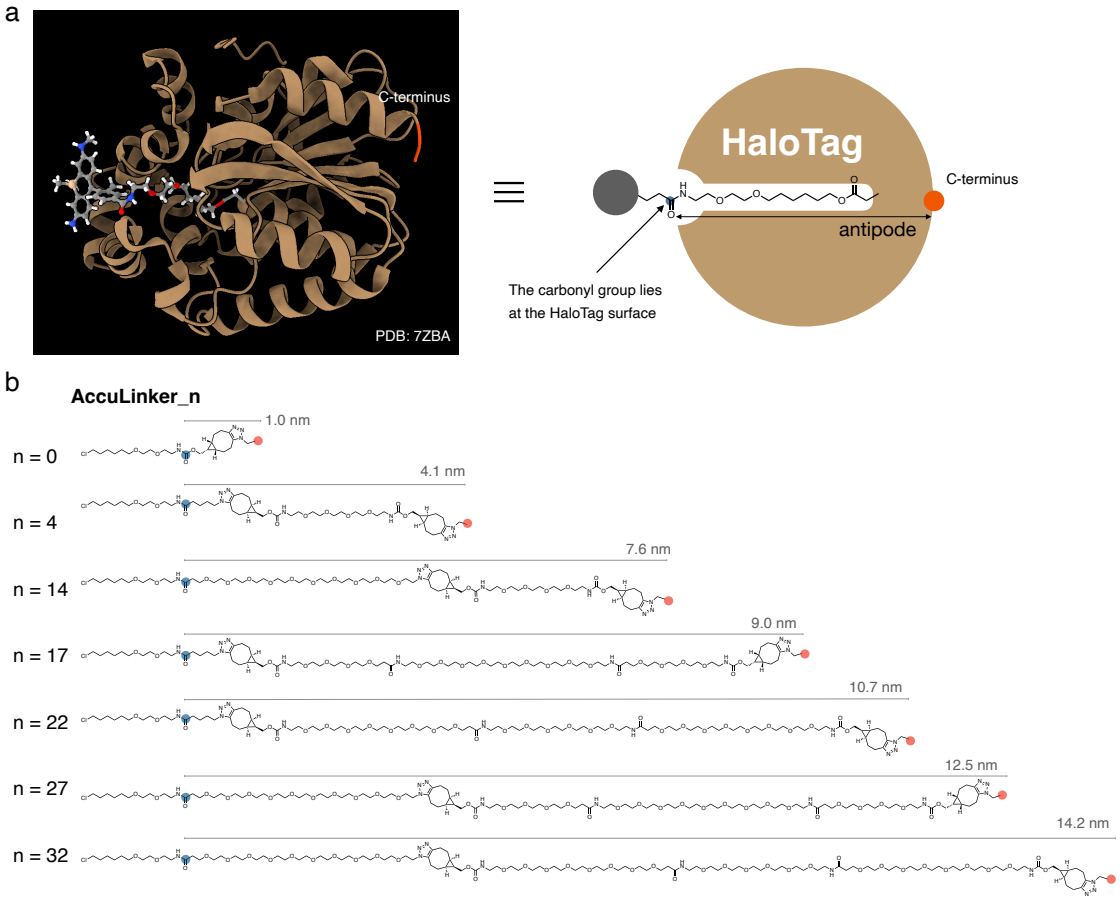
Supplementary Fig. S10 Protein tethering into DB01. a. Schematic procedure for tethering protein–AccuLinker_n conjugates to DB01. b. Relative immobilization efficiency at different equivalents of SmBiT114–AccuLinker conjugate, reacted on ice for 2 hours. Efficiency is the Cy3 fluorescence per unit DB01 concentration, normalized to its saturating value; immobilization was quantitative at 10 or more equivalents. Data are mean ± s.d. ($n = 3$). c. Cy3 fluorescence of DB01 carrying one to five LgBiT molecules, set by the sequence specificity of the AccuLinker overhangs. Values in the bars are mean relative fluorescence intensities, which scale linearly with the number immobilized. Data are mean ± s.d. ($n = 3$).



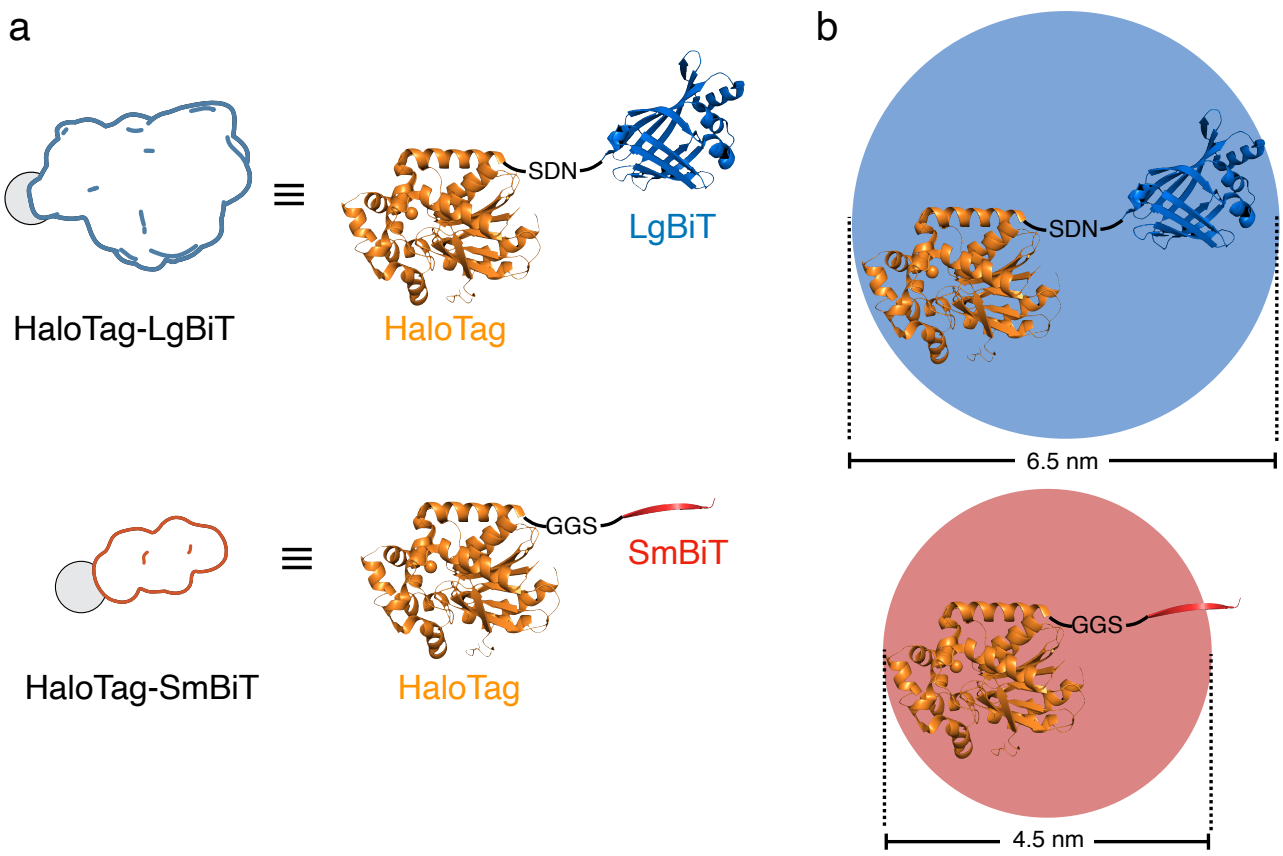
Supplementary Fig. S11 Synthetic scheme of AccuLinker_n. a. Synthetic scheme of BCN-OEGn-ssDNA-Cy3. The sequences of the azide-ssDNA-Cy3 used are listed in **Supplementary Table 6**. BCN dimers (the synthesized compounds **D** and **E**, or the commercial compound **F**; Section 3) were used for the first click reaction. b. Synthetic scheme of AccuLinker_n. The synthesized BCN-OEGn-ssDNA-Cy3 conjugates were reacted with compound **B** or **C** in a second click reaction to prepare the desired AccuLinker_n constructs of various lengths. c. Synthetic scheme of AccuLinker_0.



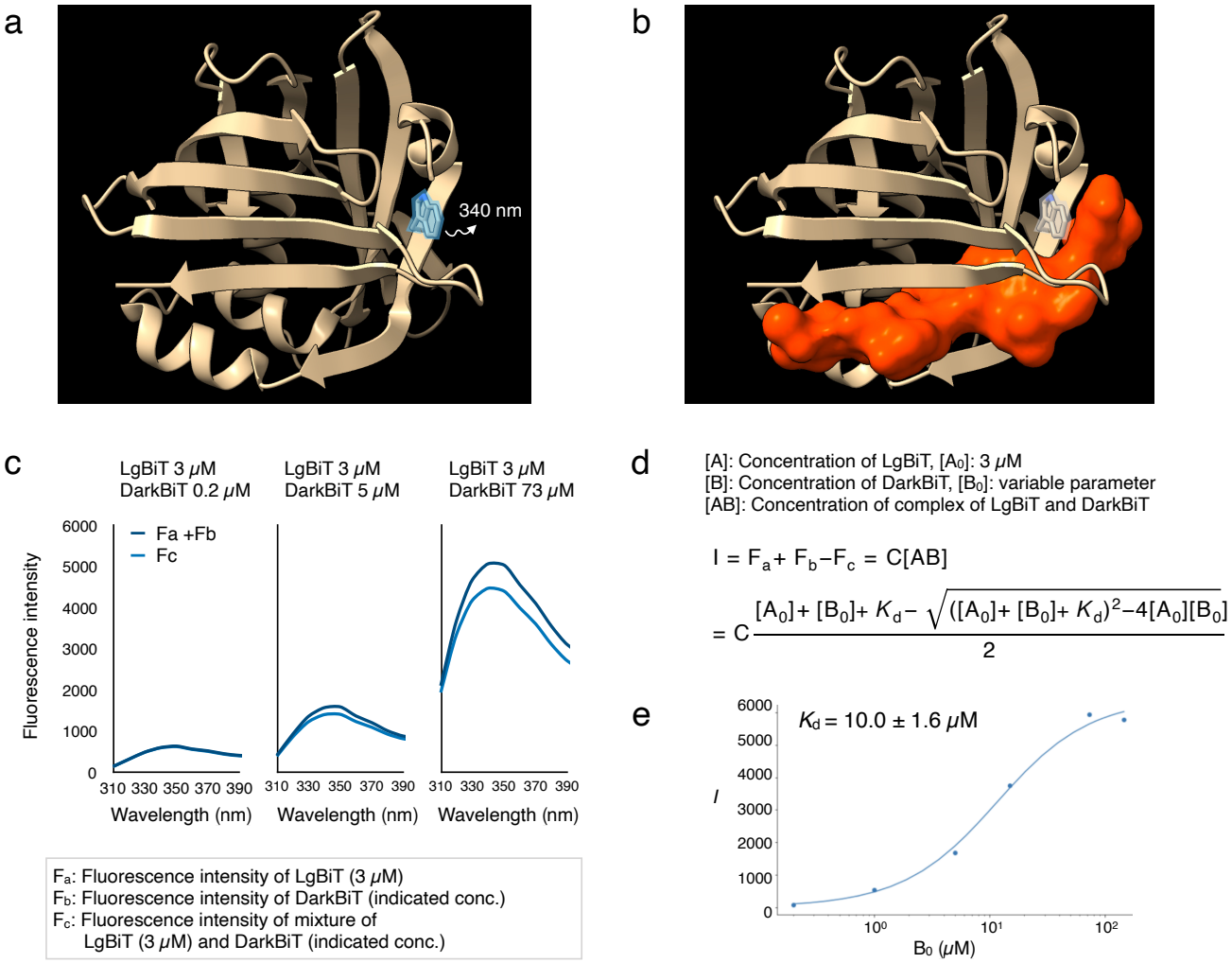
Supplementary Fig. S12 Gel-electrophoresis image of synthesized BCN-OEGn-ssDNA and AccuLinker_n. Gel mobility analysis of the unreacted azide-modified ssDNA, synthesized BCN-OEGn-ssDNAs (n = 4, 17, and 22) and synthesized AccuLinker_n (n = 0, 4, 14, 17, 22, 27, and 32). Each intermediate yields two AccuLinkers, because compound **B** adds no OEG unit and compound **C** adds ten; AccuLinker_0 follows the separate route in Supplementary Fig. S11c. The sequence of ssDNA is GTGATTTGAAAGTTGC, and the synthesized AccuLinkers correspond to the AccuLinker_n_67 series listed in Supplementary Table 7. The ssDNA carried a Cy3 label, so the purity and size of each product are read from its Cy3 fluorescence in the gel. The gel electrophoresis was conducted on a 5–20% gradient polyacrylamide gel. The gel shown is representative of independent preparations.



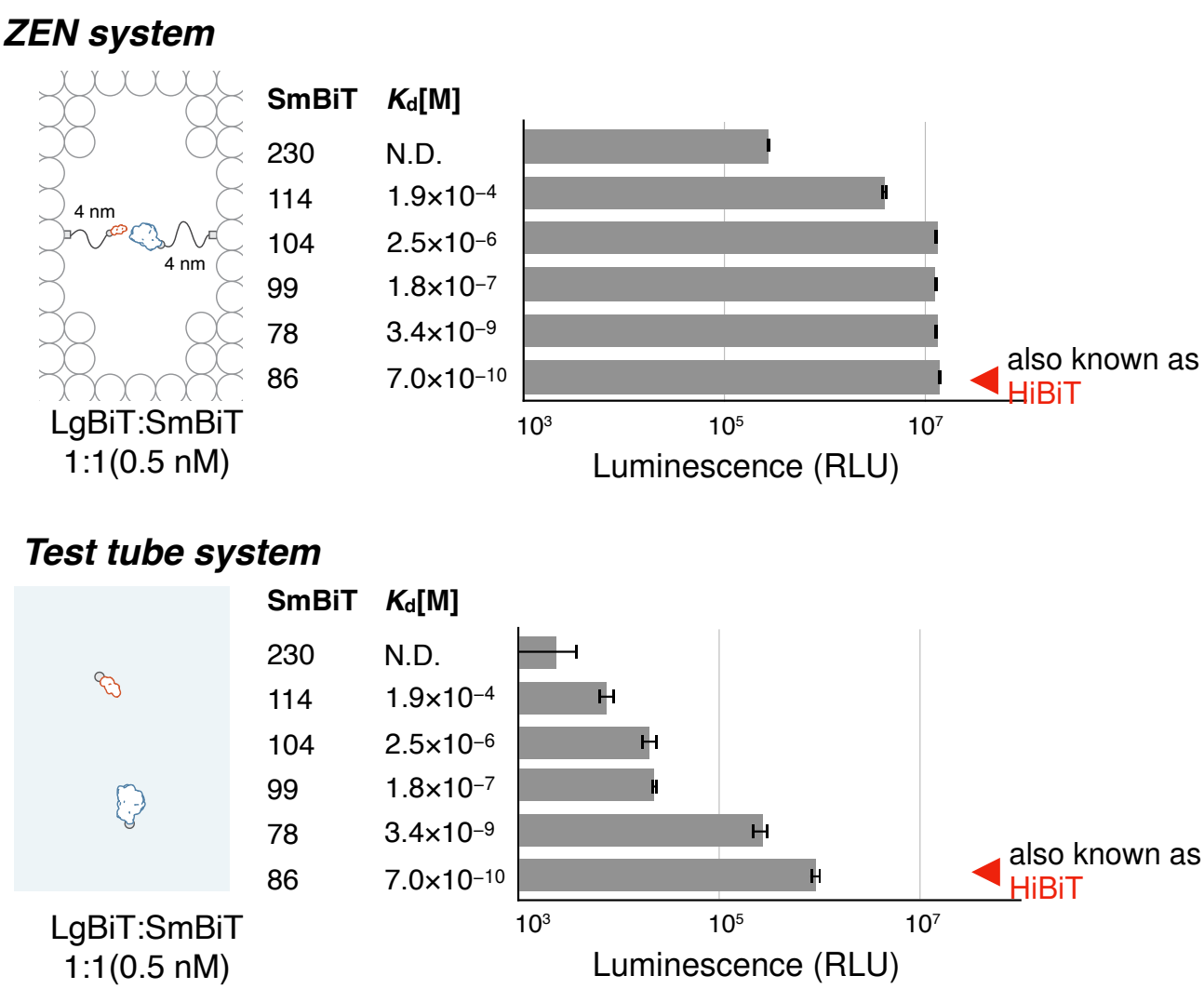
Supplementary Fig. S13 Synthetic AccuLinker_n. a. X-ray structural analysis of HaloTag protein-conjugated with specific ligand (Protein Data Bank (PDB) entry 7ZBA). b. Chemical structure of AccuLinker_n (n = 0, 4, 14, 17, 22, 27, 32). The linker length of AccuLinker_n is estimated from an OEG unit length of 0.35 nm and a BCN-azide conjugate length of 1.0 nm, both calculated using Material Studio.



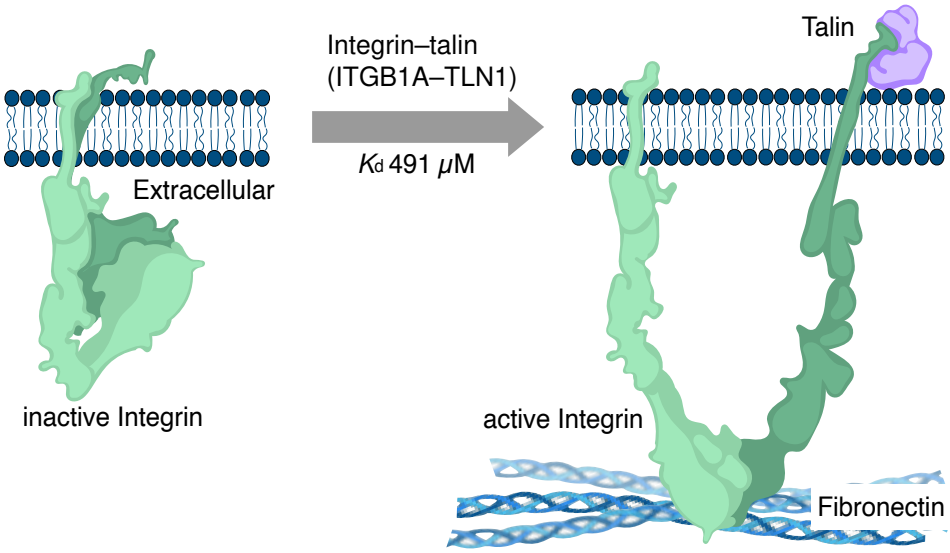
Supplementary Fig. S14 Sizes of HaloTag-fused proteins. a. Schematic illustration of HaloTag-fused LgBiT or SmBiT with a three-amino-acids spacer. b. HaloTag-fused LgBiT and SmBiT are approximated as spherical particles 6.5 and 4.5 nm in diameter, respectively for theoretical simulation. Detailed sequence information of these proteins and the other proteins was summarized in **Supplementary Tables 1–4**.



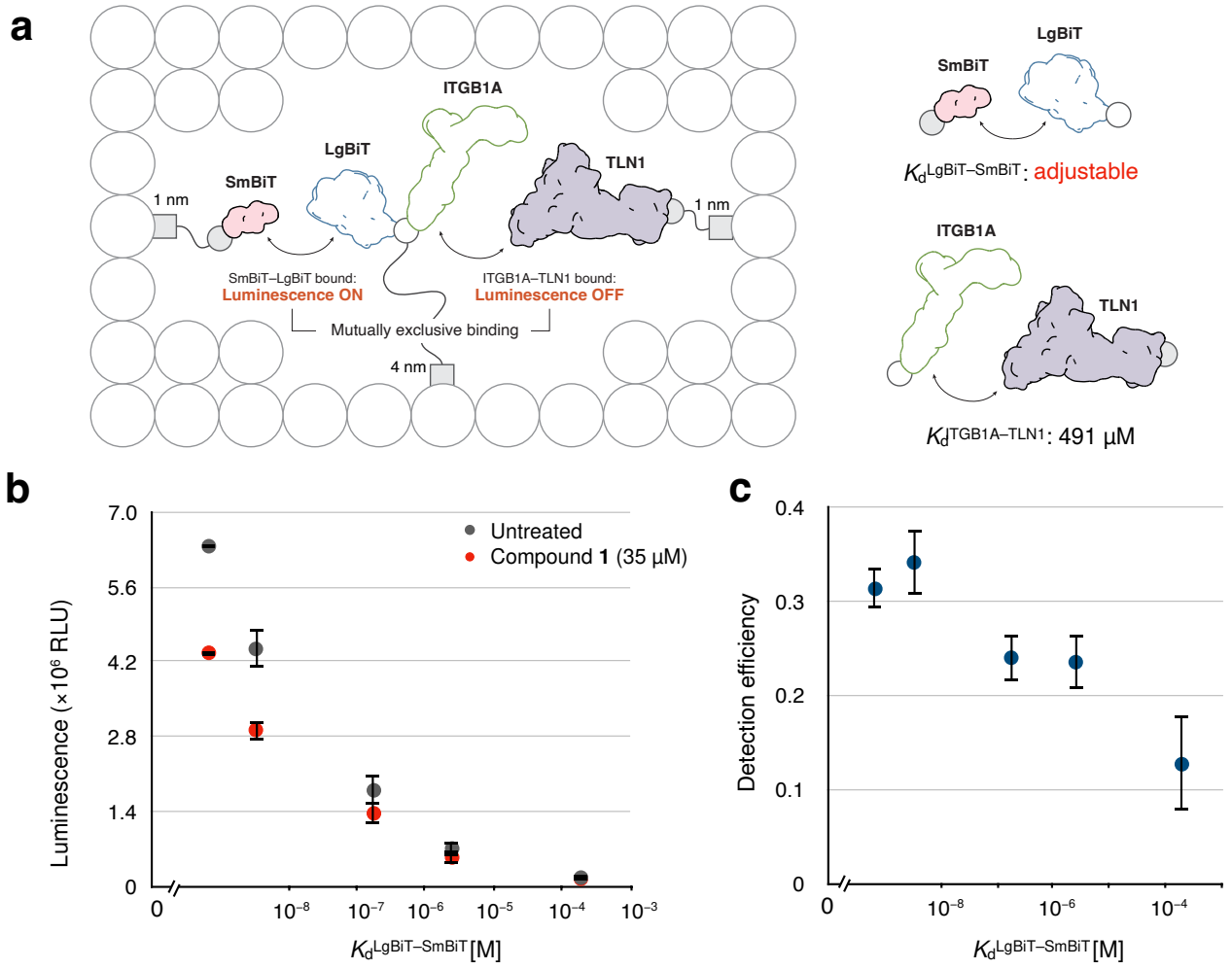
Supplementary Fig. S15 Binding analysis of DarkBiT **1** (labelled DarkBiT) to LgBiT. a. LgBiT from the LgBiT–SmBiT complex structure (PDB 7SNX), with SmBiT hidden. The tryptophan residue emitting at 340 nm is highlighted in blue. b. The same structure with SmBiT shown in orange. DarkBiT **1** competes for this site, and peptide binding quenches the tryptophan fluorescence. c. Fluorescence spectra at three DarkBiT **1** concentrations. The gap between $F_a + F_b$ and F_c is the quenching I, which grows with concentration. d. Symbol definitions and the binding equation used to obtain the LgBiT–DarkBiT **1** dissociation constant (K_d). e. Fitted curve for DarkBiT **1** binding to LgBiT. DarkBiT **1** binds to LgBiT with $K_\mathrm{d} = 10.0 \pm 1.6$ μM (standard error of the fit).



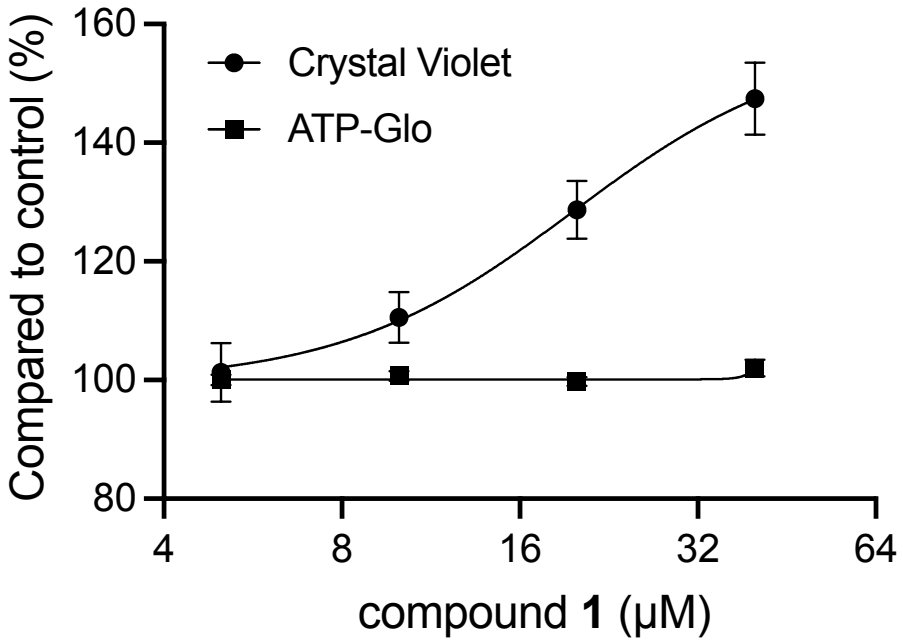
Supplementary Fig. S16 Comparison of LgBiT-SmBiT complexation in the Zonal Engineered Nano (ZEN) system and the test tube system. LgBiT-SmBiT complexation was evaluated by measuring the complexation-dependent luminescence. In the ZEN system, LgBiT and SmBiT were tethered with AccuLinker_4_91 and AccuLinker_4_67, respectively. In both systems, LgBiT and SmBiT were present at 0.5 nM each. The SmBiT numbering and the reported dissociation constants (K_d) follow the original NanoBiT report[28]. The red arrow marks SmBiT86, which is also known as HiBiT. The luminescence axis is logarithmic. Data are mean ± s.d. ($n = 3$).



Supplementary Fig. S17 Molecular mechanism of integrin activation[51]. Binding of talin to the intracellular domain of integrin promotes a structural change in the integrin. This structural change allows the integrin to bind extracellular-matrix proteins such as fibronectin.



Supplementary Fig. S18 Adjustment of PPI modulator sensitivity. a. Protein placement in DB01 for detection of a PPI modulator. HaloTag-fused SmBiT, HaloTag-fused TLN1 and LgBiT-HaloTag-ITGB1A are tethered into DB01 with AccuLinker_0_175, AccuLinker_0_45, and AccuLinker_4_91, respectively. Treatment with a PPI modulator (compound **1**) switches the binding partners, resulting in the dissociation of LgBiT from SmBiT. b. Changes in luminescence of LgBiT–SmBiT in the presence or absence of compound **1**, shown against their dissociation constants ($K_d^{LgBiT–SmBiT}$) on the x axis. Red data points represent samples treated with 35 μM of compound **1**, while grey points indicate untreated samples. Data are mean ± s.d. ($n = 3$). c. Fractional decrease in luminescence caused by treatment with compound **1**. The x axis is the LgBiT–SmBiT dissociation constant; the y axis shows 1 − (treated/untreated), so larger values indicate a stronger switching response. The response varies systematically with the LgBiT–SmBiT affinity, so the switch threshold can be set by the choice of SmBiT variant. Data are mean ± s.d. ($n = 3$).



Supplementary Fig. S19 Cell proliferation and cell biomass analyses. Crystal violet staining (circles) and the CellTiter-Glo 3D ATP signal (squares, labelled ATP-Glo in the figure) are plotted against compound **1** concentration, each as a percentage of the vehicle control. To test the effect of compound **1** on integrin-dependent cell adhesion, U87MG cells were cultured for 5 days with DMEM containing 1% FBS on fibronectin-coated dishes (10 µg/mL). Cell proliferation was quantified using the CellTiter-Glo 3D assay, which estimates viable cell number based on intracellular ATP content. In parallel, crystal violet staining was used to assess cellular biomass, providing an integrated measure of adherent cell mass that is influenced by both the number of adherent cells and their size. Data are mean ± s.d. ($n = 6$ replicate wells).

17 Bayesian estimation of the SmBiT230 K_{d}

The competitive DarkBiT **2** titration series place the six SmBiT variants on a common occupancy scale, and anchoring that scale to published affinities gives $K_{\mathrm{d}}^{\mathrm{SmBiT230}} = 9.60\ [4.24, 22.04]$ mM. The median is insensitive to the calibration and likelihood-weighting choices examined, staying between 8.82 and 9.98 mM, and the fitted effective concentration agrees to within a factor of 1.3 with the value computed independently from cavity geometry. This section sets out the model and its calibration, the estimate and its diagnostics, the sensitivity analyses, and the choices held fixed.

17.1 Analysis scope

The SmBiT230 K_{d} was estimated from six DarkBiT **2** competition titrations, using the finite-capacity ${}_2F_1$ response model derived and parameterized in the supplementary information of the companion paper[24]. The DarkBiT **2** affinity is not an input to this response model, so the reported estimate does not depend on it; the original report estimates it to be comparable to that of the parent SmBiT peptide[29]. The present section describes the external-affinity calibration, the resulting SmBiT230 estimate, and the analyses used to assess its dependence on that calibration. The full response function, prior specification for the curve-shape and observation parameters, implementation, and posterior predictive checks are given there[24].

Published SmBiT affinity measurements provide the external calibration needed to place the fitted occupancy ratios on a conventional K_{d} scale. The reported SmBiT230 value is therefore a calibrated model-based estimate whose absolute scale is set by that calibration.

The fitted data comprised six series: SmBiT86, SmBiT78, SmBiT99, SmBiT104, SmBiT114 and SmBiT230. Each contained 12 DarkBiT **2** concentrations measured in triplicate, giving $6 \times 12 \times 3 = 216$ replicate-level observations. The linker-length titration data were not included in these K_{d} analyses.

17.2 Primary external-affinity calibration

For each SmBiT series i, the response model uses

$$\rho_i = \frac{c_{\mathrm{eff}}}{K_{\mathrm{d},i}}, \tag{2}$$

where c_{eff} is a shared effective-concentration scale. The titration curves determine ρ_i more directly than they determine c_{eff} and $K_{\mathrm{d},i}$ separately. External affinity information is therefore required to calibrate the absolute K_{d} scale. The geometric meaning

of c_{eff}, and its relation to the intrinsic K_{d} through the two-state occupancy odds, are derived in Section 18 (Eqs. (12) and (14)).

The spatial-overlap calculation underlying Fig. 4b provides a position-based effective-concentration scale under its simplified geometric encounter kernel. That geometric value was not imposed as the c_{eff} of the present response model, because the simplified geometric kernel does not explicitly resolve every orientational, conformational, or molecular-shape contribution. Such contributions can in principle be incorporated into a higher-resolution encounter kernel; here their net effect is absorbed into the fitted response-model scale.

In the primary analysis, the published SmBiT99 and SmBiT104 dissociation constants were fixed at 180 nM and 1.3 μM, respectively[28]. The two reported SmBiT114 values, 190 μM and 440 μM, were obtained by different measurement procedures[28] and were not treated as error-free replicates. Instead, they were modeled as external observations of one latent SmBiT114 dissociation constant:

$$\log_{10}\left(\frac{K_{\mathrm{d,114}}^{(k)}}{\mathrm{M}}\right) \sim \mathcal{N}\left[\log_{10}\left(\frac{K_{\mathrm{d,114}}}{\mathrm{M}}\right), \sigma_{\mathrm{ext}}^2\right], \qquad k = 1, 2, \tag{3}$$

$$\sigma_{\mathrm{ext}} \sim \mathrm{HalfNormal}(0.30\,\mathrm{dex}). \tag{4}$$

This formulation treats the discrepancy between the two values as uncertainty between measurement procedures while retaining a single underlying SmBiT114 affinity.

The shared c_{eff} and the SmBiT86, SmBiT78, SmBiT114, and SmBiT230 dissociation constants were estimated simultaneously.

Each titration series was normalized to the luminescence of the corresponding single-chain HaloTag-LgBiT-SmBiT fusion (Supplementary Table 3), which reports the intact-luciferase activity of that SmBiT variant and was measured separately in the absence of competitor. The reference value was the mean of three technical replicates, each background-subtracted before averaging. A single common factor was then applied to all series so that the mean zero-competitor response of SmBiT86 equalled one; SmBiT86 binds most strongly and therefore has the bound fraction closest to one in the absence of competitor. Every titration point was measured in triplicate, and all replicates are plotted in Fig. 5c,d.

The finite-capacity response model, its fixed parameters $M = 24$ and $\beta_\nu = -0.5$, and the series-specific signal scale s_i are all defined in the supplementary information of the companion paper[24], which is the source for every equation used here. The predicted response is s_i times a bound fraction that equals $\rho_i/(1+\rho_i)$ at zero competitor, so fixing s_i does not force the zero-competitor response to one: series with small ρ_i begin below full signal. For SmBiT114 and SmBiT230, s_i was fixed at one as an explicit model constraint, because over the measured range a change in $K_{\mathrm{d},i}$ for these

two series appears mainly as a change in response amplitude, leaving s_i and $K_{\mathrm{d},i}$ not jointly identifiable. The signal scales for the other four series were estimated.

17.3 Priors, sampling, and primary estimate

For each freely estimated dissociation constant,

$$\log_{10}\left(\frac{K_{\mathrm{d},i}}{\mathrm{M}}\right) \sim \mathrm{Uniform}(-12, -1). \tag{5}$$

The shared effective concentration was given the prior

$$\log_{10}\left(\frac{c_{\mathrm{eff}}}{\mathrm{M}}\right) \sim \mathcal{N}(-5, 1.5^2) \quad \text{truncated to } [-12, 2]. \tag{6}$$

The primary fit used a shape-weighted objective based on the replicate-level Student-t_4 observation model:

$$\log \widetilde{p}(D \mid \theta) = \sum_{ij} \omega_{ij} \log p(y_{ij} \mid \theta). \tag{7}$$

The weights increase the influence of the transition and high-concentration regions on the simultaneous curve-shape fit; the group definitions and values are given in the deposited code. The weighting defines a weighted pseudo-posterior rather than an additional generative observation model.

The weighted objective was sampled with the No-U-Turn Sampler in Turing.jl using four chains, 2,000 warmup iterations per chain, 4,000 retained samples per chain, and a target acceptance probability of 0.95. This gave 16,000 retained samples; the random seed was 20260733.

The primary weighted pseudo-posterior estimate for SmBiT230 was

$$K_{\mathrm{d}}^{\mathrm{SmBiT230}} = 9.60\ [4.24,\ 22.04]\,\mathrm{mM}. \tag{8}$$

The central value is the weighted pseudo-posterior median, and the brackets give the 5th and 95th percentiles, defining a 90% weighted pseudo-posterior interval. Sampling was well behaved: the maximum monitored $\widehat{R}$ was 1.0013, the minimum effective sample size was 3,704, and no divergent transitions occurred. The corresponding latent SmBiT114 estimate was 285.5 μM (90% weighted-posterior interval : 128.3–637.4 μM), and the shared effective concentration was 0.978 mM (0.437–2.21 mM). The weighted pseudo-posterior median of σ_{ext} was 0.271 dex (0.130–0.566 dex).

Series	Literature K_d	Use in the primary fit	Median	90% interval
SmBiT86	0.70 nM	free; literature value withheld	0.699 nM	0.450–1.03 nM
SmBiT78	3.4 nM	free; literature value withheld	3.60 nM	2.34–5.47 nM
SmBiT99	180 nM	exact anchor	not estimated	—
SmBiT104	1.3 μM	exact anchor	not estimated	—
SmBiT114	190/440 μM	external-observation model	286 μM	128–637 μM
SmBiT230	none	free	9.60 mM	4.24–22.04 mM

Table S2 Literature affinities and how each entered the primary fit. The SmBiT86 and SmBiT78 literature values were withheld from fitting and used only for post-fit comparison, so their estimates test the calibrated model against affinities it was not given; both literature values fall inside the reported intervals. SmBiT99 and SmBiT104 were exact calibration anchors, and the two SmBiT114 measurements entered an external-observation model. Literature values are from the NanoBiT characterization[28]. Estimates are weighted pseudo-posterior medians with 5th–95th percentile intervals.

17.4 Stability across calibration and weighting choices

The primary analysis was compared with four alternative treatments of the SmBiT114 information. The first retained the exact SmBiT99 and SmBiT104 constraints but omitted external SmBiT114 calibration. Two further analyses placed a Normal and a Student-t_4 prior on $\log_{10}(K_{d,114}/\mathrm{M})$, centred at the geometric mean of the two reported values (289 μM) with scale 0.182 dex. The final analysis retained the external-observation formulation but increased the Half-Normal prior scale for σ_{ext} from 0.30 to 0.60 dex.

SmBiT114 treatment	SmBiT114 K_d	SmBiT230 K_d
No external SmBiT114 data; SmBiT99/104 exact constraints retained	262 [31.7, 2112] μM	8.82 [1.04, 71.26] mM
Direct Normal prior	287 [145, 559] μM	9.65 [4.79, 19.31] mM
Direct Student-t_4 prior	283 [125, 633] μM	9.52 [4.10, 21.78] mM
Two external observations; Half-Normal (0.30 dex) **s.d. prior (primary)**	286 [128, 637] μM	9.60 [4.24, 22.04] mM
Two external observations; Half-Normal (0.60 dex) s.d. prior	284 [94.2, 841] μM	9.52 [3.13, 28.47] mM

Supplementary Table 10 Sensitivity of the conditional SmBiT230 K_d estimate to the treatment of the SmBiT114 external information. Values are weighted pseudo-posterior medians with 5th–95th percentile intervals. All analyses retain the exact SmBiT99 and SmBiT104 literature constraints. The analysis without SmBiT114 external calibration is an identifiability reference, not an alternative primary estimate.

The entries in this comparison table are weighted pseudo-posterior medians and 90% weighted pseudo-posterior intervals obtained with the same shape-weighted objective; these are the intervals reported as uncertainty intervals in the main text. These

intervals summarize a weighted pseudo-posterior and should not be interpreted as nominal credible intervals for the unweighted Student-t_4 observation model.

Across the five calibration treatments, the SmBiT230 median remained within 8.82–9.65 mM. Broadening the prior for between-method variation changed the median by less than 1% while widening the interval. Omitting the SmBiT114 external calibration produced a similar median but a substantially broader interval. In that identifiability reference, the posterior correlations of $\log_{10} c_{\mathrm{eff}}$ with $\log_{10} K_{\mathrm{d},114}$ and $\log_{10} K_{\mathrm{d},230}$ were 0.9986 and 0.9977, respectively. Thus the central estimate was stable across the examined calibration treatments, whereas the interval width reflected the uncertainty in the absolute affinity scale.

As a separate likelihood-weighting sensitivity analysis, the shape weighting was disabled and mean-one observation weights were used. The highest-concentration 25% of observations contributed 25%, 33%, 40%, or 50% of the total likelihood weight; under the 25% setting every observation carried equal weight. Across these four settings, the SmBiT230 pseudo-posterior median spanned 9.25 to 9.98 mM, with 90% interval bounds from 3.77 to 23.53 mM. The equal-weight result was 9.98 [4.35, 23.53] mM. The central estimate was therefore insensitive to this weighting choice at the scale relevant to the reported affinity, although interval width remained dependent on the calibration and weighting assumptions.

Across all nine analysis variants examined here, five calibration treatments and four likelihood-weighting settings, the SmBiT230 median stayed between 8.82 and 9.98 mM, within 9% of the reported value. The calibration governs the width of the interval rather than its centre.

17.5 Calibration-free identifiability analysis

To separate what the titration data determine from what the calibration supplies, the staged finite-capacity ${}_2F_1$ analysis was repeated with all six dissociation constants treated as latent parameters. No literature K_{d} was fixed and no external-affinity observation entered the likelihood. Each $\log_{10}(K_{\mathrm{d},i}/\mathrm{M})$ was assigned a Uniform$(-14, 2)$ prior, and the shared $\log_{10}(c_{\mathrm{eff}}/\mathrm{M})$ a Normal prior with standard deviation 1.5 truncated to $[-12, 2]$. Prior means of -6, -5 and -4 were run to expose the dependence of the absolute scale on that choice. All remaining settings matched the primary analysis, including $M = 24$, $\beta_\nu = -0.5$, and the signal scales s_i fixed at one for SmBiT114 and SmBiT230. Each condition used four chains, 2,000 warmup iterations per chain, 4,000 retained samples per chain, and a target acceptance probability of 0.95. Every posterior lies at least 1.39 dex inside the Uniform bounds, so the K_{d} priors contribute no gradient along the direction described below.

All three fits met the prespecified diagnostics (maximum $\hat{R} \leq 1.003$, minimum bulk effective sample size $\geq$ 2,585, minimum tail effective sample size $\geq$ 1,128, no

divergent transitions). Convergence did not confer an absolute affinity scale. The posterior correlation between $\log_{10} K_\mathrm{d}$ and $\log_{10} c_\mathrm{eff}$ exceeded 0.999 for both SmBiT114 and SmBiT230, and moving the prior mean from -6 to -4 moved the c_eff median from 43.4 to 708 μM and the SmBiT230 median from 0.429 to 6.99 mM, while $K_\mathrm{d}/c_\mathrm{eff}$ stayed at 9.84–9.86 (Table 11).

The response model is invariant under

$$\log_{10} c'_\mathrm{eff} = \log_{10} c_\mathrm{eff} + \delta, \qquad \log_{10} K'_{\mathrm{d},i} = \log_{10} K_{\mathrm{d},i} + \delta, \qquad \log_{10} \nu'_0 = \log_{10} \nu_0 - \beta_\nu \delta, \tag{9}$$

so the likelihood constrains ratios, $K_{\mathrm{d},i}/c_\mathrm{eff}$ and $K_{\mathrm{d},i}/K_{\mathrm{d},j}$, rather than either factor alone. The identifiable combinations are $\eta_i = \log_{10}(K_{\mathrm{d},i}/c_\mathrm{eff})$ and $\omega = \log_{10} \nu_0 + \beta_\nu \log_{10} c_\mathrm{eff}$. Where the absolute scale settles is set jointly by the c_eff, ν_0 and K_d priors and their bounds, not by the c_eff prior alone: the $\log_{10} \nu_0$ medians of -1.316, -1.193 and -1.080 move by 0.11–0.12 dex, whereas Eq. (9) alone would move them by 0.29–0.32 dex.

What the data do determine transfers unchanged to the calibrated fit. The SmBiT230-to-SmBiT114 ratio was 33.61 [28.16, 40.50] without any literature input and 33.56 [28.23, 40.61] with it, a difference of 0.15%. Combining that ratio with an independently computed effective concentration therefore yields an affinity without any affinity standard: the position-based $c_\mathrm{eff}^\mathrm{spatial} = 1.20$ mM of Section 17.6 gives $K_\mathrm{d}^\mathrm{SmBiT230} = 11.8$ mM and $K_\mathrm{d}^\mathrm{SmBiT114} = 352\,\mu$M, within a factor of 1.23 of the calibrated values in both cases. Extending this route requires only a more accurate c_eff, which follows from geometry.

The calibration-free fits are therefore reported as an identifiability and prior-sensitivity reference. The reported estimate remains the calibrated, explicitly conditional $K_\mathrm{d}^\mathrm{SmBiT230} = 9.60$ [4.24, 22.04] mM. Machine-readable tables, the complete per-series results, and the sampler diagnostics are provided under `docs/calibration_free_tables/` in the deposited analysis code (https://github.com/FujitaG/zen-kd-estimation).

Prior mean	SmBiT114 K_d (μM)	SmBiT230 K_d (mM)	SmBiT114 $K_\mathrm{d}/c_\mathrm{eff}$	SmBiT230 $K_\mathrm{d}/c_\mathrm{eff}$
-6	12.6 [0.215, 1,045]	0.429 [0.00722, 35.3]	0.293 [0.262, 0.329]	9.84 [8.63, 11.43]
-5	47.4 [0.710, 5,108]	1.60 [0.0243, 170]	0.294 [0.262, 0.329]	9.86 [8.62, 11.45]
-4	206 [2.57, 28,034]	6.99 [0.0859, 964]	0.294 [0.262, 0.328]	9.86 [8.64, 11.46]

Supplementary Table 11 Dependence of the calibration-free absolute scale on the $\log_{10} c_\mathrm{eff}$ prior mean. Intervals are 90% weighted pseudo-posterior intervals. The K_d values are deliberately uncalibrated and are not independent affinity measurements; the $K_\mathrm{d}/c_\mathrm{eff}$ ratios are the identifiable quantities.

Series	Median	90% interval
SmBiT86	0.0139 nM	0.000246–0.611 nM
SmBiT78	0.0750 nM	0.00134–3.50 nM
SmBiT99	3.58 nM	0.0619–165 nM
SmBiT104	0.116 μM	0.00146–14.98 μM
SmBiT114	47.4 μM	0.710–5,108 μM
SmBiT230	1.60 mM	0.0243–170 mM

Supplementary Table 12 Calibration-free estimates for all six series at the reference condition ($\log_{10} c_{\mathrm{eff}}$ prior mean -5). Values lie on an arbitrary reference scale set by the priors and are not independent absolute affinities; their ratios are the identifiable content.

17.6 Agreement with the geometric effective concentration

The position-based spatial-overlap calculation gave an effective-concentration scale of $c_{\mathrm{eff}}^{\mathrm{spatial}} = 1.20\,\mathrm{mM}$. This value was not fixed as the shared response-model scale in the primary affinity analysis, which instead sampled c_{eff} jointly with the unknown dissociation constants. The fitted median of 0.978 mM agrees with the spatial estimate to within a factor of 1.3, although this agreement was not imposed.

The spatial implementation resolves tether geometry, steric exclusion, and positional overlap at its present resolution. A higher-resolution treatment could be developed to represent linker bending stiffness, detailed molecular shape, conformational flexibility, cavity fluctuations, and orientation-dependent reactivity, and to assess how uncertainty in these effects influences future affinity inference.

17.7 Model choices held fixed

Three response-model choices remained fixed across the primary fit and the calibration and likelihood-weighting sensitivity analyses above; the reported estimate and intervals are conditional on these choices.

For SmBiT114 and SmBiT230, the signal scale s_i was fixed at one because s_i and $K_{\mathrm{d},i}$ are not jointly identifiable over the measured range; the signal scales for the other variants were estimated under a weakly informative prior[24].

Finite local capacity is physically motivated by the limited occupancy of a single cavity. Its numerical value $M = 24$ was chosen after exploratory comparisons among candidate integer values and then held fixed during the reported Markov chain Monte Carlo (MCMC) sampling. Because M remained fixed, uncertainty from this exploratory selection is not included in the reported intervals.

The empirical coefficient β_ν, which describes the affinity dependence of curve shape, is not microscopically derived. It was fixed at -0.5 after exploratory model checks to stabilize that trend and was not sampled during the reported MCMC[24].

18 Accessible volume, state occupancy, and the definition of K_d

This section explains why the accessible-volume expression in the main text does not imply that the intrinsic dissociation constant changes with confinement. The apparent contradiction arises from applying a bulk concentration identity to state-conditioned microscopic volumes. In a homogeneous bulk solution, the concentrations of A, B, and AB are defined in the same physical volume, and their ratio already contains the equilibrium balance between unbound and bound populations. After mutually isolated local states are resolved, that population balance must instead be retained explicitly.

Throughout this section, concentrations are number concentrations. Conversion to molar units introduces only the corresponding constant factor. We also use an idealized state-counting model to expose the relevant probability term. In this minimal notation, geometry-independent internal and solvent contributions are coarse-grained into an effective non-spatial binding term; retaining them as separate partition-function factors gives the same result.

18.1 A mutually isolated pair is a two-state system

Consider one mutually isolated compartment containing one specified A–B pair. The compartment has two mutually exclusive states,

$$\mathrm{A} + \mathrm{B} \rightleftharpoons \mathrm{AB}, \tag{10}$$

which we call the unbound and bound states, respectively. Let $\overline{v}_A$ and $\overline{v}_B$ be the volumes accessible to the unbound partners, and let $\overline{v}_{AB}$ be the volume accessible to the complex. In a minimal state-counting representation, the statistical weights of the two states are

$$q_\mathrm{u} = \frac{\overline{v}_A \overline{v}_B}{v_0^2}, \qquad q_\mathrm{b} = \frac{\overline{v}_{AB}}{v_0} \exp(\beta\epsilon), \tag{11}$$

where v_0 is a microscopic reference volume, $\epsilon > 0$ denotes the geometry-independent binding-energy gain in this minimal model, and $\beta = (k_\mathrm{B}T)^{-1}$. Additional non-spatial state factors can be retained explicitly or absorbed into the corresponding effective Boltzmann factor without changing the argument. We define the geometric effective

concentration and the geometry-independent concentration scale K_0 as

$$C_{\mathrm{eff}} := \frac{\overline{v}_{AB}}{\overline{v}_A \overline{v}_B}, \qquad K_0 := \frac{1}{v_0 \exp(\beta\epsilon)}. \tag{12}$$

Both quantities are number concentrations, as is every concentration in this section. Calibrating the minimal state-counting model to its homogeneous bulk limit identifies K_0 with the intrinsic dissociation constant K_{d}, as derived in Section 18.3. Thus $K_0 = K_{\mathrm{d}}$, and Eqs. (11) and (12) give

$$\frac{q_{\mathrm{b}}}{q_{\mathrm{u}}} = \frac{C_{\mathrm{eff}}}{K_0} = \frac{C_{\mathrm{eff}}}{K_{\mathrm{d}}}. \tag{13}$$

Expressing every concentration in molar units divides each by the Avogadro constant and leaves these ratios unchanged, so the same relations hold for the molar $c_{\mathrm{eff}} = C_{\mathrm{eff}}/N_{\mathrm{A}}$ and K_{d} reported elsewhere in this work.

Let p be the equilibrium probability of the bound state. The normalized two-state probabilities are $P_{\mathrm{b}} = p$ and $P_{\mathrm{u}} = 1 - p$, and therefore

$$\frac{p}{1-p} = \frac{q_{\mathrm{b}}}{q_{\mathrm{u}}} = \frac{C_{\mathrm{eff}}}{K_{\mathrm{d}}}. \tag{14}$$

Equivalently,

$$\boxed{K_{\mathrm{d}} = \frac{\overline{v}_{AB}}{\overline{v}_A \overline{v}_B} \frac{1-p}{p}} \tag{15}$$

and

$$p = \frac{C_{\mathrm{eff}}}{K_{\mathrm{d}} + C_{\mathrm{eff}}}. \tag{16}$$

Equation (15) is the complete form of the schematic accessible-volume expression in the main text. The factor $(1-p)/p$ is the missing balance between the unbound and bound states. Changing accessible volume changes C_{eff} and therefore changes p according to Eq. (16); it does not require K_{d} to change.

The unbound probability in Eq. (15) is a joint-state probability. Within an isolated compartment, A and B are unbound together or are converted together into AB. It would therefore be incorrect to replace $1 - p$ by the product of two independent marginal probabilities, $(1-p)^2$. Mutual isolation removes cross-pair encounters and creates this A–B pairing constraint, so the factorization underlying the ordinary bulk product [A][B] no longer applies at the single-pair level.

18.2 The occupancy factor from an ensemble of isolated compartments

The same result follows by considering N mutually isolated, equivalent compartments. If n compartments are bound, the statistical weight of that population state is

$$W_n = \binom{N}{n} q_{\mathrm{u}}^{N-n} q_{\mathrm{b}}^{n}. \tag{17}$$

The binomial coefficient counts the ways of choosing which compartments are bound; equivalently, it removes the overcounting among the n bound and $N-n$ unbound compartments. Its contribution can be written as the combinatorial entropy

$$S_{\mathrm{comb}}(n) = k_{\mathrm{B}} \log \binom{N}{n}. \tag{18}$$

For large N, with $p = n/N$, the change in this entropy upon increasing the number of bound compartments is

$$\frac{1}{k_{\mathrm{B}}} \frac{\partial S_{\mathrm{comb}}}{\partial n} \simeq \log \frac{N-n}{n} = -\log \frac{p}{1-p}. \tag{19}$$

This is the origin of the bound–unbound odds term in an entropy derivation. Without taking the large-N derivative, the corresponding exact finite-system statement is obtained directly from adjacent population states:

$$\frac{W_{n+1}}{W_n} = \frac{N-n}{n+1} \frac{C_{\mathrm{eff}}}{K_{\mathrm{d}}}. \tag{20}$$

Thus, the combinatorial state count supplies precisely the occupancy information that disappears if molecule number is cancelled against a species-specific occupied volume. The normalized distribution generated by Eq. (17) is binomial, with mean bound fraction $\langle n/N \rangle = p$ given by Eq. (16). For a large ensemble, the adjacent-state ratio crosses unity near the most probable n, and Eq. (20) reduces to Eq. (14) with $p \simeq n/N$.

The substitution $V_X = N_X \overline{v}_X$ makes

$$\frac{N_X}{V_X} = \frac{1}{\overline{v}_X} \tag{21}$$

a density conditioned on state X already being present. Because both numerator and denominator change with occupancy, recovering the bulk activity additionally requires the probability that state X occurs. Equation (15) supplies that state probability.

18.3 Where the same probability balance appears in bulk

In a homogeneous bulk system, the equilibrium composition encodes the probability balance. Let the conserved molecular totals be N_A^0 and N_B^0, and let j complexes be present. The particle numbers in state j are

$$n_A = N_A^0 - j, \qquad n_B = N_B^0 - j, \qquad n_{AB} = j. \tag{22}$$

For an ideal, homogeneous solution of volume V, the equilibrium probability P_j is proportional to the state weight

$$\Omega_j \propto \frac{1}{n_A! n_B! j!} \left(\frac{V}{v_0}\right)^{n_A+n_B+j} \exp(\beta j \epsilon). \tag{23}$$

The factorials are the combinatorial terms associated with indistinguishable bulk molecules. Taking the ratio of adjacent states gives the exact finite-system expression

$$\frac{P_{j+1}}{P_j} = \frac{\Omega_{j+1}}{\Omega_j} = v_0 \exp(\beta\epsilon) \frac{n_A n_B}{V(j+1)} = \frac{1}{K_0} \frac{[\mathrm{A}][\mathrm{B}]}{[\mathrm{AB}] + 1/V}, \tag{24}$$

where $[\mathrm{A}] = n_A/V$, $[\mathrm{B}] = n_B/V$, and $[\mathrm{AB}] = j/V$.

The bulk equilibrium distribution has a maximum near some $j = j_*$. For a finite discrete system, the adjacent ratios on the two sides of the maximum bracket unity, attaining it only in the degenerate case of two equally probable neighbouring states. In the macroscopic limit, however, the distribution is sharply peaked and

$$\frac{P_{j_*+1}}{P_{j_*}} \longrightarrow 1. \tag{25}$$

Equation (24) then yields

$$K_0 \simeq \frac{[\mathrm{A}][\mathrm{B}]}{[\mathrm{AB}] + 1/V} \longrightarrow \frac{[\mathrm{A}][\mathrm{B}]}{[\mathrm{AB}]} \equiv K_\mathrm{d}. \tag{26}$$

The last step is the thermodynamic limit at fixed concentrations and establishes the promised identification

$$K_\mathrm{d} = K_0 = \frac{1}{v_0 \exp(\beta\epsilon)}. \tag{27}$$

This relation is therefore a consequence of calibrating the minimal statistical model to the conventional bulk definition, rather than an independent assumption about K_d. The relative size of the finite-particle correction is $1/(V[\mathrm{AB}]) = 1/j$. The probability term is not discarded as an arbitrary constant. Its composition-dependent part becomes the concentration ratio, while the remaining local slope of the equilibrium probability distribution, $\log(P_{j+1}/P_j)$, approaches zero at the bulk peak.

The different appearances of the same information can now be summarized directly. A mutually isolated pair has only two states, so equilibrium is represented by their explicit odds $p/(1-p)$. A bulk system has many possible values of j, so equilibrium is represented primarily by the location of a sharply peaked distribution, which is, equivalently, the equilibrium concentration ratio. The standard bulk formula already contains the bound–unbound balance and should not be reapplied to volumes conditioned separately on A, B, and AB occupancy.

18.4 Interpretation and scope

The thermodynamically general statement is written in terms of activities rather than raw concentrations. In a homogeneous ideal solution, activities reduce to concentration factors and the familiar expression $K_\mathrm{d} = [\mathrm{A}][\mathrm{B}]/[\mathrm{AB}]$ follows. In a mutually isolated microscopic system, correlations and pairing prevent the unbound joint state from being represented by the product of two independently averaged local concentrations. The explicit state odds in Eq. (15), or an equivalent correlated activity, must be used instead.

Accordingly, accessible volume controls occupancy through C_eff, whereas K_d describes the intrinsic A–B binding thermodynamics under the volume-only assumption used here: geometry changes translational accessibility while the binding energy and the internal state factors of A, B, and AB remain fixed. An extended state-weight treatment could represent confinement-induced strain, surface interactions, electrostatic changes, or conformational selection through geometry-dependent free-energy factors and, where necessary, additional conformational states. These contributions are outside the present treatment and could change the intrinsic or apparent affinity. Within the volume-only treatment, the apparent volume dependence of K_d is not a physical prediction but a consequence of omitting the bound–unbound occupancy factor when transferring a bulk concentration expression to resolved local states.